



## 저작자표시-비영리-변경금지 2.0 대한민국

이용자는 아래의 조건을 따르는 경우에 한하여 자유롭게

- 이 저작물을 복제, 배포, 전송, 전시, 공연 및 방송할 수 있습니다.

다음과 같은 조건을 따라야 합니다:



저작자표시. 귀하는 원저작자를 표시하여야 합니다.



비영리. 귀하는 이 저작물을 영리 목적으로 이용할 수 없습니다.



변경금지. 귀하는 이 저작물을 개작, 변형 또는 가공할 수 없습니다.

- 귀하는, 이 저작물의 재이용이나 배포의 경우, 이 저작물에 적용된 이용허락조건을 명확하게 나타내어야 합니다.
- 저작권자로부터 별도의 허가를 받으면 이러한 조건들은 적용되지 않습니다.

저작권법에 따른 이용자의 권리는 위의 내용에 의하여 영향을 받지 않습니다.

이것은 [이용허락규약\(Legal Code\)](#)을 이해하기 쉽게 요약한 것입니다.

[Disclaimer](#)

공학박사 학위논문

**Estimation of Geotechnical  
Properties on Highly and  
Completely Weathered Granite  
using Chemical Weathering Index**

화학적 풍화지수를 이용한 화강 풍화암의  
지반정수 평가

2020년 2월

서울대학교 대학원

건설환경공학부

이 승 환

# Estimation of Geotechnical Properties on Highly and Completely Weathered Granite using Chemical Weathering Index

지도 교수 정 충 기

이 논문을 공학박사 학위논문으로 제출함  
2019 년 11월

서울대학교 대학원  
건설환경공학부  
이 승 환

이승환의 공학박사 학위논문을 인준함  
2020 년 1월

위 원 장 박 준 범



부위원장 정 충 기

(인)

위 원 김 성 렬

(인)

위 원 전 석 원

(인)

위 원 조 환 제

(인)

## **Abstract**

# **Estimation of Geotechnical Properties on Highly and Completely Weathered Granite using Chemical Weathering Index**

Lee, Seung-Hwan

Department of Civil & Environmental Engineering

The Graduate School

Seoul National University

Granite is one of the major rock types in South Korea, and its weathered layers including residual soil, and weathered granite from highly to completely weathered grades are thickly developed. Since the weathered granites are used as a bearing stratum of various structures, such as roads, bridges, and tunnels, it is important to evaluate the geotechnical properties of the weathered granite for securing the performance and safety of the structures.

Focusing on the effects of weathering on geotechnical properties of rocks, previous researchers tried to accurately evaluate the geotechnical properties of rocks investigating the changes in the geotechnical properties of rocks with degree of weathering. To quantitatively evaluate the degree of weathering, various weathering indices have been proposed based on the petrographic characteristics, engineering characteristics, and chemical characteristics. The correlations between such weathering indices and geotechnical properties of rocks have been extensively studied. However, most of the previous studies dealt with the geotechnical properties in the weathering grades from fresh rock to moderately weathered rocks. Moreover, the previously suggested relationships, presenting simple correlations between weathering indices and



geotechnical properties, have limitations in that the site-specific characterization is not considered even though the geotechnical properties of highly and completely weathered rocks are assumed to follow the relationship between the degree of weathering and the change of the geotechnical properties.

In most cases, it is difficult to evaluate reliable geotechnical properties such as stiffness and strength parameters of the highly and completely weathered granite because it tends to be easily fractured during sampling or retrieving due to its weathered nature and thus is not suitable for lab tests unlike the slightly or moderately weathered ones. Furthermore, field tests are often not suitable due to the limitation of the field test itself or high cost for the highly and completely weathered soils. Standard penetration test (SPT) widely used for investigating soil properties, often cannot provide reliable N value due to the insufficient penetrability for the highly and completely weathered granite and pressuremeter test (PMT) is rarely performed due to the high cost and time-consuming procedures even though it can provide reliable stiffness values. Therefore, the research to quantitatively evaluate the geotechnical properties of highly and completely weathered rocks has rarely performed and the geotechnical properties of highly and completely weathered rock are still vague. Therefore, this dissertation analyzed geotechnical properties of highly and completely weathered granite with the degree of weathering and proposed a new method to estimate the geotechnical properties of a highly and completely weathered granite considering not only the degree of weathering but also the site-specific characteristics.

In this study, several *in situ* tests and laboratory tests were conducted to measure the geotechnical properties of highly and completely weathered granite at three test sites, and geochemical analysis using X-ray fluorescence for retrieved samples were performed to measure the chemical weathering indices. The distribution of the geotechnical properties, resulted from each *in situ* tests and laboratory tests, were evaluated, which showed a general increasing tendency with a local decrease of the degree of weathering.

Thus, an estimation method was newly proposed using the chemical weathering indices with a consideration of site-specific characteristics of weathered granite. The newly proposed method estimates the geotechnical properties of highly and completely weathered granite based on those of

residual soil and moderately weathered granite applying the degree of weathering concept. From the test sites, the acquired geotechnical properties and chemical weathering indices were applied to the new estimation method to validate the method and find out the fitting constant of each geotechnical properties defining the relationship between the geotechnical properties and the chemical weathering indices. As a result, the new method showed a strong correlation in most of geotechnical properties, and especially very strong correlations in the pressuremeter modulus and maximum shear modulus.

The results of this thesis can be utilized for the simple and reliable estimation of the geotechnical properties of highly and completely weathered granite based on the measured chemical weathering indices and geotechnical properties from residual soil to moderately weathered granite. With additional researches using more data, it is expected that the more reliable estimation model can be acquired and utilized for economical evaluation of the geotechnical properties of highly and completely weathered granite.

**Keywords:** Site investigation, Geotechnical properties, Weathering, Chemical weathering index, Weathered granite

**Student Number:** 2015-30281

# Contents

<b>Chapter 1. Introduction.....</b>	<b>1</b>
1.1 Research Background .....	1
1.2 Objective and Scope of Research.....	7
1.3 Organization and Structure .....	8
 <b>Chapter 2. Literature review.....</b>	 <b>10</b>
2.1 Introduction.....	10
2.2 Weathering Process and Weathering Indices.....	11
2.2.1 Weathering Processes.....	11
2.2.2 Weathering Indices.....	18
2.3 Relationship between Geotechnical Properties and Chemical Weathering Indices.....	26
2.4 Classifications of Highly and Completely Weathered Rock ...	31
 <b>Chapter 3. Experiment and Analysis Procedure .....</b>	 <b>36</b>
3.1 Introduction.....	36
3.2 Site Investigation .....	37
3.2.1 Test Sites .....	37
3.2.2 <i>In Situ</i> Test.....	40
3.2.3 Sampling Method .....	53
3.3 Laboratory Test .....	55
3.4 Geochemical Analysis.....	56
3.5 Estimation Method of Geotechnical Property .....	57

<b>Chapter 4. Experiment Results and Discussion .....</b>	<b>60</b>
4.1 Introduction.....	60
4.2 Geotechnical Properties Measured by <i>In Situ</i> Testing.....	61
4.2.1 Pressuremeter Test Results ( $E_m$ , $E_{ur}$ , $P_L$ ).....	61
4.2.2 Geophysical Test Results ( $\gamma_t$ , $V_p$ , $V_s$ , $G_{max}$ ).....	65
4.3 Geotechnical Properties Measured by Lab. Testing.....	71
4.3.1 Unconfined Compressive Strength ( $q_u$ ) .....	71
4.3.2 Shear Strength Parameters ( $c$ and $\phi$ ) .....	75
4.4 Geochemical Analysis Results .....	85
4.4.1 Major Oxide Composition .....	85
4.4.2 Chemical Weathering Indices .....	92
4.5 Discussion of Geotechnical Properties.....	104
4.5.1 Comparative study .....	104
4.5.2 Soil – Rock Transition State .....	110
 <b>Chapter 5. Proposed Method for Estimating Geotechnical Properties.....</b>	 <b>121</b>
5.1 Correlation Analysis .....	121
5.2 Prediction of Geotechnical Property .....	132
5.3 Application of the Proposed method .....	141
 <b>Chapter 6. Conclusions and Recommendations .....</b>	 <b>143</b>
 <b>List of References .....</b>	 <b>147</b>

## List of Tables

Table 1-1 The classification of weathering grades based on field tests and observations (Ulsay and Hudson, 2007).....	4
Table 2-1 Some processes of physical weathering (Blyth and Freitas, 2017)	13
Table 2-2 Some processes of chemical weathering (Blyth and Freitas, 2017)	17
Table 2-3 Summary of chemical weathering indices evaluated in this study .	25
Table 2-4 Classification of weathered granite in Hong Kong in terms of dry density (Irfan, 1996).....	27
Table 2-5 Empirical equations for predicting uniaxial compressive strength (Arel and Tugrul, 2001) .....	28
Table 2-6 Classification of rock with respect to strength (after Marinos and Hoek, 2001).....	32
Table 2-7 Classification of weathered rock (Seoul, 2006) .....	33
Table 2-8 Classification of weathered rock (Korean Express Corporation,2009) .....	34
Table 2-9 Classification of weathered rock (Korean Geotechnical Society, 2009) .....	34
Table 2-10 Classification of weathered rock (Korea Rail Network Authority, 2011).....	35
Table 4-1 PMT results: $E_m$ , $E_{ur}$ , $P_L$ .....	64

Table 4-2 Normalized mean value of the PMT results .....	65
Table 4-3 Geophysical test results: $\gamma_t$ , $V_p$ , $V_s$ , $G_{max}$ .....	69
Table 4-4 Normalized mean value of the geophysical test results .....	70
Table 4-5 Average unconfined compressive strength measured by uniaxial compressive test, point load test and estimated by SPT- $N_{60}$ .....	74
Table 4-6 Normalized mean value of average unconfined compressive strength .....	74
Table 4-7 Shear strength parameters measured by triaxial test .....	75
Table 4-8 Range of the shear strength parameters in previous studies .....	79
Table 4-9 Equivalent friction angle evaluated using limit pressure .....	84
Table 4-10 Normalized mean value of average unconfined compressive strength .....	84
Table 4-11 Weight percentage of major oxide measured by XRF (G site) .....	89
Table 4-12 Weight percentage of major oxide measured by XRF (S site).....	90
Table 4-13 Weight percentage of major oxide measured by XRF (A site) .....	91
Table 4-14 Chemical weathering indices (G site) .....	101
Table 4-15 Chemical weathering indices (S site) .....	102
Table 4-16 Chemical weathering indices (A site).....	103
Table 4-17 Relationship between SPT-N and friction angle of sand (Terzaghi and Peck, 1948).....	109
Table 4-18 Empirical equations of $E_m$ . ....	114
Table 4-19 Empirical equations of $\phi$ .....	114

Table 4-20 Empirical equations of $V_S$ .....	114
Table 4-21 Empirical equations of $E_m$ .....	118
Table 4-22 Empirical equations of $\phi$ .....	118
Table 4-23 Estimated $E_m$ .....	120
Table 4-24 Estimated $\phi$ .....	120
Table 5-1 Relationship between the property ratio and the weathering index ratio ( $R_P = (R_W)^k$ ) .....	131

## List of Figures

Figure 1-1 Weathering profile of granite (Shirlaw et al., 2000).....	1
Figure 1-2 Highly and completely weathered granite piece .....	2
Figure 1-3 Highly and completely weathered granite sample.....	3
Figure 2-1 Diagrammatic representation of a rock weathering. An increase in the surface area of rock will increase the rate at which it is weathered (Lech and Trewin, 2013). .....	12
Figure 2-2 Suggested relative importance of various types of weathering (Peltier, 1950).....	15
Figure 2-3 Variation in chemical composition of Hong Kong granite with weathering (Irfan, 1996). .....	16
Figure 2-4 Schematic diagram describing a relationship between weathering and geotechnical properties of rock materials .....	19
Figure 2-5 Typical process of calculating chemical weathering indices.....	20
Figure 2-6 Mobiles index versus dry density (Irfan, 1996).....	27
Figure 2-7 Relationship between uniaxial compressive strength and loss on ignition (Arel and Tugrul, 2001).....	28
Figure 2-8 Variation of various indices with dry density .....	30
Figure 3-1 Schematic diagram of research procedure.....	36
Figure 3-2 Location of each test site: G site, S site, A site.....	38



Figure 3-3 Subsurface information with <i>in situ</i> tests and sampling depth.....	39
Figure 3-4 Elastometer-2 test apparatus set made by Oyo Corp.....	43
Figure 3-5 Interpretation of PMT curve: (a) pressuremeter modulus and unloading-reloading modulus; (b) limit pressure .....	44
Figure 3-6 Test procedure of pressuremeter test.....	45
Figure 3-7 Density logging test device set made by Robertson Geo. Corp. ...	47
Figure 3-8 Z/A ratio versus atomic number (Lacerda, 2010).....	47
Figure 3-9 Test procedure of density logging.....	48
Figure 3-10 Downhole seismic test device set .....	51
Figure 3-11 Test procedure of downhole seismic test .....	52
Figure 3-12 Schematic diagram of triple core barrel and retrieved sample ....	54
Figure 3-13 The procedure of direct shear test for pseudo highly and completely weathered granite .....	56
Figure 3-14 Concept of the estimation method of geotechnical properties of highly and completely weathered granite .....	59
Figure 3-15 Procedure of estimating geotechnical properties of highly and completely weathered granite using chemical weathering indices .....	59
Figure 4-1 Distribution of PMT results ( $E_m$ ; $E_{ur}$ ; $P_L$ ) at each site: (a) G site; (b) S site; (c) A site .....	62
Figure 4-2 Distribution of geophysical test results ( $\gamma_t$ , $V_p$ , $V_s$ ) at each site: (a) G site; (b) S site; (c) A site .....	67
Figure 4-3 Distribution of $G_{max}$ at each site: (a) G site; (b) S site; (c) A site ..	68

Figure 4-4 Correlation between unconfined compressive strengths and penetration resistance of weak rock (Gannon et al., 1999). ....	71
Figure 4-5 Distribution of unconfined compressive strength results ( $q_u$ ) at each site: (a) G site; (b) S site; (c) A site.....	72
Figure 4-6 Failure envelopes for granite weathered to varying degree (Baynes and Dearman, 1978).....	76
Figure 4-7 A simple model to illustrate the microfabric consequences (Baynes and Dearman, 1978).....	77
Figure 4-8 Mohr-Coulomb failure envelope of pseudo highly and completely weathered granite .....	78
Figure 4-9 Distribution of cohesions suggested in the previous studies.....	80
Figure 4-10 Distribution of the equivalent friction angle at each site: (a) G site; (b) S site; (c) A site.....	81
Figure 4-11 Comparison of the equivalent friction angles with the friction angles in previous studies .....	83
Figure 4-12 Distribution of the weight percentage of the alkalis and alkaline oxides with weathering grade: (a) used in VR, (b) used in CIA and $I_{mob}$ , (c) used in MWPI .....	86
Figure 4-13 Distribution of the weight percentage of LOI, sesquioxides, and $SiO_2$ with weathering grade: (a) used in LOI, (b) used in CWI, (c) used in PI and RR .....	88
Figure 4-14 Distribution of the chemical weathering indices evaluated at G site	

.....	94
Figure 4-15 Distribution of the chemical weathering indices evaluated at S site	
.....	95
Figure 4-16 Distribution of the chemical weathering indices evaluated at A site	
.....	96
Figure 4-17 Distribution of the chemical weathering indices with weathering grade : (a) VR, (b) CIA, (c) $I_{mob}$ , (d) MWPI.....	98
Figure 4-18 Distribution of the chemical weathering indices with weathering grade : (a) LOI, (b) PI, (c) RR, (d) CWI.....	100
Figure 4-19 Comparison of pressuremeter modulus ( $E_m$ ).....	105
Figure 4-20 Comparison of unit weight ( $\gamma_t$ ).....	106
Figure 4-21 Comparison of P-wave velocity ( $V_p$ ).....	106
Figure 4-22 Comparison of S-wave velocity ( $V_s$ ).....	107
Figure 4-23 Comparison of unconfined compressive strength ( $q_u$ ) .....	108
Figure 4-24 Comparison of equivalent friction angle ( $\phi_{equi.}$ ) .....	108
Figure 4-25 Distribution both $E_m$ and $\sigma_v'$ : (a) G site; (b) S site; (c) A site....	111
Figure 4-26 Relationship between geotechnical properties and SPT $N$ : (a) $E_m$ ; (b) $\phi$ ; (c) $V_s$ .....	116
Figure 4-27 Chart for determining GSI (Hoek and Brown, 1997).....	119
Figure 5-1 The relationship between the property ratio ( $R_p$ ) and the weathering index ratio ( $R_w$ ) based on VR.....	124
Figure 5-2 The relationship between the property ratio ( $R_p$ ) and the weathering	

index ratio ( $R_w$ ) based on CIA .....	126
Figure 5-3 The relationship between the property ratio ( $R_p$ ) and the weathering	
index ratio ( $R_w$ ) based on $I_{mob}$ .....	128
Figure 5-4 The relationship between the property ratio ( $R_p$ ) and the weathering	
index ratio ( $R_w$ ) based on MWPI .....	130
Figure 5-5 Comparison the predicted and measured $E_m$ : (a) Plot of predicted $E_m$	
– measured $E_m$ ; (b) Histogram of predicted $E_m$ / measured $E_m$ .....	134
Figure 5-6 Comparison the predicted and measured $G_{max}$ : (a) Plot of predicted	
$G_{max}$ – measured $G_{max}$ ; (b) Histogram of predicted $G_{max}$ / measured $G_{max}$	
.....	135
Figure 5-7 Comparison the predicted and measured geotechnical properties: $E_{ur}$ ,	
$P_L$ , $V_s$ , and $q_u$ .....	137
Figure 5-8 Histogram of predicted properties / measured properties: $E_{ur}$ , $P_L$ , $V_s$ ,	
and $q_u$ .....	138
Figure 5-9 Comparison the predicted and measured geotechnical properties: $\gamma_t$ ,	
$\phi$ , and $V_p$ .....	139
Figure 5-10 Histogram of predicted properties / measured properties: $\gamma_t$ , $\phi$ , and	
$V_p$ .....	140
Figure 5-11 Procedure for determining fitting constant $k$ (other types of rock)	
.....	142
Figure 5-12 Application of $k$ for HW and CW granite.....	142

# Chapter 1. Introduction

## 1.1 Research Background

Granite is a representative rock type that accounts for approximately 35% of the geological strata in South Korea, and its weathered zones from highly weathered granite to residual soil were often thickly developed (Lee, 1993). In particular, thick layers of highly and completely weathered granites lying between moderately weathered granites and residual soil are usually used as the bearing stratum in geotechnical structures (Figure 1-1). Therefore, it is crucial to evaluate the geotechnical properties of highly and completely weathered granites.

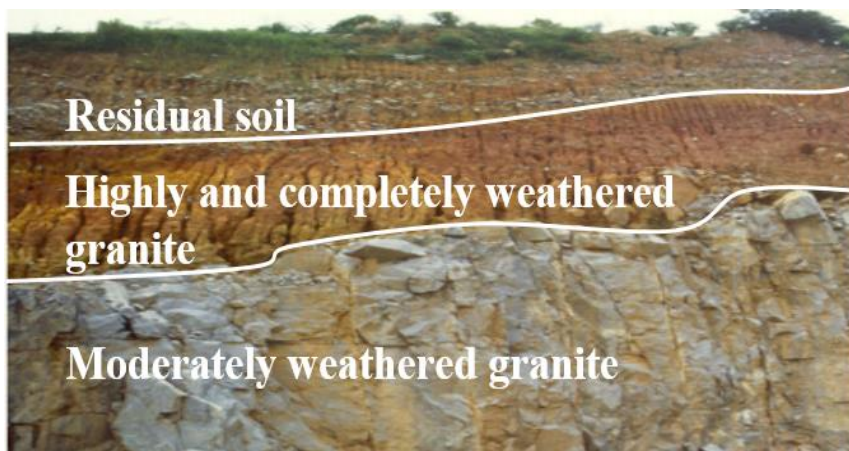


Figure 1-1 Weathering profile of granite (Shirlaw et al., 2000)

Highly and completely weathered rock are IV and V grade in the weathering classification suggested by the International Society of Rock Mechanics and Rock Engineering (Table 1-1) (Ulsay and Hudson, 2007). The highly and completely weathered granite shows typical visible characteristics. The color is intensively changed from white grey to reddish-brown, grains which consist of the weathered granite are visible to the naked eye and the rock pieces are easily breakable by hands (Figure 1-2 and Figure 1-3). The geotechnical properties of rock materials are dependent on the characteristics of both intact rock and discontinuity, however, the influence of discontinuity is greatly reduced in the highly and completely weathered rock and both the mineralogy and fabric of the rock control the geotechnical properties (Irfan, 1996).



Figure 1-2 Highly and completely weathered granite piece



Figure 1-3 Highly and completely weathered granite sample

Some critical issues for highly and completely weathered rock have been raised in the engineering field (Kanji, 2014). First of all, the weathered rock shows undesirable behaviors, such as low strength, disaggregation and crumbling. Secondly, they have intermediate strength between soil and hard rock, which indicates that they are too soft or too hard to be tested in conventional rock or soil test equipment. The third type of problem is sampling and site investigation. The samples retrieved using rotary drilling with triple core barrel which rarely affects the sample disturbance are usually destroyed so they are not suitable for a laboratory test. Also, standard penetration test N value (SPT-N value) is usually much greater than 50, because the penetrability of split spoon sampler is insufficient, which implies that the geotechnical properties of the weathered rock estimated by using SPT are unreliable.

Table 1-1 The classification of weathering grades based on field tests and observations (Ulsay and Hudson, 2007)

Weathering grade	Description
Slightly weathered (II)	Discoloration indicates weathering of rock materials and discontinuity surfaces. Fresh appearance is not still visible. A sharp sound upon hammer blow
Moderately weathered (III)	The rock material is slightly decomposed, but totally discolored, thus no original color is there. The rock is present as a continuous framework. A dull sound upon hammer blow, but not easy to break.
Highly weathered (IV)	Most of the rock material is decomposed with intense discoloration. Discolored rock is present either as a continuous framework or as coarse stones. All grains are visible to naked eye. The rock mass can be broken by hand in water. Even fine grains are visible to naked eye.
Completely weathered (V)	All rock material is decomposed and the original mass structure is still largely intact or with preserved rock texture, the foliation is still defined by biotite grains. Most grains are within the rock aggregate. Mineral grains are visible to naked eye especially graphite. The rock mass can be crumbled with fingers.



*In-situ* tests are usually performed to estimate the geotechnical properties of the highly and completely weathered rock because suitable specimens to laboratory tests are rarely retrieved, as mentioned above. The representative *in-situ* tests available to the weathered rock are SPT, pressuremeter test (PMT) and borehole geophysical tests such as density logging and seismic downhole logging. As mentioned above, the geotechnical properties estimated by SPT are less reliable, on the other hand, PMT and borehole geophysical tests have good applicability and can reliably evaluate the properties. In practical terms, however, the PMT and borehole geophysical tests are limitedly conducted or omitted because of their high cost and time-consuming procedure.

Due to the above-mentioned limitations of laboratory tests and *in-situ* tests, many researchers have focused on the changes in the geotechnical properties of rocks with weathering. To quantitatively evaluate weathering, they have proposed weathering indices based on the analysis of petrographic characteristics (Irfan and Dearman, 1978; Onodera et al., 1974), engineering characteristics (Franklin and Chandra, 1972; Hamrol, 1961; Iliev, 1966), and chemical characteristics (Irfan, 1996; Nesbitt et al., 1982; Reiche, 1943; Ruxton, 1968; Sueoka, 1988; Sueoka et al., 1985; Vogel, 1975; Vogt, 1927). The correlations between such weathering indices and geotechnical properties of rocks (e.g., dry density, uniaxial compressive strength (UCS), point load strength, and tensile strength) have been extensively studied (Chiu and Ng, 2014; Kim and Park, 2003; Rigopoulos et al., 2015; Udagedara et al., 2017). Chiu and Ng (2014) reported that weathering potential index (WPI), loss on ignition (LOI) and mobile index ( $I_{mob}$ ) had a linear relationship with a dry

density of highly weathered and completely weathered granite in Hong Kong. Kim and Park (2003) evaluated the change of geotechnical properties and chemical weathering indices of artificially weathered granite, they found that LOI and modified weathering potential index (MWPI) had a relatively good correlation with dry density and uniaxial compressive strength, respectively. Also, Udagedara et al. (2017) investigated the change of a bulk density and point load strength of gneiss with a number of chemical weathering indices. Rigopoulos et al. (2015) found that WPI and LOI showed the best correlation with geotechnical parameters of ultramafic and mafic rocks, respectively. However, most previous relevant studies dealt with the geotechnical properties in the weathering grades from fresh rock to moderately weathered rock (see Table 1-1), so that research on highly and completely weathered rocks, which are difficult to retrieve rock core sample, is rather lacking. Moreover, they had the limitation of not considering site-specific characteristics, which affect the geotechnical properties of rocks, by presenting simple correlations between weathering indices and geotechnical properties. To overcome the limitations of previous researches, this dissertation explores and proposes a new method to estimate the geotechnical properties of a highly and completely weathered granite.

## 1.2 Objective and Scope of Research

The main objective of this dissertation is to estimate the geotechnical properties of the highly and completely weathered granite using chemical weathering indices. Particular attention was given to the investigation of the relationship between the geotechnical properties and the chemical weathering indices, suggesting the estimation method considering both the degree of weathering and site-specific characteristics.

A series of *in-situ* tests were performed on three different test sites where thick granite weathered zones have developed, and laboratory tests and X-ray Fluorescence (XRF) were also performed on the retrieved samples to obtain the geotechnical properties and the chemical weathering indices. The distribution of geotechnical properties of highly and completely weathered granite and chemical weathering indices was analyzed with depth at each test site. Also, the suitable chemical weathering indices that well represent the degree of weathering of the granite in all of the test sites were investigated. After then, particular attention was given to the development of a new geotechnical properties estimation method that could consider the degree of weathering and site-specific characteristics using *in-situ* and laboratory test results and chemical weathering indices. Then, applicability of the proposed estimation method was evaluated by comparing the predicted geotechnical property values with the measured test results.

### 1.3 Organization and Structure

This dissertation lays out a basic framework to investigate the estimation method of highly and completely weathered granite using chemical weathering indices based on in-situ and laboratory tests, and it is structured in the following manner.

A comprehensive literature review on the relationship between weathering indices and geotechnical properties of rock is presented in Chapter 2. Weathering process of rock and weathering indices are outlined, and the result of several case studies about the relationship between chemical weathering indices and geotechnical properties of the rock are reviewed with an analysis of the weakness of previous researches.

Chapter 3 introduces *in-situ* and laboratory tests performed in this study. Site investigation, which is performed in this study, including the sampling method, the *in-situ* and laboratory tests are firstly described. And then, geochemical analysis to evaluate the chemical weathering indices are presented. Finally, the concept of how to develop the new estimation method of geotechnical properties is given in detail.

In Chapter 4, the results including both geotechnical properties and chemical weathering indices are presented; all of the *in-situ* and laboratory test results are analyzed to characterize the highly and completely weathered granite, and geochemical analysis results for evaluating the main chemical composition of the weathered granite, also, are described. The manuscript in Chapter 4 was submitted to “*Bulletin of Engineering Geology and the Environmental*,” and is

under review at the time this dissertation is submitted.

In Chapter 5, the newly proposed method to estimate the geotechnical properties of the weathered granite using the chemical weathering indices are applied to the test results and derived the fitting constants defining the relationship between geotechnical properties of highly and completely weathered rock and chemical weathering indices.

The conclusions and recommendations of this dissertation are presented in Chapter 6.

## **Chapter 2. Literature review**

### **2.1 Introduction**

In this research, the variation of rock properties with weathering was the main issue developing a new estimation method of geotechnical properties of highly and completely weathered granite. Therefore, understanding of both a weathering process and how to quantitatively evaluate the weathering is needed.

Weathering process according to their mechanisms were briefly reviewed and weathering indices which are quantitative values that evaluate the degree of weathering were presented in section 2 of this chapter. After that, several previous researches about the relationship between geotechnical properties of rock and weathering indices were summarized and suggested with their limitations in section 3.

Also, it is important that classifying the subsurface layer such as residual soil, highly and completely weathered rock, and moderately weathered rock. So the previously suggested classifications were described in the last section.

## **2.2 Weathering Process and Weathering Indices**

### **2.2.1 Weathering Processes**

Weathering is the breakdown and alteration of minerals near the earth's surface to products that are more in equilibrium under newly imposed physico-chemical conditions (Ollier, 1984). In other words, rocks were formed at high pressure and temperature, and the change of the surrounding environmental condition, such as low pressure, low temperature, water, and air, etc., resulted in weathering. The weathering process is subdivided into three types according to their mechanisms as follows.

#### *Physical weathering*

Physical weathering involves the disintegration of rocks and minerals by mechanical processes. Such processes break down the materials into smaller portions without change of chemical composition. Table 2-1 shows the most common processes resulted in the physical weathering of rocks. Boundaries of the grains which composed rocks are gradually opening resulting in microfractures when rock material undergoes physical weathering. Once the microfractures are developed, their length and thickness are more and more extended to be recognizable with the naked eye, but for the clear observation to quantify the characteristics of the microfractures the use of a microscope is needed.

Physical weathering originally does not include the chemical change, as

mentioned before, but, rocks with increased numbers of joints and fractures resulted from physical weathering are weathered more quickly than a solid mass of rock with the same dimensions. This is because the internal surface of the rock is accessible to water and air, as described in Figure 2-1 Diagrammatic representation of a rock weathering. An increase in the surface area of rock will increase the rate at which it is weathered (Lech and Trewin, 2013). Real rocks in nature will be weathered as the shape of spheroids, because weathering agents can be contacted with the corners (in Figure 2-1) from two sides, but the cube faces are attacked only one side, which results in a more quick weathering on the corners of the cube.

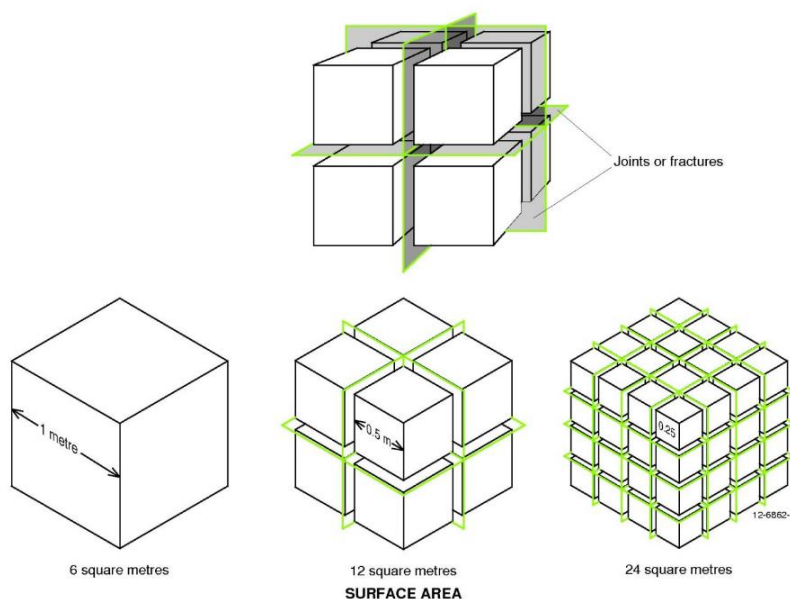


Figure 2-1 Diagrammatic representation of a rock weathering. An increase in the surface area of rock will increase the rate at which it is weathered (Lech and



Trewin, 2013).

Table 2-1 Some processes of physical weathering (Blyth and Freitas, 2017)

Process	Description
Mechanical unloading	Vertical expansion due to the reduction of vertical load by erosion. This will open existing fractures and may permit the creation of new fractures.
Mechanical loading	Impact on rock, and abrasion, by sand and silt size wind borne particles in deserts. Impact on soil and weak rocks by rain drops during intense rainfall storms.
Thermal loading	Expansion by the freezing of water in pores and fractures in cold regions, or by the heating of rocks in hot regions. Contraction by the cooling of rocks and soils in cold regions.
Wetting and drying	Expansion and contraction associated with the repeated absorption and loss of water molecules from mineral surface and structures
Crystallization	Expansion of pores and fissures by crystallization within them of minerals that were originally in solution. Note: expansion is only severe when crystallization occurs within a confined space.
Pneumatic loading	The repeated loading by waves of air trapped at the head of fractures exposed in the wave zone of a sea cliff.

### *Chemical weathering*

Chemical weathering involves the breakdown of rocks and minerals through changes in the chemical composition of the material. These changes are predominantly the result of interactions with air and water and chemical compounds contained within them (Lech and Trewin, 2013). Table 2-2 shows the most common processes resulted in the chemical weathering of rocks.

Climatic conditions, particularly temperature and rainfall, are the main factors that affect the chemical weathering. Chemical reaction resulting in weathering of rocks occurs when the high temperature and humid condition. Figure 2-2, Peltier's diagram shows the relationship between mean annual rainfall and temperature in determining the intensity of chemical weathering (Peltier, 1950). This concept is useful for preliminary assessment of likely weathering conditions wherever climatic characteristics are known. For example, applying the average annual rainfall (57 inches) and temperature (55 °F) of Seoul from 1981 to 2010, which have been investigated by Statistics Korea, to the Peltier's diagram, strong chemical weathering condition is derived.

The concentration of major oxide in the rock materials starts to be changed by chemical weathering especially from the weathering grade of highly weathered. As shown in Figure 2-3, alkali and alkaline oxides such as  $K_2O$ ,  $Na_2O$ ,  $CaO$ , and  $MgO$  show dramatically decreasing trend in highly and completely weathered condition (Irfan, 1996). These variations of the chemical

composition of rock materials are applied to chemical weathering indices that quantitatively estimate the degree of weathering. The chemical weathering indices are described in detail in the following section.

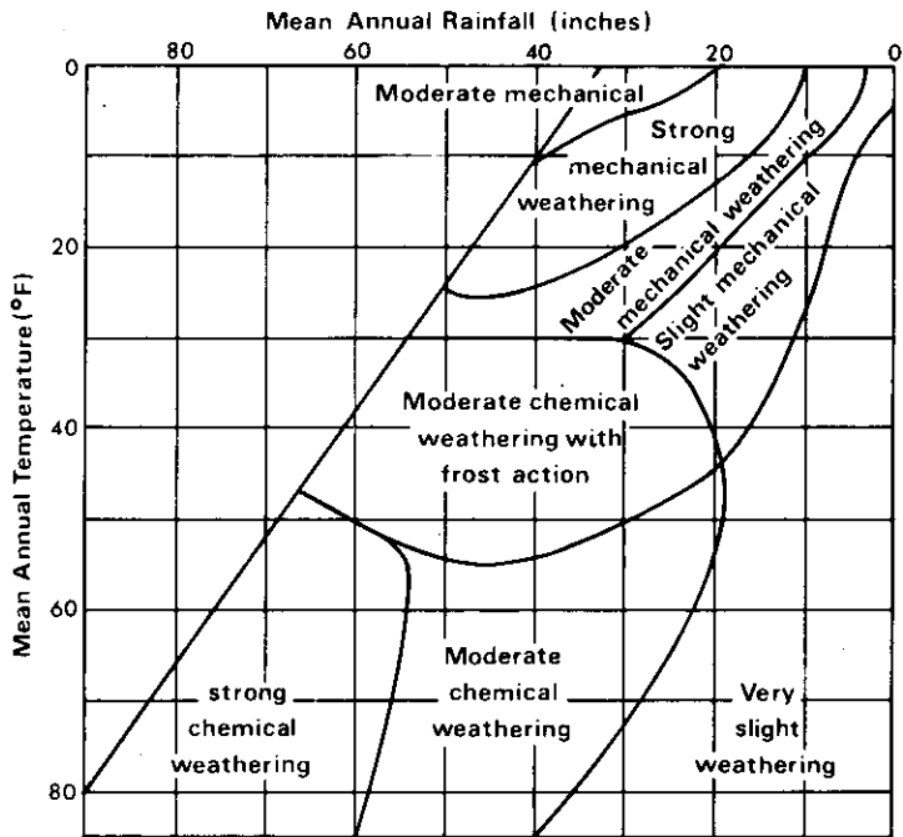


Figure 2-2 Suggested relative importance of various types of weathering (Peltier, 1950).

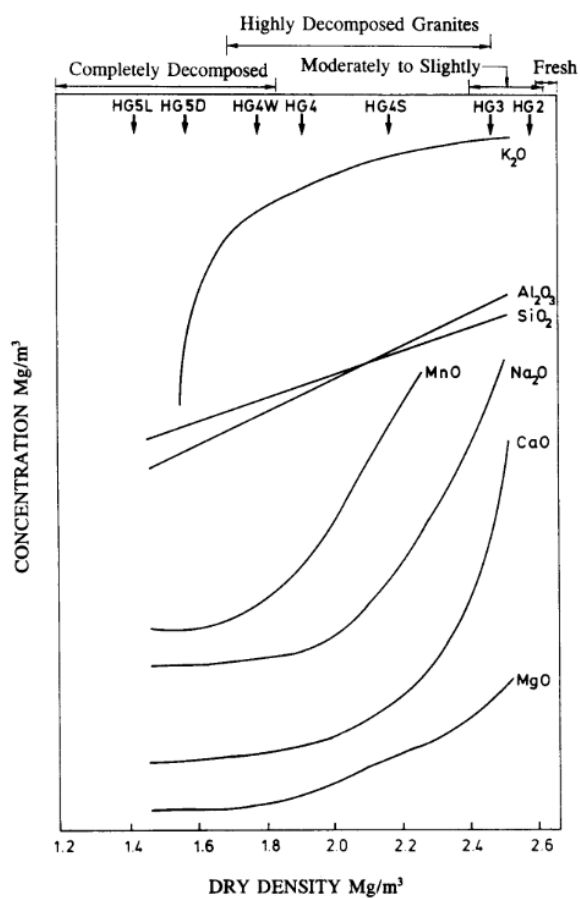


Figure 2-3 Variation in chemical composition of Hong Kong granite with weathering (Irfan, 1996).

Table 2-2 Some processes of chemical weathering (Blyth and Freitas, 2017)

Process	Description
Solution	Dissociation of minerals into ions, greatly aided by the presence of CO <sub>2</sub> in the soil profile, which forms carbonic acid (H <sub>2</sub> CO <sub>3</sub> ) with percolating rainwater.
Oxidation	The combination of oxygen with a mineral to form oxides and hydroxides or any other reaction in which the oxidation number of the oxidized elements is increased.
Reduction	The release of oxygen from a mineral to its surrounding environment: ions leave the mineral structure as the oxidation number of the reduced elements is decreased.
Hydration	Absorption of water molecules into the mineral structure. Note: this normally results in expansion, some clays expand as much as 60 %, and by admitting water hasten the processes of solution, oxidation, reduction and hydrolysis.
Hydrolysis	Hydrogen ions in percolating water replace mineral cations: no oxidation-reduction occurs.
Leaching	The migration of ions produced by the above processes. Note: the mobility of ions depends upon their ionic potential: Ca, Mg, Na, K are easily leached by moving water, Fe is more resistant. Si is difficult to leach and Al is almost immobile.

Cation exchange	Absorption onto the surface of negatively charged clay of positively charged cation in solution, especially Ca, H, K, Mg.
--------------------	---

### 2.2.2 Weathering Indices

Weathering indices are defined as quantitative values describing the degree of weathering. Weathering is a natural phenomenon that results in breakdown and alteration of minerals composed on rock materials, and it was already known that geotechnical properties of the rock, such as strength, density, stiffness, and porosity, change when fresh rock is transferred to residual soil by weathering (Figure 2-4). However, it was needed how to quantitatively evaluate the weathering in an engineering field to establish the relationship between the geotechnical properties and the weathering. With this background, many researchers have developed a variety of weathering indices using quantitative characteristics of rock shown in the weathering process.

Weathering indices are divided into three types with the quantitative characteristics used to evaluate the degree of weathering: petrographic weathering indices; physical weathering indices; chemical weathering indices. The petrographic and physical weathering indices, which need undisturbed rock samples, are not covered in this paper, because the useful samples of highly and completely weathered rock are rarely retrieved. In this section, chemical weathering indices including the principal assumption and several chemical weathering indices suggested by previous researches are to be described.

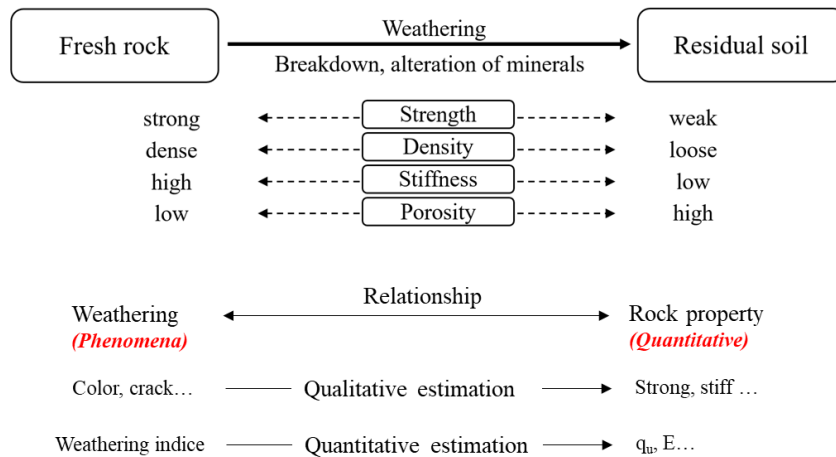


Figure 2-4 Schematic diagram describing a relationship between weathering and geotechnical properties of rock materials

Chemical weathering indices are commonly used for characterizing weathering profiles. The indices are typically applied to investigate how much the parent rock is weathered by plotting the specific chemical weathering index versus depth, which provides a visual change of the index with increasing or decreasing.

Chemical weathering indices have been developed using the mobility of chemical elements with weathering, some assumptions applied to develop the indices are as follows: (1) certain major oxides, including  $Al_2O_3$ ,  $Fe_2O_3$ , and  $TiO_2$ , considered as ‘immobile’, remain constant; (2)  $SiO_2$ ,  $Na_2O$ ,  $K_2O$ ,  $CaO$ , and  $MgO$  considered as ‘mobile’, decrease with weathering; (3) LOI (loss on ignition) content increases with weathering (Duzgoren-Aydin et al., 2002). These assumptions, however, are not always warranted (Duzgoren-Aydin et al.,

2002; Gardner et al., 1978; Price, 1995).

The chemical weathering indices indicating the degree of weathering conventionally have been calculated using the molecular proportions of major element oxides. The molecular proportion of each oxide is easily calculated from the percent of the oxide based on the weight percentage measured from X-ray fluorescence analysis (Figure 2-5). The representative chemical weathering indices used in this study are described as follows.

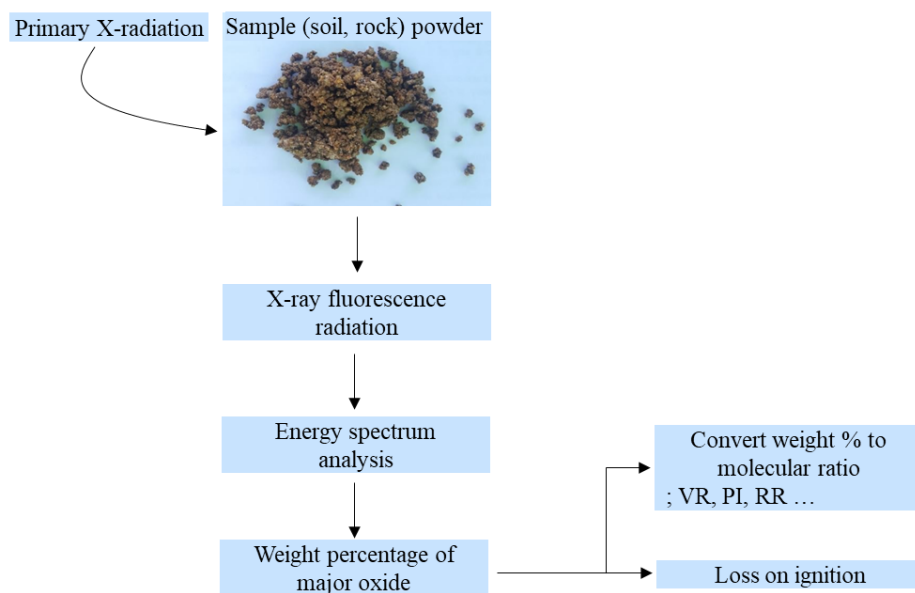


Figure 2-5 Typical process of calculating chemical weathering indices.



*Vogt's ratio (VR)* (Vogt, 1927)

Vogt's ratio was suggested based on geochemical analysis of completely weathered residual sediments (equation 2-1). Since this index treated that aluminum is immobile and other alkali and alkaline oxides are decreased with weathering, a higher value of *VR* means further weathering.

$$VR = \frac{Al_2O_3 + K_2O}{MgO + CaO + Na_2O} \quad 2-1$$

*Product index (PI)* (Reiche, 1943)

Product index was suggested based on the tendency that the ratio of  $SiO_2$  to the sum of silica and sesquioxides appears to be highly sensitive to the silica content (equation 2-2). Since this index developed based on mobility (decreasing) of  $SiO_2$  and immobility of sesquioxides, the *PI* value decreases with increasing of weathering intensity.

$$PI = \frac{SiO_2}{SiO_2 + TiO_2 + Fe_2O_3 + FeO + Al_2O_3} \quad 2-2$$

*Ruxton Ratio, (RR)* (Ruxton, 1968)

Ruxton ratio was proposed based on the result performed on igneous and metamorphic rocks from humid regions (equation 2-3). This ratio relates to silica loss and considers aluminum to be immobile during weathering, so this index has a decreasing tendency as increasing of weathering intensity.

$$RR = \frac{SiO_2}{Al_2O_3} \quad 2-3$$

*Modified weathering potential index, (MWPI)* (Vogel, 1975)

Vogel (1975) suggested this index, a modified version of the Weathering Potential Index (WPI) (Reiche 1943), where the element of water ( $H_2O$ ) was removed from WPI (equation 2-4). Since the MWPI was developed based on decreasing tendency of the mobile element such as alkali and alkaline oxides, this index has a decreasing tendency as weathering intensity increases.

$$MWPI = \frac{100 \times (K_2O + Na_2O + CaO + MgO)}{SiO_2 + Al_2O_3 + Fe_2O_3 + FeO + TiO_2 + CaO + Na_2O + MgO + K_2O} \quad 2-4$$

*Chemical index of alteration, (CIA)* (Nesbitt and Young, 1982)

Nesbitt and Young proposed the chemical index of alteration based on the investigation performed on lutites (equation 2-5). They found that feldspars were the most abundant of the reactive minerals; the degradation of feldspars was dominant during the weathering process and calcium, sodium and potassium generally were removed from the feldspars with weathering. Therefore, this index represented the proportion of aluminum to alkalis typically increasing in the more weathered condition.

$$CIA = \frac{100 \times Al_2O_3}{Al_2O_3 + CaO + Na_2O + K_2O} \quad 2-5$$

*Loss on ignition (LOI) and Chemical weathering index (CWI)* (Sueoka, 1985, 1988)

Loss on ignition is the loss in weight of samples after heating to 1000 °C, and the LOI increases with the weathering process because of the abundant secondary minerals. The chemical weathering Index (CWI) proposed based on the increasing tendency of sesquioxides and H<sub>2</sub>O (equation 2-6), so this index increases with weathering.

$$CWI = \frac{100 \times (Al_2O_3 + Fe_2O_3 + TiO_2 + LOI)}{\text{All chemical components}} \quad 2-6$$

*Mobiles index ( $I_{mob}$ )* (Irfan, 1996)

Mobiles index, which is a normalized form, was suggested based on the observation of deep granitic weathering profiles, and this index used the decreasing tendency of alkali and alkaline oxides to evaluate the degree of weathering. Since the composition of alkali and alkaline oxide decreased with weathering, the mobiles index has an increasing tendency as the intensity of weathering increases.

$$I_{mob} = \frac{I_{fresh} - I_{weathered}}{I_{fresh}}, \quad I = K_2O + Na_2O + CaO \quad 2-7$$

All of the chemical weathering indices described above are summarized in Table 2-3 and used to quantitatively evaluate the weathering in this study.

Table 2-3 Summary of chemical weathering indices evaluated in this study

Weathering Index	Weathering Index Equation	Ideal trend with weathering	Note
Vogt's Ratio, VR (Vogt, 1927)	$(Al_2O_3 + K_2O)/(MgO + CaO + Na_2O)$	↑	Molecular ratio
Product Index, PI (Reiche, 1943)	$SiO_2/(SiO_2 + TiO_2 + Fe_2O_3 + FeO + Al_2O_3)$	↓	
Ruxton Ratio, RR (Ruxton, 1968)	$SiO_2/Al_2O_3$	↓	
Modified Weathering Potential Index, MWPI (Vogel, 1975)	$100(K_2O + Na_2O + CaO + MgO)/(SiO_2 + Al_2O_3 + Fe_2O_3 + FeO + TiO_2 + CaO + Na_2O + MgO + K_2O)$	↓	
Chemical Index of Alteration, CIA (Nesbitt and Young, 1982)	$100Al_2O_3/(Al_2O_3 + CaO + Na_2O + K_2O)$	↑	
Loss on Ignition, LOI (Sueoka et al., 1985)	$H_2O$	↑	Weight %.
Chemical Weathering Index, CWI (Sueoka, 1988)	$100(Al_2O_3 + Fe_2O_3 + TiO_2 + LOI)/\text{all chemical components}$	↑	Molecular ratio
Mobles Index, $I_{mob}$ (Irfan, 1996)	$(I_{fresh} - I_{weathered})/I_{fresh}, \quad I = (K_2O + Na_2O + CaO)$	↑	

## **2.3 Relationship between Geotechnical Properties and Chemical Weathering Indices**

Weathering affects a change of geotechnical properties of rock materials, as mentioned in section 2. Therefore, lots of researches for the relationship between chemical weathering indices and geotechnical properties have been conducted. The representative case studies about the relationship are summarized as follows.

Irfan (1996) proposed various indices to characterize the degree of weathering with the engineering classification schemes of the weathered granites in Hong Kong. Mobiles index ( $I_{mob}$ ), firstly suggested in this study, was used to quantify the degree of weathering, and the relevance of some chemical weathering indices including  $I_{mob}$  to dry density was assessed, which was shown the linear relationship (Figure 2-6). A classification of weathering grades in Hong Kong granites with respect to their dry densities was also proposed based on the linear relationship between  $I_{mob}$  and dry density (Table 2-4).

Arel and Tugrul (2001) suggested relationships between various chemical weathering indices and the uniaxial strength of Cavusbasi granitic rocks in northwestern Turkey. Uniaxial compressive strength test and point load test for the granitic rocks whose weathering grades were from fresh to residual soil were conducted (point load tests were not applied to residual soil), and the relationship with chemical weathering indices analyzed using linear correlation analysis (Table 2-5). However, the samples used in this study were very limited, especially for highly and completely weathered rock.

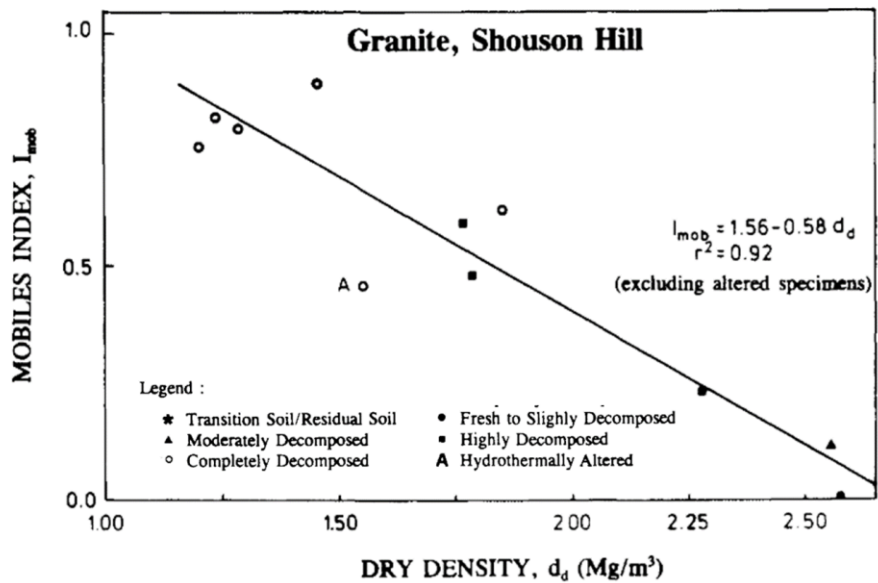


Figure 2-6 Mobiles index versus dry density (Irfan, 1996)

Table 2-4 Classification of weathered granite in Hong Kong in terms of dry density (Irfan, 1996)

Weathering grade	(subgrade) or strength	Dry density (Mg/m³)
Fresh	-	2.58 – 2.63
Slightly decomposed	-	2.55 – 2.60
Moderately decomposed	-	2.30 – 2.58
Highly decomposed	Moderately weak	2.00 – 2.40
	Very weak to weak	1.70 - 2.00
Completely decomposed	Very dense	1.60 – 1.80
	Dense	1.40 – 1.60
	Loose	1.20 – 1.40
Residual soil	-	1.25 -1.60

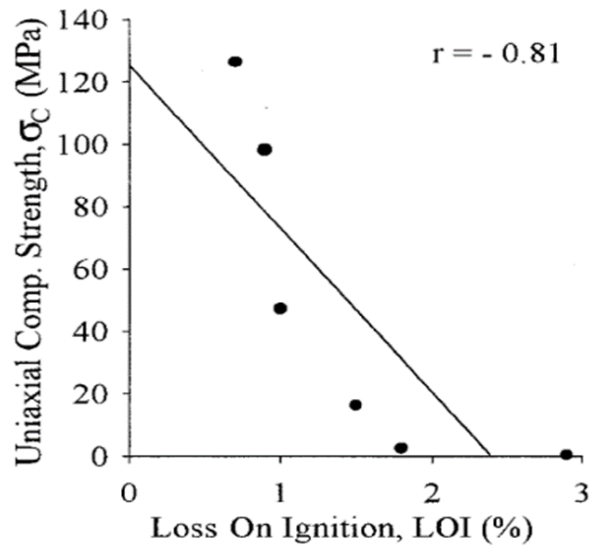


Figure 2-7 Relationship between uniaxial compressive strength and loss on ignition (Arel and Tugrul, 2001)

Table 2-5 Empirical equations for predicting uniaxial compressive strength (Arel and Tugrul, 2001)

Chemical weathering index*	Uniaxial compressive strength (MPa)	
	Equation	Correlation coefficient (r)
MWPI	$q_u = 92.4 - 1213 \text{ MWPI}$	0.71
RR	$q_u = 277 - 1851 \text{ RR}$	0.75
VR	$q_u = 810 - 818 \text{ VR}$	-0.75
CWI	$q_u = 1412 - 26 \text{ CWI}$	-0.71
CIA	$q_u = 1437 - 27.79 \text{ CIA}$	-0.71
LOI	$q_u = 125 - 52.39 \text{ LOI}$	-0.81

\* See Table 2-3



Chiu and Ng (2014) reported that weathering potential index (WPI), loss on ignition (LOI) and mobile index ( $I_{mob}$ ) had a linear relationship with a dry density of highly and completely weathered granite in Hong Kong (Figure 2-8). In addition, Kim and Park (2003) evaluated the change of geotechnical properties and chemical weathering indices of artificially weathered granite, they found that LOI and modified weathering potential index (MWPI) had a relatively good correlation with dry density and uniaxial compressive strength respectively. Also, Udagedara et al. (2017) investigated the change of a bulk density and point load strength of gneiss with a number of chemical weathering indices, and they found that chemical index of alteration (CIA) had a good correlation ( $r > 0.6$ ). Rigopoulos et al. (2015) found that weathering potential index (WPI) and loss on ignition (LOI) showed the best correlation with engineering parameters of ultramafic and mafic rocks respectively.

Most previous relevant studies mainly dealt with the geotechnical properties in the weathering grades from fresh rock to moderately weathered rock so that research on highly and completely weathered rocks is rather lacking. Moreover, the previous researches have not considered site-specific characteristics, which affect the geotechnical properties of rock, by presenting simple correlations between weathering indices and geotechnical properties.

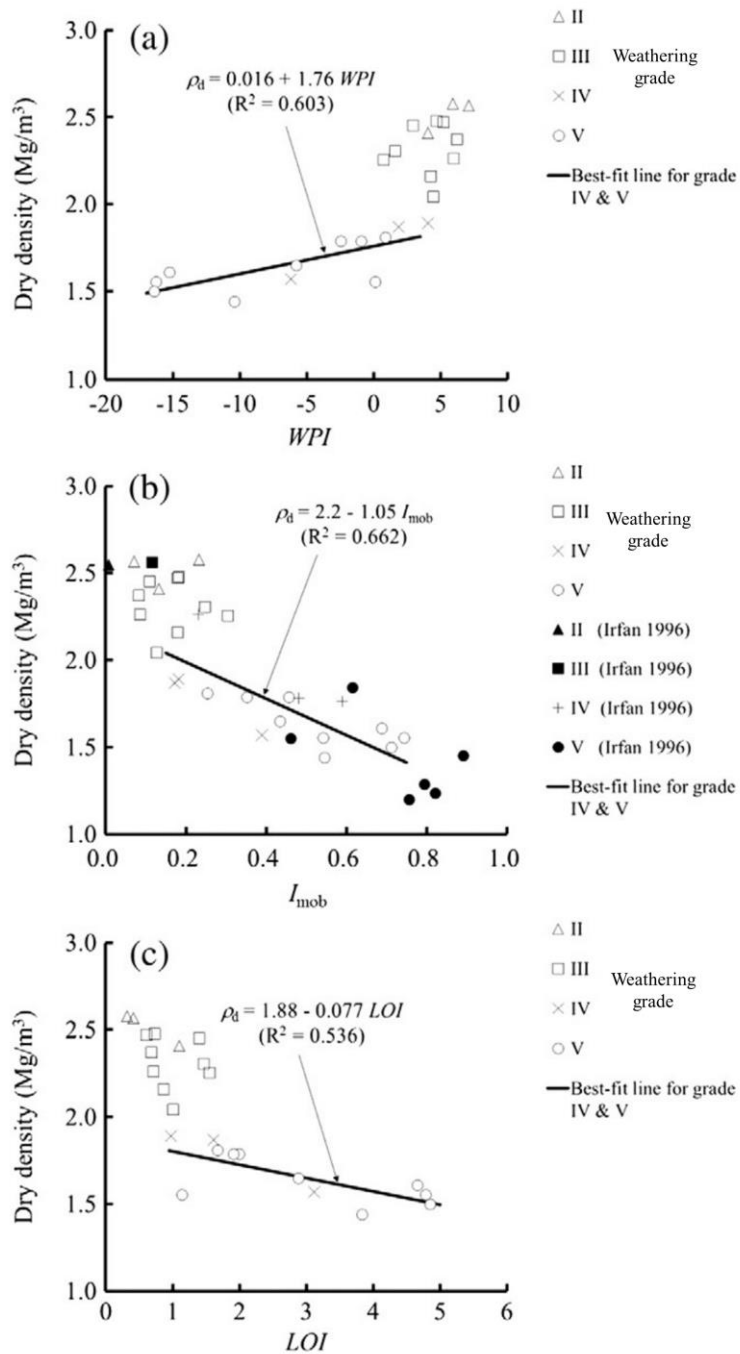


Figure 2-8 Variation of various indices with dry density

## 2.4 Classifications of Highly and Completely Weathered Rock

There are many criteria for classifying rock material. In this section, the classification criteria suggested in the various institutions are going to be described and determined the criterion applying to distinguish the subsurface into residual soil, highly and completely weathered rock, and moderately weathered rock in this study.

*Federal Highway Administration (FHWA)*

FHWA (1999) firstly suggested the IGM (Intermediate geo-material) defined as the earth materials that are transitional from soil to rock, and IGM include hard soil and weak rock such as residual soil and highly and completely weathered rock. FHWA (1999) classified the geo-material into 4 types as follows.

- 1) Cohesive soil: Clay or plastic silt with  $s_u \leq 0.25$  MPa.
- 2) Granular soil: Sand, gravel or non-plastic silt with  $SPT-N \leq 50$  blows / 30 cm
- 3) Intermediate Geo-material
  - Cohesive IGM: clay shales or mudstones with  $0.25 \text{ MPa} \leq s_u \leq 2.5$  MPa.
  - Cohesionless IGM: granular tills, granular residual soils with  $SPT-N > 50$  blows / 30 cm.

#### 4) Rock

Cohesive, cemented geo-material with  $s_u \geq 2.5$  MPa or  $q_u \geq 5.0$  MPa.

#### *International Society for Rock Mechanics (ISRM)*

ISRM classified the rock material with scale: intact rock, rock mass. The engineering characteristics of the rock material were respectively suggested about the intact rock and the discontinuity.

The intact rock was classified into 7 grade with respect to the unconfined compressive strength, and weathering grade was suggested as presented in Table 1-1. In addition, the characteristics of discontinuity (orientation, strength, spacing) were suggested.

Table 2-6 Classification of rock with respect to strength (after Marinos and Hoek, 2001)

Grade	Description	Range of $q_u^*$ (MPa)
R0	Extremely weak	0.25 – 1.0
R1	Very weak	1.0 – 5.0
R2	Weak	5.0 – 25
R3	Medium strong	25 – 50
R4	Strong	50 – 100
R5	Very strong	100 – 250
R6	Extremely strong	> 250

\*  $q_u$  is unconfined compressive strength.

Also, various institutions in Korea suggested the classification criteria as follows (Table 2-7 ~ Table 2-10). The institutions distinguished residual soil and highly and completely weathered rock with SPT-N value of 50 blows / 10 cm. However, the range of the other engineering properties of the highly weathered rock and moderately weathered rock were differently suggested, as follows.

Table 2-7 Classification of weathered rock (Seoul, 2006)

Grade	Range of engineering properties						
	$\gamma_t$ (kN/m <sup>3</sup> )	c (MPa)	$\phi$ (deg.)	$E_m$ (MPa)	$q_u$ (MPa)	RQD (%)	$V_p$ (km/s)
Highly and completely weathered	20 - 22	0.1– 0.3	30 - 35	100-200	< 10	-	1.0-2.5
Moderately weathered	23 - 25	0.3– 0.6	30 - 40	200-400	10-50	$\geq 25$	2.0-3.2

Table 2-8 Classification of weathered rock (Korean Express Corporation,2009)

Grade	Range of engineering properties		
	$q_u$ (MPa)	RQD (%)	$V_p$ (km/s)
Highly and completely weathered	25 - 60	20 - 40	2.0 – 3.5
Moderately weathered	60 - 80	20 - 40	3.5 – 4.0

Table 2-9 Classification of weathered rock (Korean Geotechnical Society, 2009)

Grade	Range of engineering properties	
	$q_u$ (MPa)	$V_p$ (km/s)
Highly and completely weathered	10 - 70	0.7 – 1.8
Moderately weathered	20 - 100	2.7 – 4.3

Table 2-10 Classification of weathered rock (Korea Rail Network Authority, 2011)

Grade	Range of engineering properties		
	$q_u$ (MPa)	RQD (%)	$V_P$ (km/s)
Highly and completely weathered	$\leq 5$	-	$\leq 1.2$
Moderately weathered	5 - 25	$\leq 10$	1.2 – 2.5

As described above, many institutions suggested the quantitative criteria of the weathered rock but the range of the engineering properties was different. Also, although ASTM D6032 suggested that highly weathered rock core should not be included when the engineers evaluate the RQD (Rock quality designation), the KEC presented the RQD of highly weathered rock was from 20 to 40 %. So it is very confusing that engineers determined the rock condition only using the engineering properties values of the rock.

Therefore, many engineers determine the subsurface layer using boring log described by field boring engineers. The field boring engineers usually judged the boundary between the residual soil and highly weathered rock with SPT N value of 50 blows / 10 cm, and they classified the weathered rock observing the sample condition as described in Table 1-1. So, in this study, the subsurface layers were determined with the boring log.

## Chapter 3. Experiment and Analysis Procedure

### 3.1 Introduction

In this research, site investigation including some *in situ* tests and laboratory tests to obtain geotechnical properties of highly and completely weathered granite were performed. Geochemical analysis for the retrieved sample, also, was conducted to quantify the degree of weathering that affects the geotechnical properties of the weathered granites. After then, the estimation method to predict the geotechnical properties using chemical weathering indices was developed based on general assumptions that can be acceptable in the weathered zone. The research procedure was simply represented in Figure 3-1.

In this chapter, site investigation, laboratory tests, geochemical analysis, and the estimation method of geotechnical properties, which were adopted to this study, are introduced.

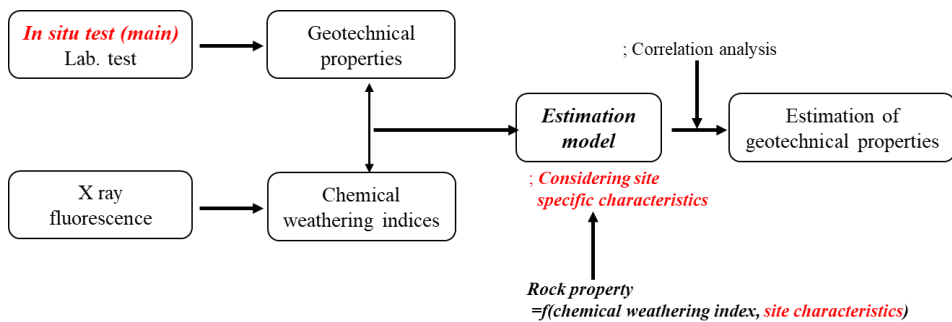


Figure 3-1 Schematic diagram of research procedure



## **3.2 Site Investigation**

### **3.2.1 Test Sites**

The objective of this study is to estimate the highly and completely weathered granite using chemical weathering indices, so test sites where weathered granite layer was thickly developed were needed. Eventually, three test sites (G site: Goyang, S site: Sejong, and A site: Ansong) were determined as the research area based on the review of lots of previous site investigation reports. The location of the three test sites was shown in Figure 3-2.

Borehole investigation to find out the compositions of subsurface was performed with standard penetration test (SPT) at all of the test sites and the boreholes at each test sites were referred to as GBH-1, SBH-1, and ABH-1 (Figure 3-3). The compositions of subsurface were verified based on the measured SPT N values and the state of the retrieved samples by split spoon sampler. The boundary between the residual soil layer and highly and completely weathered granite layer was distinguished based on the criterion where the SPT penetration depth was less than 10 cm after 50 blows (Seoul, 2006). Rock coring using a triple barrel was conducted from the depth where SPT was refused; if there is no observed advance of the split spoon sampler during 10 times successive blows, SPT can be stopped (ASTM D1586). After then, highly and completely weathered granite and moderately weathered granite were distinguished by checking the condition of the rock core according to Table 1-1.

The G site had a thick layer of alluvial soil down to a depth of 22 m, below which there were 1 m-thick residual soil and 13 m-thick highly and completely weathered granite. On the other hand, S site was composed of residual soil down to a depth of 7 m and approximately 18 m-thick highly and completely weathered granites below that residual soil. The A site had alluvial soil layer down to a depth of 3.2 m, below which 12.8 m-thick of residual soil and 19 m-thick of highly and completely weathered granite were developed. The subsurface composition of the test sites was shown in Figure 3-3.

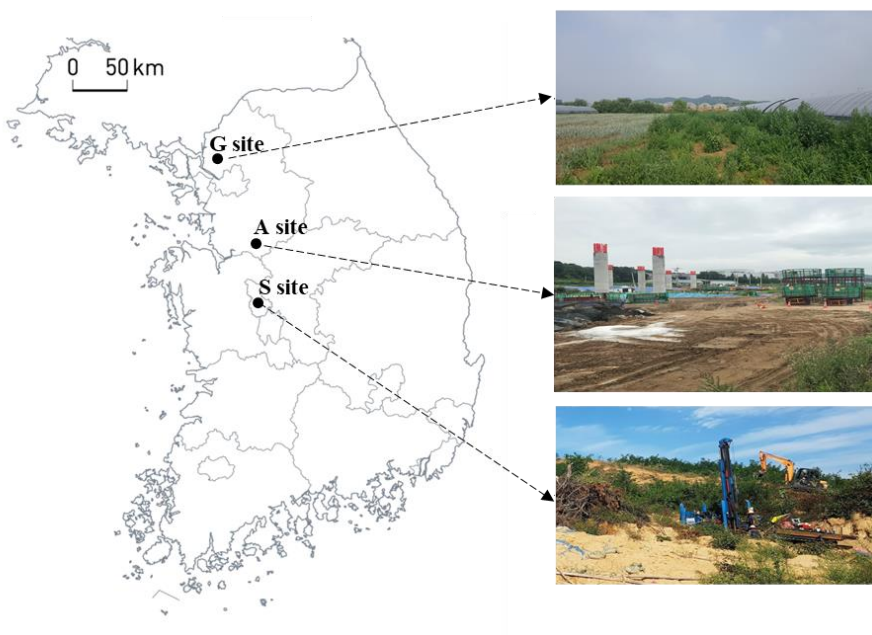
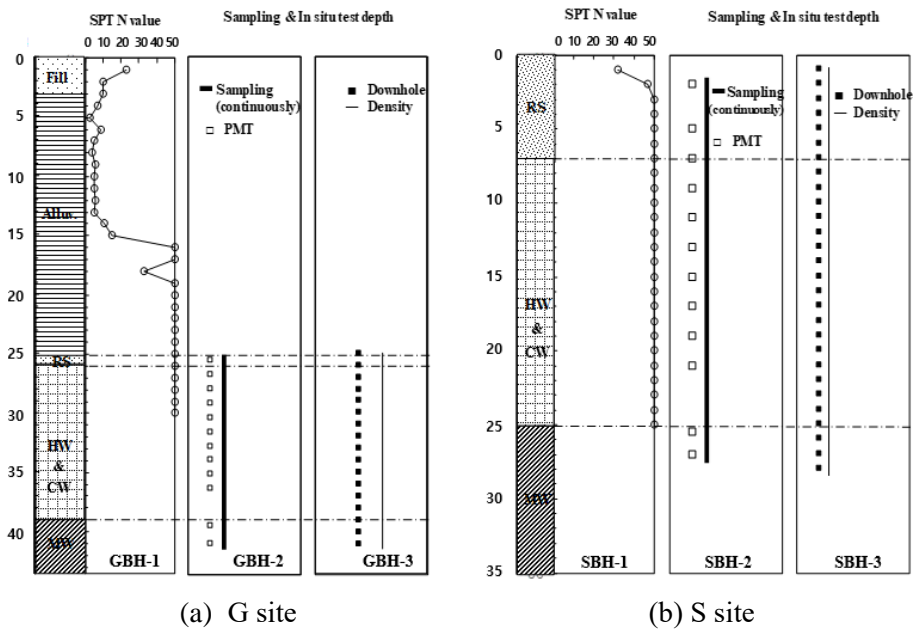
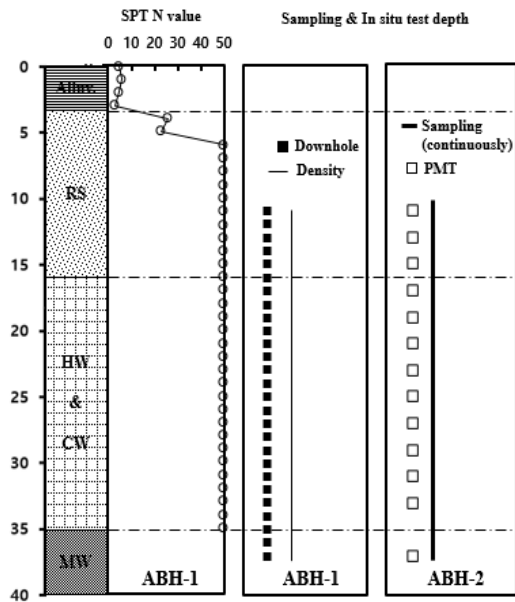


Figure 3-2 Location of each test site: G site, S site, A site



(a) G site (b) S site



(c) A site

Figure 3-3 Subsurface information with *in situ* tests and sampling depth

### 3.2.2 *In Situ* Test

*In situ* tests including pressuremeter test (PMT), density logging, and downhole seismic test were performed at all of the test sites to estimate geotechnical properties of residual soil, highly and completely weathered granite, and moderately weathered granite. PMTs were conducted with a depth interval of approximately 1.5 – 2.0 m in second boreholes which have 1 m spacing with first boreholes at all of the sites (GBH-1, SBH-1, and ABH-1). Geophysical loggings (density logging and downhole seismic test) were performed in third boreholes which were 1-m apart from the second borehole at G site and S site (GBH-3, SBH-3), but conducted in the first borehole at A site (ABH-1). The *in situ* test depth of each site was presented in Figure 3-3. The procedures and simple interpretation methods of each *in situ* test are as follows:

#### *Pressuremeter test (PMT)*

PMTs were performed using Elastometer-2 made by Oyo Corp., which could measure the radius of the borehole (Figure 3-4). Pressure – borehole radius curve could be obtained after the test, and this curve typically shows 3 steps of behaviors (Figure 3-5):

- 1) Non-contact and disturbed zone: while being in its free inflation, the probe has not yet been in contact with the borehole wall and accordingly no stress has been transmitted to the ground. And then the disturbed borehole wall was recompressed by the probe until earth

pressure at rest ( $P_0$ ), and the gradual increase of ground reaction and the decrease with its deformation speed is accompanied.

- 2) Pseudo elastic zone: This indicate the initial linearity stage in the pressure loading process to generate the passive earth pressure within the ground. The pressure-deformation curve is approximately linear while the deformation speed indicates the values almost constant.
- 3) Plastic zone: After the yield pressure ( $P_y$ ) at which the pressure-deformation curve deviating from the linear section, the deformation speed accelerated, and the pressure-deformation curve tended to be gradually inflected towards the right direction.

Pressuremeter modulus ( $E_m$ ) can be obtained by interpreting the linear section in the pseudo elastic zone.  $E_m$  can be calculated by the following equation.

$$E_m = (1 + \nu) \cdot r \cdot \frac{\Delta P}{\Delta R} \quad 3-1$$

Where,  $\nu$  represents Poisson's ratio,  $r$  represents the intermediate radius for the section to calculate the slope ( $\Delta P / \Delta R$ ) of the linear section (Figure 3 5-a). The unloading-reloading elastic modulus, also, can be calculated in the same manner as the pressuremeter modulus from the unloading-reloading cycle

section.

Limit pressure ( $P_L$ ) is defined as the pressure where the probe volume reaches twice the original ground cavity volume, which was expressed by the following equation:

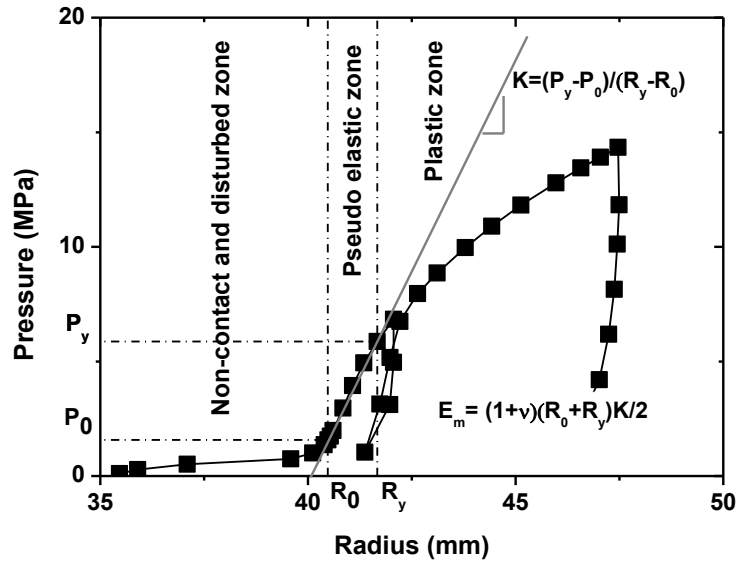
$$P_L = P|_{at V=V_L}, \quad V_L = 2V_c \quad 3-2$$

Where,  $V_L$  and  $V_C$  are the probe volumes corresponding to the limit pressure ( $P_L$ ) and the earth pressure at rest ( $P_0$ ), respectively.

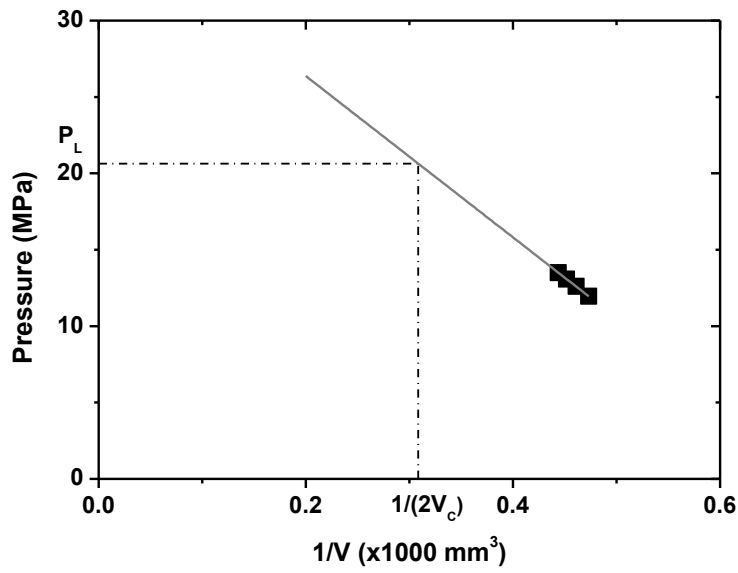
The limit pressure is usually not obtained by direct measurements during the test due to limitation in the probe expansion or excessively high pressure, so the limit pressure generally can be determined by an extrapolated  $1/V$  to  $P$  plot, as shown by Figure 3-5-b. In this research, PMTs were conducted from residual soil layer to moderately weathered granite layer at each test site for determining the variation of the geotechnical properties with depth. Firstly, a borehole was drilled to a target test depth, and then the drilling bit was retrieved. Secondly, the PMT device was connected to SPTs' rods and located at the target test depth, and PMT was performed according to ASTM D 4719. After the PMT, the test device was retrieved and successive drilling and PMTs were conducted (Figure 3-6).



Figure 3-4 Elastometer-2 test apparatus set made by Oyo Corp.



(a)



(b)

Figure 3-5 Interpretation of PMT curve: (a) pressuremeter modulus and unloading-reloading modulus; (b) limit pressure



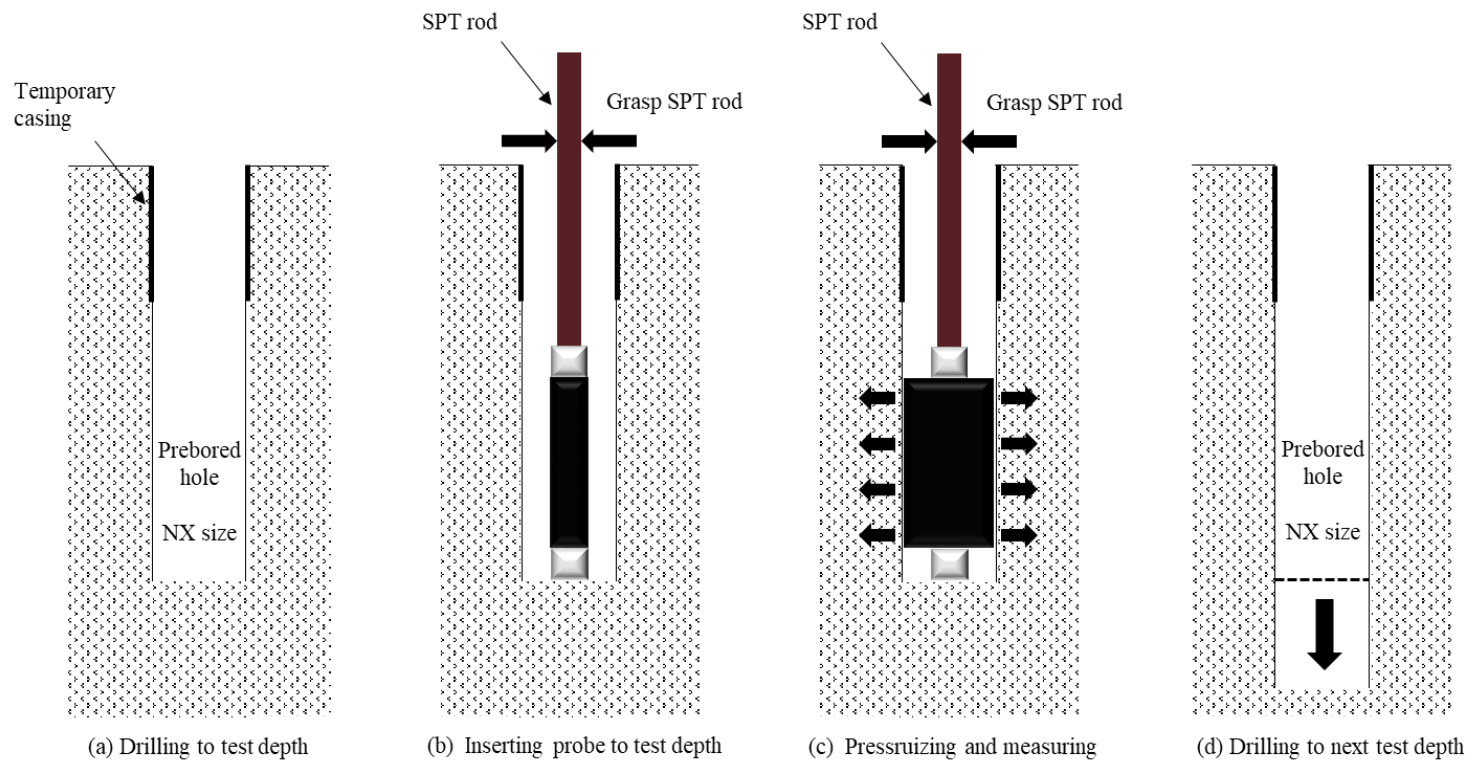


Figure 3-6 Test procedure of pressuremeter test

### *Density logging*

Density loggings were performed using the test devices set made by Robertson Geotechnical Inc., which could measure the *in situ* bulk density that can be easily converted to unit weight of the ground. The test set consisted of density probe, source, winch, tripod, and measuring program (Figure 3-7).

Density is primarily depends on the number of atoms packed into a given volume of material. Each atom consists of a nucleus containing  $N$  neutrons and  $Z$  protons surrounded by a cloud of  $Z$  electrons, where  $Z$  is the atomic number. The density could be estimated using the proton density ( $n_p$ ), Avogadro's number ( $N_A = 6.022 \times 10^{23}$ ), and the ratio of atomic number ( $Z$ ) over atomic weight ( $A$ ), as shown in equation 3-3 (Lacerda, 2010).

$$\rho = \frac{n_p}{N_A(Z / A)} \quad 3-3$$

The atomic weight  $A$  can be simply determined as the sum of the number of neutrons and protons, and the ratios ( $Z/A$ ) of most rock-forming elements are to be close to 0.5 (Figure 3-8). Thus in order to determine the density, it is necessary to measure the proton density ( $n_p$ ), but  $n_p$  is difficult to measure directly. So, the electron density ( $n_e$ ) is applied to estimating the density instead of  $n_p$ , because an electrically neutral atom has the same number of protons with electrons. The  $n_e$  can be measured by density logging.

In this study, density loggings were conducted from residual soil layer to

moderately weathered granite layer at each test site. After drilling a borehole, the density probe was located to the bottom of the borehole, and the density of the ground was measured with depth (Figure 3-9).

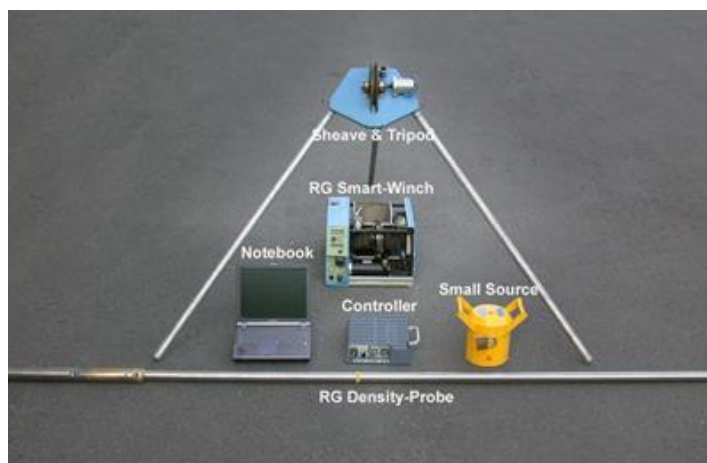


Figure 3-7 Density logging test device set made by Robertson Geo. Corp.

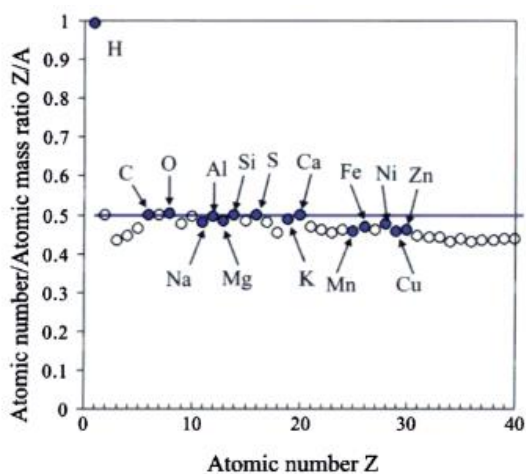


Figure 3-8 Z/A ratio versus atomic number (Lacerda, 2010)

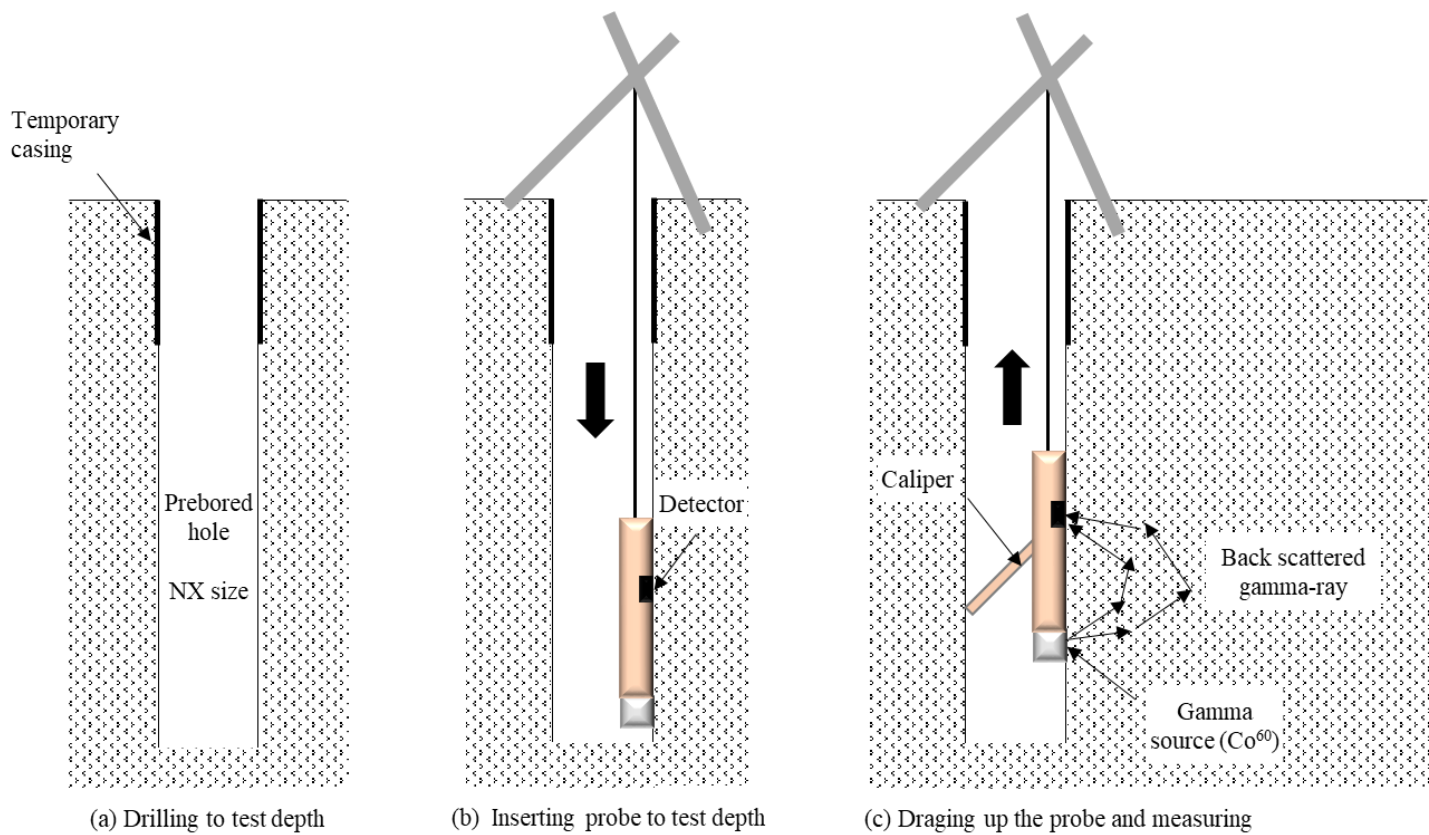


Figure 3-9 Test procedure of density logging

### *Downhole seismic test*

Downhole seismic tests were performed using the test devices set made by OYO Corporation, which could measure the P- and S-wave that triggered by seismic source (Figure 3-10). The P- and S-wave velocities of the material could be simply interpreted and directly transferred to the important geotechnical properties such as Poisson's ratio, maximum shear modulus, and dynamic elastic modulus. The test and interpretation procedure of the wave velocities and how to estimate the geotechnical properties are described as follows (Figure 3-11):

- 1) Drilling borehole to the target test depth from residual soil to moderately weathered granite, in this study.
- 2) After the drilling was completed, case the borehole with PVC pipes.
- 3) Set the downhole seismic test set: locating the sonde (receiver) at the start point of the test; preparing the wave plate and hammer as a seismic source; turning on the measuring program.
- 4) Activate the seismic source by hitting the wave plate with hammer, and measure the P- and S-wave arrival time, respectively.
- 5) The wave velocities could be calculated by considering the wave propagation length and arrival time:

$$L(\text{wave propagation length}) = \sqrt{H^2 + V^2} \quad 3-4$$

$$V(\text{wave velocity}) = L / \Delta T \quad 3-5$$

Where,  $H$  is a horizontal distance between the center of the seismic source and the receiver borehole, and  $V$  is a vertical depth of the receiver.

- 6) The Poisson's ratio, maximum shear modulus, and dynamic elastic modulus could be calculated using P- and S- wave velocities:

$$\nu(\text{Poisson's ratio}) = \frac{(V_P / V_S)^2 - 2}{2[(V_P / V_S)^2 - 1]} \quad 3-6$$

$$G_{\max}(\text{maximum shear modulus}) = \rho V_S^2 \quad 3-7$$

$$E_{dy}(\text{dynamic elastic modulus}) = 2G_{\max}(1 + \nu) \quad 3-8$$

Where,  $V_P$  and  $V_S$  is P- and S-wave velocity, and  $\rho$  is density evaluated by density logging.



Figure 3-10 Downhole seismic test device set

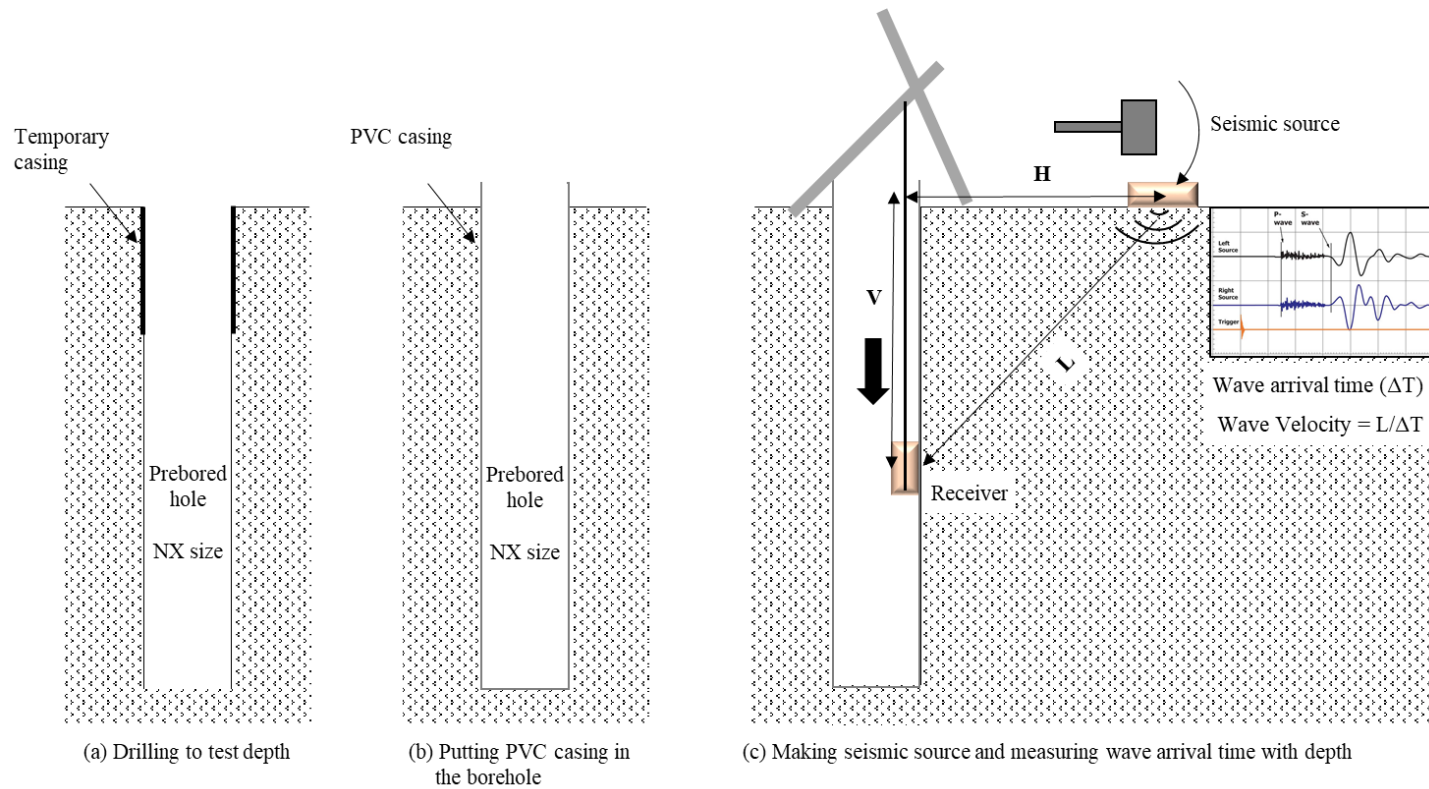


Figure 3-11 Test procedure of downhole seismic test



### **3.2.3 Sampling Method**

Samples from residual soil to moderately weathered granite were continuously retrieved at all of the test sites (GBH-3, SBH-3, and ABH-2). All samples were used in laboratory tests and geochemical analysis which estimated the geotechnical properties and chemical weathering indices, respectively.

For the least disturbance, all samples were retrieved using a triple core barrel which has been widely used for coring of severely weathered and fractured rock. The triple core barrel consisted of an outer tube, inner tube, and splitting inner liner (Figure 3-12). When drilling the ground, the outer tube rotates with rods and the bit crushes the ground. On the other hand, the inner tube and the splitting liner remain stationary during drilling, and the core samples retrieved in the splitting liner are blocked off drilling fluid such as water, which reduces the sample disturbance.

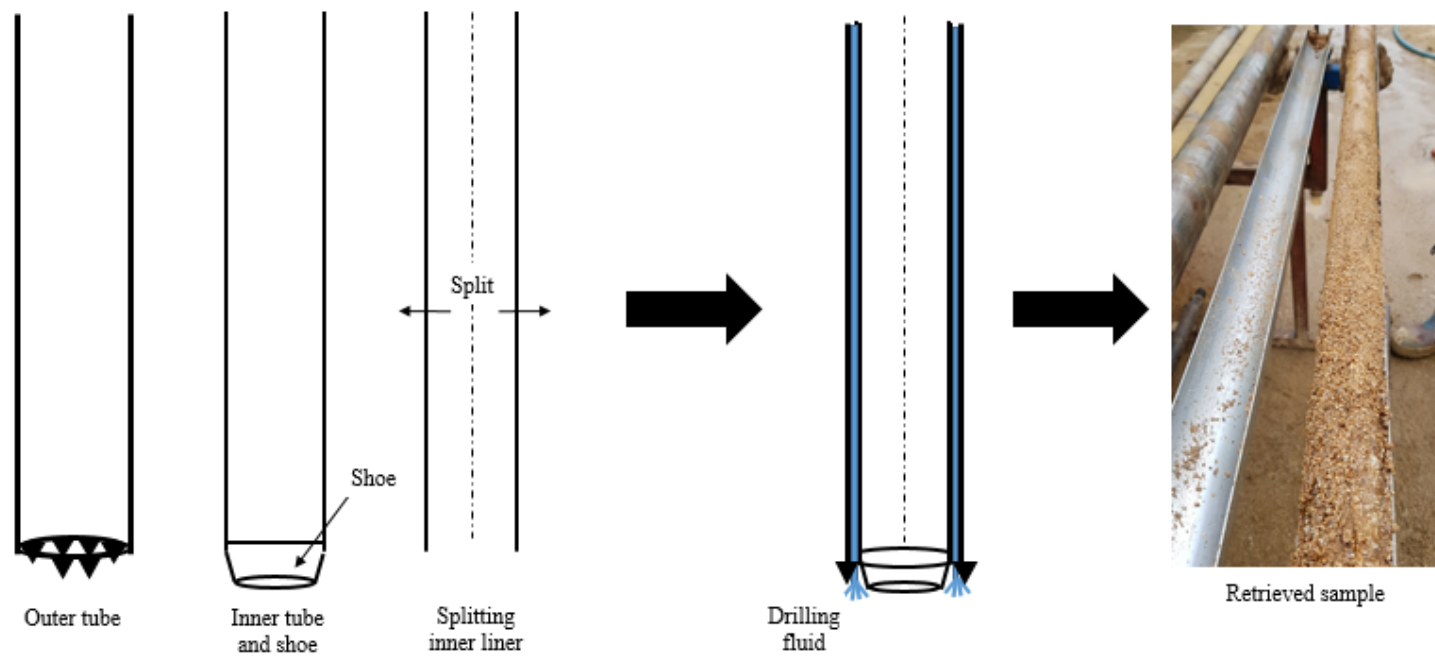


Figure 3-12 Schematic diagram of triple core barrel and retrieved sample

### 3.3 Laboratory Test

Laboratory tests such as point load strength test, unconfined compressive strength test, and triaxial compressive test for retrieved highly and completely granite, and moderately weathered granite core samples were conducted to estimate geotechnical properties. However, lots of the rock core samples of the highly and completely weathered granite were heavily disturbed, so the number of laboratory tests was limited.

On the other hand, direct shear tests for pseudo highly and completely weathered granite made by the mixture of cement mortar and residual soil were conducted to overcome the limited number of laboratory tests and to estimate shear strength parameters of the highly and completely weathered granite. The pseudo highly and completely weathered granites were made to have the representative unconfined compressive strength of the weathered granite measured by laboratory tests for simulating the *in situ* granite. The procedure of the direct shear tests for pseudo highly and completely weathered granite are shown in Figure 3-13.

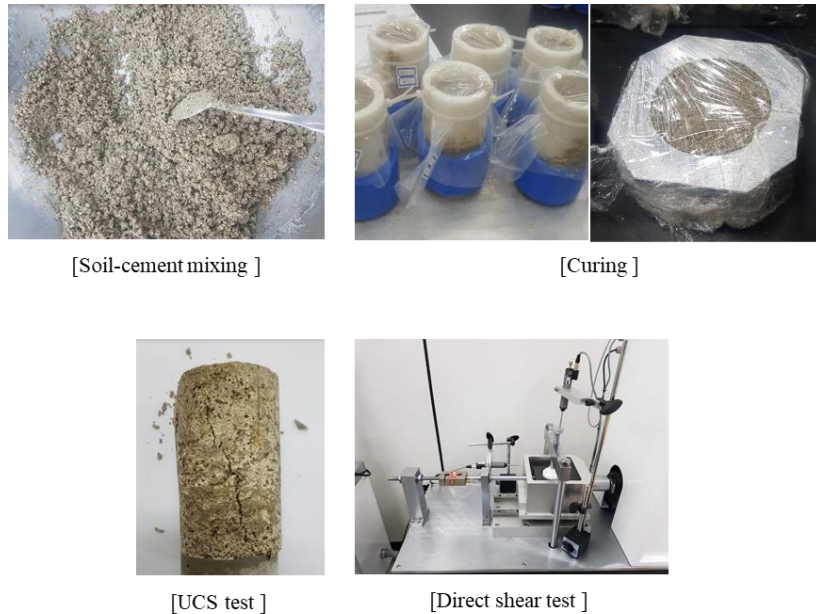


Figure 3-13 The procedure of direct shear test for pseudo highly and completely weathered granite

### 3.4 Geochemical Analysis

To measure the chemical composition of the retrieved samples from residual soil to moderately weathered granite, X-ray fluorescence (XRF) analysis was performed using a WD (wavelength dispersive)-XRF spectrometer installed at the National Center for Inter-university Research Facilities at Seoul National University. The samples retrieved from the depth, at which in situ tests were performed, were used to analyze the chemical weathering indices with the geotechnical properties. The weight percentages of the major oxide resulted from XRF analysis were transferred to the mole ratio and then chemical weathering indices applied in this study(see Table 2-3) were calculated.

### 3.5 Estimation Method of Geotechnical Property

As described in Chapter 1, even if weathered rocks originate from the same parent rock, when evaluating the geotechnical properties, it is important to consider both the weathering and site-specific characteristics. This study proposed a geotechnical properties evaluation method that can consider the chemical weathering indices and site-specific characteristics of highly weathered granite.

First, three basic assumptions were established to evaluate the geotechnical properties of highly weathered granite, which are described in Figure 3-14:

- 1) The geotechnical properties of residual soil and moderately weathered granite represent site-specific characteristics.
- 2) The geotechnical properties of the residual soil and moderately weathered granite affect those of highly and completely weathered granite.
- 3) The degree of weathering, quantitatively defined using chemical weathering indices, affects the change of the geotechnical properties of the granite.

Based on the above assumptions, the geotechnical properties of highly and completely weathered granite can be expressed as follows:

$$\zeta_{HW\&CW} = \left( \frac{WI_{MW} - WI_{HW\&CW}}{WI_{MW} - WI_{RS}} \right)^k \zeta_{RS} + \left\{ 1 - \left( \frac{WI_{MW} - WI_{HW\&CW}}{WI_{MW} - WI_{RS}} \right)^k \right\} \zeta_{MW} \quad 3-9$$

where  $\xi$  and  $WI$  are the geotechnical property and chemical weathering indices evaluated by *in situ* and laboratory tests and XRF analysis respectively. The subscripts  $MW$ ,  $HW$ ,  $CW$  and  $RS$  represent moderately weathered, highly weathered, completely weathered, and residual soil, respectively;  $k$  is a curve-fitting parameter determined by the relationship between the geotechnical properties and chemical weathering indices. Equation 3-9 can be simplified as a normalized form:

$$\left( \frac{\xi_{MW} - \xi_{HW\&CW}}{\xi_{MW} - \xi_{RS}} \right) = \left( \frac{WI_{MW} - WI_{HW\&CW}}{WI_{MW} - WI_{RS}} \right)^k \Rightarrow R_p = (R_w)^k \quad 3-10$$

where  $R_p$  and  $R_w$  are defined as the property ratio and weathering index ratio.  $R_w$  has a value between 0 and 1. If  $R_w$  is 0, the chemical weathering index of the highly and completely weathered granite is identical to that of the moderately weathered granite; from Equation 3-10, the geotechnical properties of highly and completely weathered granite are the same as those of moderately weathered granite. If  $R_w$  is 1, the chemical weathering index of highly and completely weathered granite is the same as that of the residual soil and the geotechnical properties of highly weathered granite are the same as those of residual soil.

Applying the geotechnical properties and chemical weathering indices measured in each test site to the described estimation model (equation 3-10), the curve fitting parameters ( $k$ ) of each geotechnical property are to be determined (Figure 3-15).

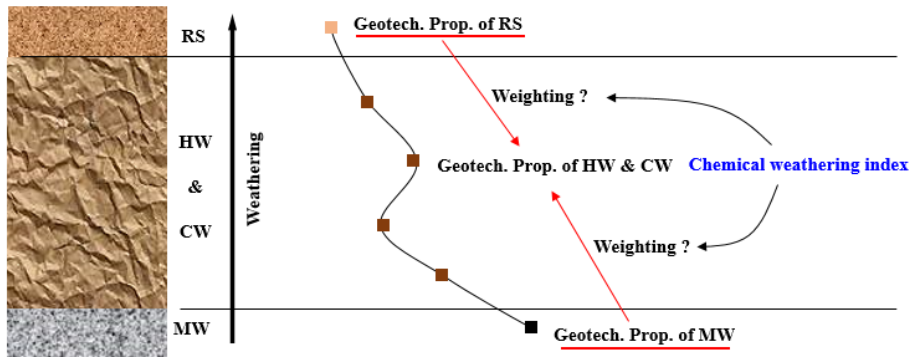


Figure 3-14 Concept of the estimation method of geotechnical properties of highly and completely weathered granite

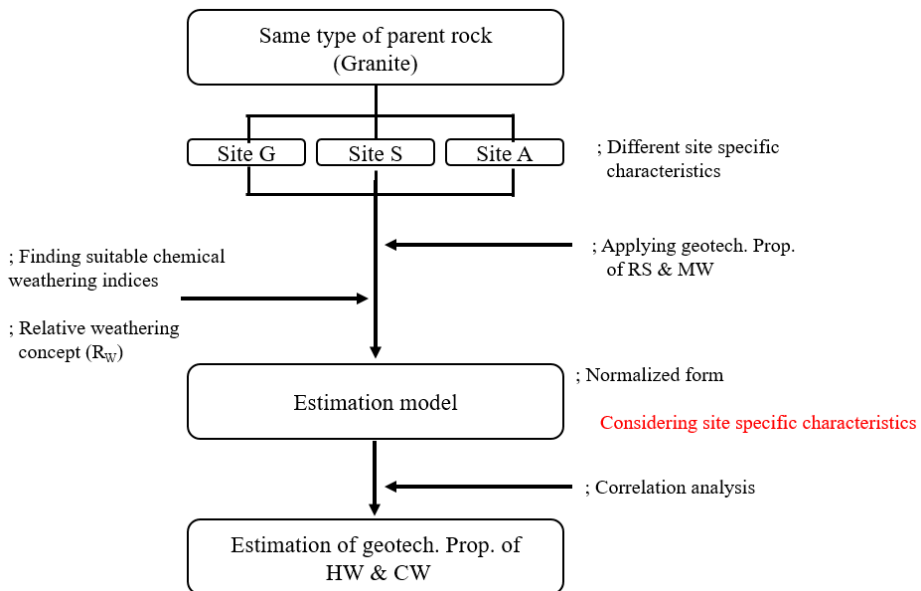


Figure 3-15 Procedure of estimating geotechnical properties of highly and completely weathered granite using chemical weathering indices

## **Chapter 4. Experiment Results and Discussion**

### **4.1 Introduction**

This chapter covered results and discussion of the geotechnical properties and chemical weathering indices of the weathered granite from residual soil and moderately weathered granite. The geotechnical properties were measured by *in situ* and laboratory tests, and the chemical weathering indices were analyzed based on the major oxide proportion measured by XRF.

Section 2 of this chapter presented the results of *in situ* tests including pressuremeter test, density logging, and seismic downhole test, and the distribution of the test results at each test site was compared with each other.

In section 3 of this chapter covered the results of laboratory tests conducting on retrieved samples, such as unconfined compressive test, point load test, triaxial test. And also, the results of direct shear tests using pseudo weathered granite for estimating the shear strength parameters were presented.

In section 4 of this chapter presented the results of major oxide proportion measured by XRF, and chemical weathering indices calculated based on the major oxide proportion.

In section 5 of this chapter, the geotechnical properties measured at all test sites were discussed with the various classification criteria, and the soil-rock transition stated of the highly and completely weathered granite was discussed.



## 4.2 Geotechnical Properties Measured by *In Situ* Testing

### 4.2.1 Pressuremeter Test Results ( $E_m$ , $E_{ur}$ , $P_L$ )

Pseudo elastic modulus so-called pressuremeter modulus ( $E_m$ ), unloading-reloading elastic modulus ( $E_{ur}$ ), and limit pressure ( $P_L$ ) from residual soil to moderately weathered granite layer at each site were measured by PMT. Figure 4-1 presents the distribution of the test results with depth at each site.

Elastic modulus ( $E_m$ , and  $E_{ur}$ ) and limit pressure at all sites show a generally increasing tendency with depth and the average values of the results of each layer were increased as the layer changes from residual soil to moderately weathered granite because of the higher effective vertical stress level and the lower degree of weathering (Figure 4-1 and Table 4-1). Especially, all the test results were significantly increased as the layer changes from highly and completely weathered granite to moderately weathered granite. Even though the effective vertical stress should be increased with depth, the results measured in highly and completely weathered granite decreased or rarely changed in particular depth range, which is representing the effect of the weathering.

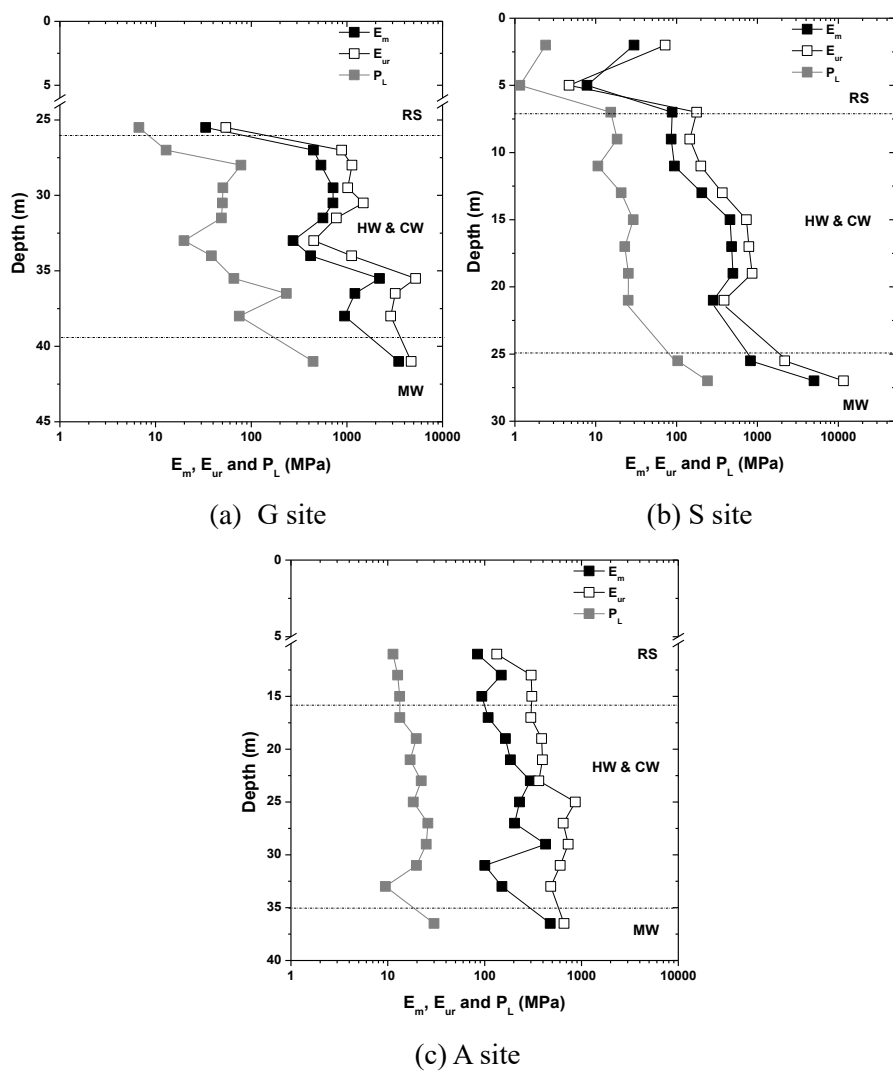


Figure 4-1 Distribution of PMT results ( $E_m$ ;  $E_{ur}$ ;  $P_L$ ) at each site: (a) G site; (b) S site; (c) A site

Comparing the mean values of the results at each site, the difference resulted from the test sites can be identified (Table 4-1). All the test results measured at G site were the highest values, because the weathered layers including residual soil, highly and completely weathered granite, and moderately weathered granite were developed from the depth of 25 m which was deeper than the other sites. On the other hands, all the test results of S site where the weathered layers were developed from more shallow depth than A site showed a different tendency with the layers: in residual soil layer, the results were lower than those of A site; in highly and completely weathered granite layer the results were similar with those of A site; in moderately weathered granite, the results were much higher than those of A site.

Also, the relative changes in the test results of the subsurface layer were differently presented at each test site. The mean value of all the test results at each subsurface layer was normalized by that of the moderately weathered granite layer for comparing the relative changes of the test results (Table 4-2). The normalized mean values of the test results at highly and completely weathered granite layer in G site and S site respectively ranged from 0.15 - 0.39 and 0.07 - 0.12, respectively. On the other hand, in A site, the normalized mean values were range from 0.44 – 0.80, which means that the geotechnical properties of G site and S site were more significantly decreased in the highly and completely weathered granite comparing with moderately weathered granite. These different tendencies of the test results represented the different site-specific characteristics resulted from the complicated effects such as weathering condition and the geotechnical properties of parent rock.

Table 4-1 PMT results:  $E_m$ ,  $E_{ur}$ ,  $P_L$

Property	Layer	G site			S site			A site		
		Min.	Mean	Max.	Min.	Mean	Max.	Min.	Mean	Max.
$E_m$ (MPa)	RS	-*	33.4	-	7.8	18.8	29.9	84.4	108.9	148.4
	HW & CW	274.0	802.8	2195.5	85.7	274.1	498.1	100.7	207.3	426.4
	MW	-	3480	-	822.4	2911.8	5001.1	-	475.9	-
$E_{ur}$ (MPa)	RS	-	54.4	-	4.7	38.4	72.2	133.4	247.8	307.5
	HW & CW	451.0	1819.5	5240.3	145.3	456.0	858.3	300.3	530.9	864.2
	MW	-	4700.0	-	2170.1	6889.5	11609.0	-	661.7	-
$P_L$ (MPa)	RS	-	6.7	-	1.2	1.78	2.4	11.3	12.4	13.3
	HW & CW	12.9	67.3	233.2	10.6	20.9	29.1	9.4	19.0	26.0
	MW	-	443.8	-	103.5	172.4	241.3	-	30.0	-

\* Not measured or invalid

Table 4-2 Normalized mean value of the PMT results

Property	Layer	Normalized mean value		
		G site	S site	A site
$E_m$	RS	0.01	0.01	0.23
	HW & CW	0.23	0.09	0.44
	MW	1.00	1.00	1.00
$E_{ur}$	RS	0.01	0.01	0.37
	HW & CW	0.39	0.07	0.80
	MW	1.00	1.00	1.00
$P_L$	RS	0.02	0.01	0.41
	HW & CW	0.15	0.12	0.63
	MW	1.00	1.00	1.00

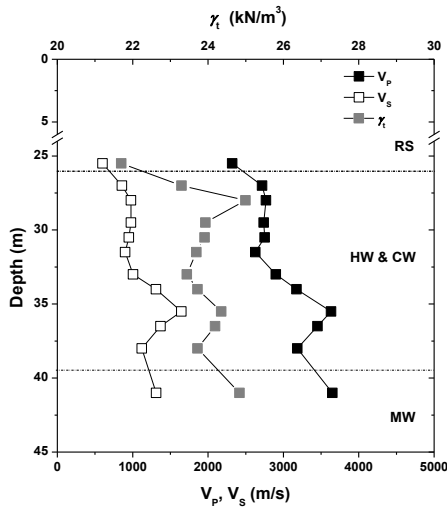
#### 4.2.2 Geophysical Test Results ( $\gamma_t$ , $V_p$ , $V_s$ , $G_{max}$ )

Unit weight ( $\gamma_t$ ), P-wave and S-wave velocity ( $V_p$ ,  $V_s$ ), and maximum shear modulus ( $G_{max}$ ) from residual soil to moderately weathered granite layer at each site were measured by geophysical tests such as density logging, and downhole seismic test. Figure 4-2 and Figure 4-3 present the distribution of the test results with depth at each site. All geotechnical properties measured by geophysical testing at each site were generally increased as the layer changes from residual soil to moderately weathered granite. In G site, all the test results measured at highly and completely weathered granite layer presented a significant increase

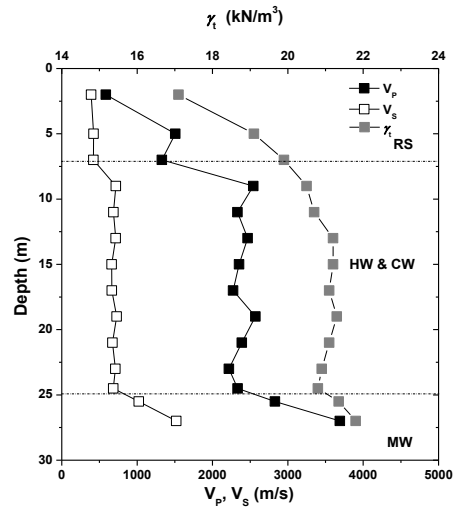
near the depth of 35 m, which was higher value than that measured at moderately weathered granite layer. On the other hand, all the test results were little changed at highly and completely weathered granite layer in S site and A site, except for the distribution of unit weight in A site which was significantly decreased near the depth of 25 – 30 m.

Comparing the mean values of the results at each site (Table 4-3), all the test results measured at G site, except for  $\gamma_t$ , were generally higher than those of the other sites, because of their higher overburden pressure as described in section 4.2.1. On the other hands, all the test results of S and A site presented a different tendency with the layers: in residual soil layer, the results were generally lower than those of A site; in highly and completely weathered granite layer, the results were a little higher than those of A site; in moderately weathered granite, the results were much higher than those of A site.

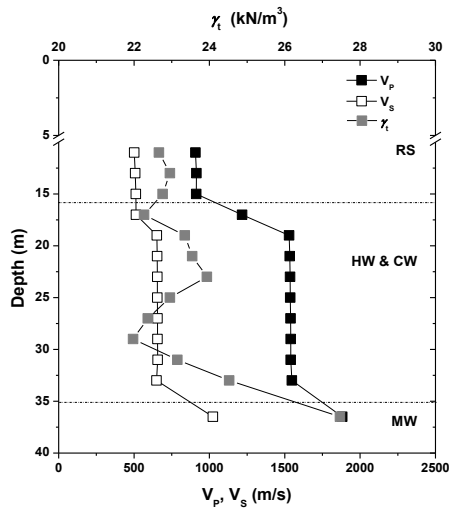
Also, the relative changes in the test results of the subsurface layer were differently presented at each test site. The mean value of all the test results at each subsurface layer was normalized as described in section 4.2.1 (Table 4-4). The normalized mean values of the  $\gamma_t$  and  $V_p$  at highly and completely weathered granite layer in all test sites were over 0.69, which were representing a relatively low variation between highly and completely weathered granite layer and moderately weathered granite layer. On the other hand, the normalized mean values of the  $V_s$  and  $G_{max}$  at each test site respectively ranged from 0.73 – 0.85 (G site), 0.23 – 0.50 (S site), and 0.36 – 0.60 (A site), which means that the  $V_s$  and  $G_{max}$  of G site were slightly decreased in the highly and completely weathered granite comparing with moderately weathered granite.



(a) G site

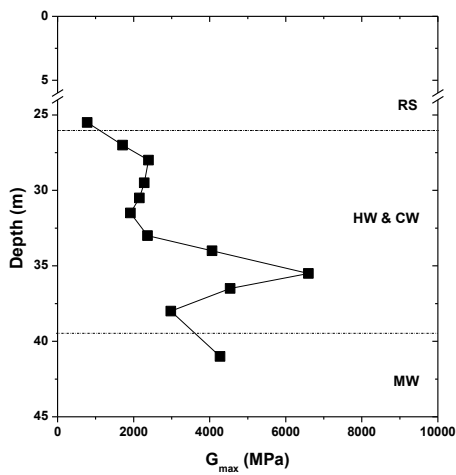


(b) S site

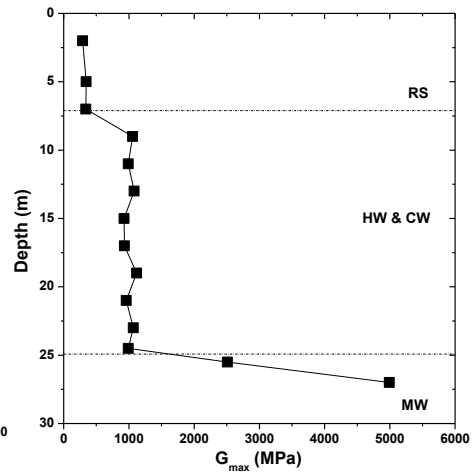


(c) A site

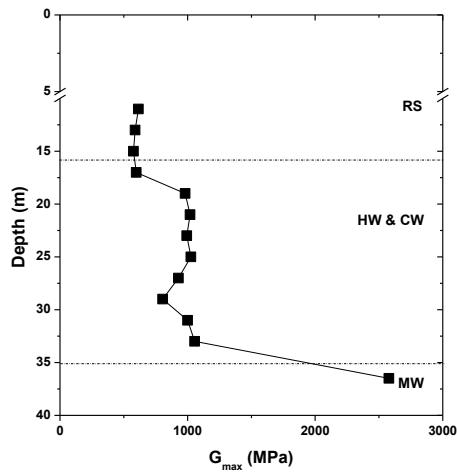
Figure 4-2 Distribution of geophysical test results ( $\gamma_t$ ,  $V_p$ ,  $V_s$ ) at each site: (a) G site; (b) S site; (c) A site



(a) G site



(b) S site



(c) A site

Figure 4-3 Distribution of  $G_{max}$  at each site: (a) G site; (b) S site; (c) A site



Table 4-3 Geophysical test results:  $\gamma_t$ ,  $V_p$ ,  $V_s$ ,  $G_{max}$

Property	Layer	G site			S site			A site		
		Min.	Mean	Max.	Min.	Mean	Max.	Min.	Mean	Max.
$\gamma_t$ (kN/m <sup>3</sup> )	RS	- *	21.7	-	17.1	18.1	19.1	22.7	22.8	22.9
	HW & CW	23.3	23.9	25.0	19.9	20.9	21.3	22.0	23.1	24.5
	MW	-	24.8	-	21.4	21.6	21.8	-	27.5	-
$V_p$ (m/s)	RS	-	2320	-	586	1047	1507	908	912	914
	HW & CW	2628	2995	3633	1329	2281	2569	1218	1502	1548
	MW	-	3650	-	2828	3310	3691	-	1882	-
$V_s$ (m/s)	RS	-	600	-	389	406	423	501	507	512
	HW & CW	857	1111	1646	339	666	1119	513	638	567
	MW	-	1312	-	1022	1334	1520	-	1023	-
$G_{max}$ (MPa)	RS	-	781	-	291	318	423	576	593	615
	HW & CW	1711	3100	6597	420	946	728	598	934	1056
	MW	-	4275	-	2511	4056	4992	-	2578	-

\* Not measured or invalid

Table 4-4 Normalized mean value of the geophysical test results

Property	Layer	Normalized mean value		
		G site	S site	A site
$\gamma_t$	RS	0.87	0.84	0.83
	HW & CW	0.96	0.96	0.84
	MW	1.00	1.00	1.00
$V_P$	RS	0.64	0.32	0.48
	HW & CW	0.82	0.69	0.80
	MW	1.00	1.00	1.00
$V_S$	RS	0.46	0.30	0.50
	HW & CW	0.85	0.50	0.62
	MW	1.00	1.00	1.00
$G_{\max}$	RS	0.18	0.08	0.23
	HW & CW	0.73	0.23	0.36
	MW	1.00	1.00	1.00

## 4.3 Geotechnical Properties Measured by Lab. Testing

### 4.3.1 Unconfined Compressive Strength ( $q_u$ )

Unconfined compressive strength ( $q_u$ ) from residual soil to moderately weathered granite layer at each site was determined by uniaxial compressive test, and point load test (PLT). Also,  $q_u$  of residual soil, highly and completely weathered granite was estimated using the correlation with SPT  $N_{60}$  which was suggested for weak rock (Figure 4-4), because the samples retrieved each test site were much fractured that the suitable specimens were limited.

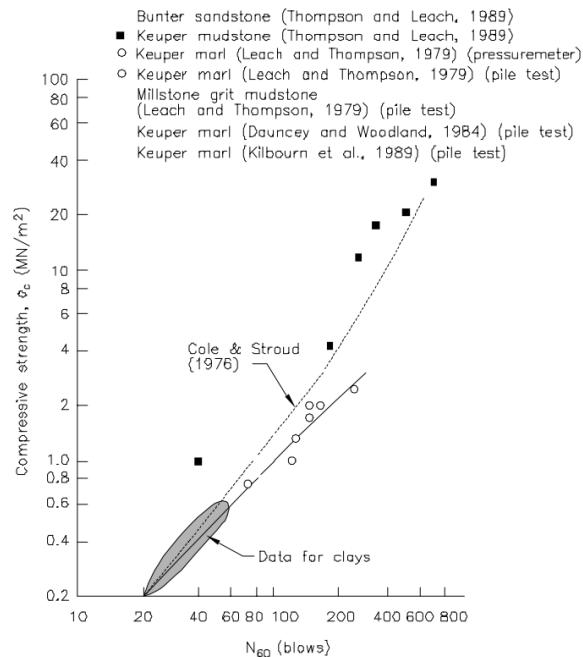


Figure 4-4 Correlation between unconfined compressive strengths and penetration resistance of weak rock (Gannon et al., 1999).

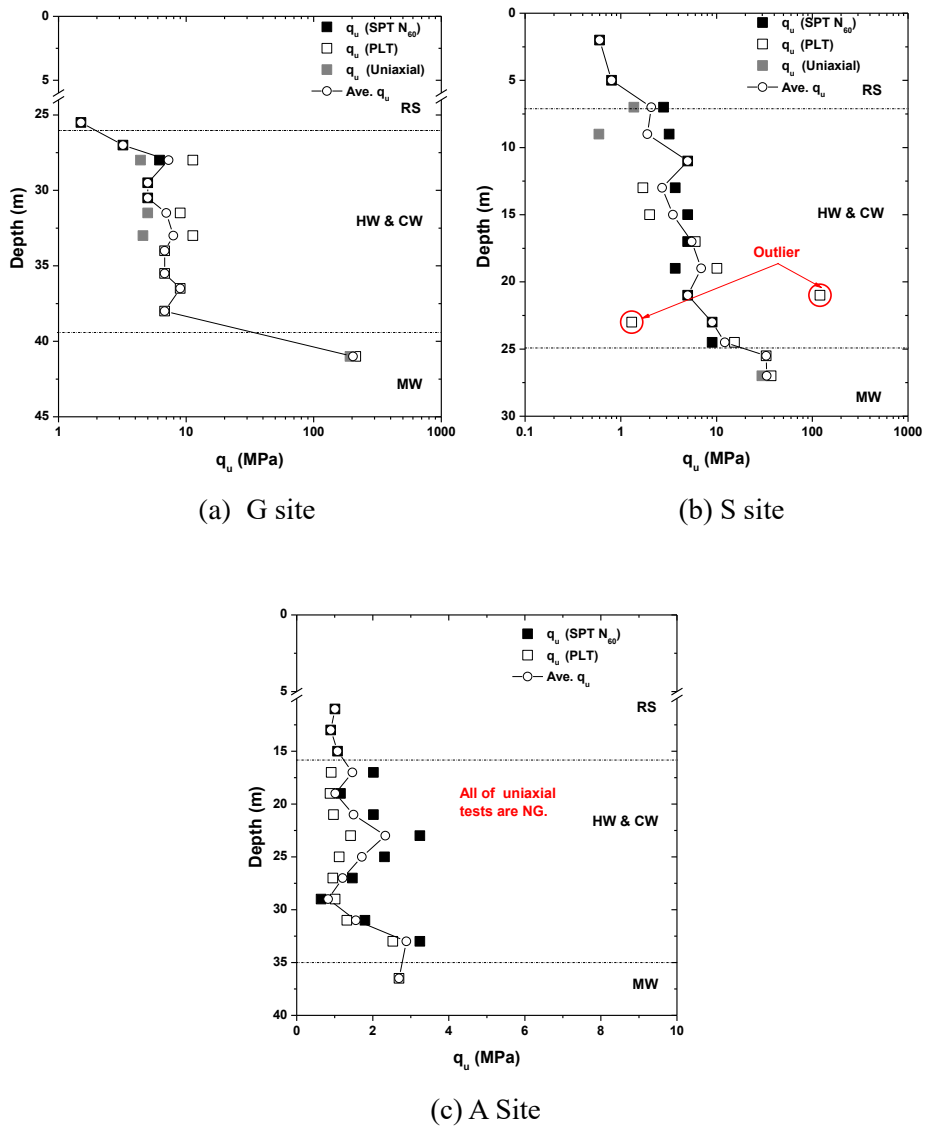


Figure 4-5 Distribution of unconfined compressive strength results ( $q_u$ ) at each site: (a) G site; (b) S site; (c) A site

The measured and estimated  $q_u$  were plotted with depth in Figure 4-5, and the representative  $q_u$  which was the average value of  $q_u$  evaluated by using each test method also were presented in the same figure. The representative  $q_u$  were generally increased as the layer changes from residual soil to moderately weathered granite at G and S site, especially, the representative  $q_u$  at G site were significantly increased in moderately weathered granite layer. On the other hand, in A site, the representative  $q_u$  was shown a repetitive decreasing and increasing tendency in highly and completely weathered granite layer.

Comparing the mean value of the representative  $q_u$  at each test site, G site had the highest  $q_u$  in all of the layers (Table 4-5). And the representative mean value of  $q_u$ , normalized by that of moderately weathered granite, in highly and completely weathered granite layer at G and S site were very low, compared to that of in A site (Table 4-6).

As described in section 4.2.1, the magnitude and the distribution of the geotechnical properties of the weathered zone were affected by the site-specific characteristics which were hard to be clearly estimated in spite of the same parent rock type of granite. Therefore, it is important to consider the site-specific characteristics for estimating geotechnical properties using general correlation, which results in a more reliable evaluation. So, in this study, as described in section 3.5, a particular method, using the own site test results of residual soil and moderately weathered granite, is suggested to consider the site-specific characteristics, and the details and applied results are to be described in section 4.5.

Table 4-5 Average unconfined compressive strength measured by uniaxial compressive test, point load test and estimated by SPT-N<sub>60</sub>

Property	Layer	G site			S site			A site		
		Min.	Mean	Max.	Min.	Mean	Max.	Min.	Mean	Max.
q <sub>u</sub> (MPa)	RS	- *	1.5	-	0.6	0.7	0.8	0.9	1.0	1.1
	HW & CW	3.2	6.5	9.0	1.9	5.4	12.2	0.8	1.6	2.9
	MW	-	203.2	-	29.8	32.1	33.5	-	2.7	-

\* Not measured or invalid

Table 4-6 Normalized mean value of average unconfined compressive strength

Property	Layer	Normalized mean value		
		G site	S site	A site
q <sub>u</sub>	RS	0.01	0.02	0.37
	HW & CW	0.03	0.17	0.60
	MW	1.00	1.00	1.00

#### 4.3.2 Shear Strength Parameters ( $c$ and $\phi$ )

Shear strength parameters ( $c$ : cohesion,  $\phi$ : friction angle) from residual soil to moderately weathered granite layer at each site were measured by the triaxial test and evaluated using limit pressure resulted from PMTs. Also, the direct shear tests for pseudo highly and completely weathered granite to evaluate the shear strength parameters were conducted, because of very limited specimens suitable for the triaxial test. And all the test results were compared with the shear strength parameters presented in several previous studies.

The triaxial test results were only obtained from the specimens retrieved at G site because the sample conditions of the other sites were no good. The cohesions and friction angles derived from Mohr-Coulomb failure envelope show a particular tendency, respectively. Comparing the results of highly and completely weathered granite layer to moderately weathered granite, the friction angles approximately remain, but the cohesions were significantly decreased (Table 4-7). Baynes and Dearman (1978) explained this tendency us-

Table 4-7 Shear strength parameters measured by triaxial test

Layer	Depth (m)	$\phi'$ (deg.)	$c'$ (MPa)
MW	41.0	59.0	26.0
	29.5	61.0	1.0
HW & CW	31.5	61.0	1.0
	33.0	61.0	1.0

ing the failure envelopes of unweathered and highly and completely weathered granite, and simple model to illustrate the microfabric consequences of different degree of weathering (Figure 4-6 and Figure 4-7). They mentioned that the cohesion and friction were developed due to the strength of the intergranular bonds and the interlocking texture, respectively. When granite is highly and completely weathered state, grain boundaries are opening due to microfracturing, which results in a significant reduction of cohesion. On the other hand, the friction angles are only slightly reduced by this degree of weathering, due to minor mineralogical changes and internal weakening of the grains resulting in a high interlocking. After further weathering, the grains have become completely separated or converted to a weathering product (Figure 4-7), so that the friction angles also fall markedly.

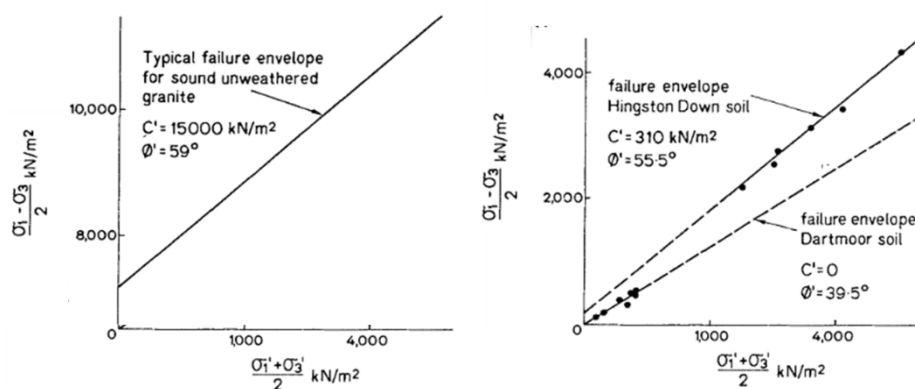


Figure 4-6 Failure envelopes for granite weathered to varying degree (Baynes and Dearman, 1978)



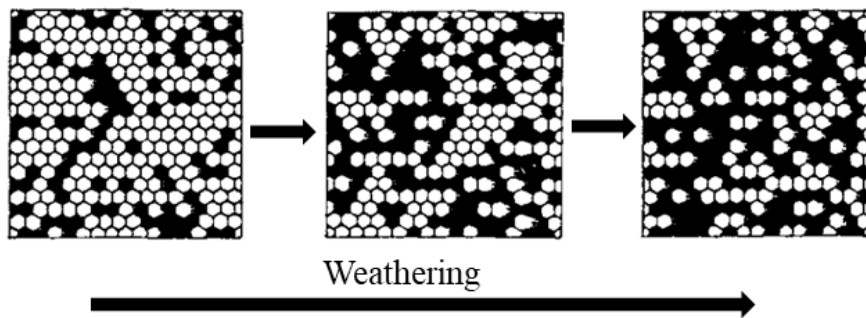


Figure 4-7 A simple model to illustrate the microfabric consequences (Baynes and Dearman, 1978)

Two sets of direct shear tests using the pseudo highly and completely weathered granite, also, were conducted, and the results were compared with the shear strength parameters suggested in several previous studies. Unconfined compressive strengths of the pseudo weathered rock specimens were 3 MPa and 9 MPa, which represented the first and third quartile of the unconfined compressive strengths in all test sites (see Table 4-5). Figure 4-8 shows Mohr-Coulomb failure envelope of the pseudo highly and completely weathered granite and the upper and lower bound of residual soil and moderately weathered rock suggested in previous studies. The shear strength parameters in the previous studies are presented in Table 4-8. As shown in Figure 4-8, the cohesions were ranged between the upper bound of residual soil and the lower bound of the moderately weathered granite. On the other hand, the friction angles of the pseudo weathered granites were over the lower bound of the moderately weathered granite, presumably due to the lower bound including discontinuity characteristics, which were not clearly described in the previous studies.

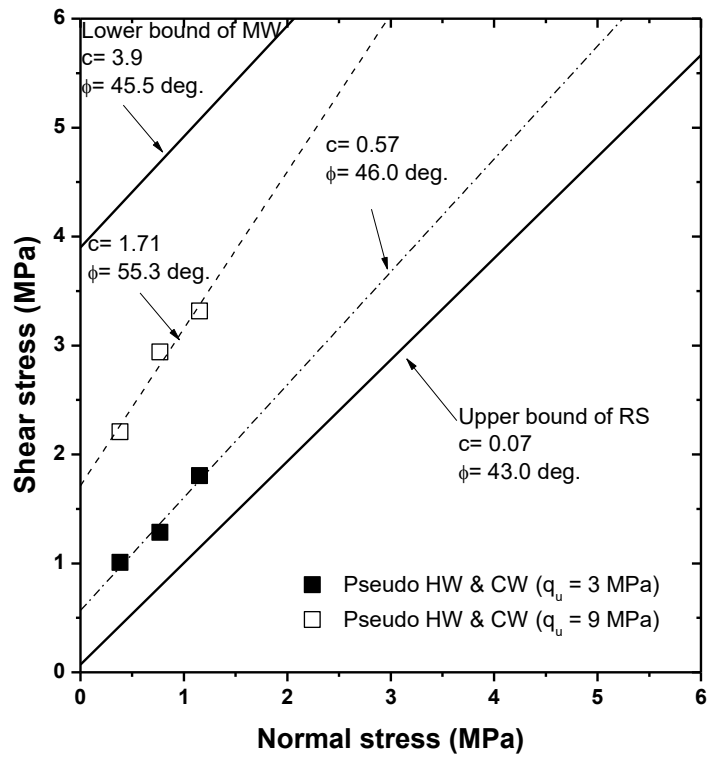


Figure 4-8 Mohr-Coulomb failure envelope of pseudo highly and completely weathered granite

Table 4-8 Range of the shear strength parameters in previous studies

Weathering grade	$\phi'$ (deg.)	c' (MPa)	Source
FS	59.0	15.0	(Baynes and Dearman, 1978)
MW	45.5 – 49.0	3.9 – 8.3	(Seo et al., 2016)
HW & CW	28.0 – 55.5	0.00 – 0.31	(Dearman et al., 1978; Seo et al., 2016)
RS	20.0 – 43.0	0.00 – 0.23	(Kwon, 1998)

Most previous studies suggested that 50 % of the cohesions of highly and completely weathered granite were below 0.03 MPa, which is the median value (Figure 4-9). So in this study, the equivalent friction angles that assume the zero cohesion were evaluated using the limit pressure ( $P_L$ ) which suggested by the Menard (1975) as presented in equation 4.1.

$$P_L = b \cdot 2^{(\phi' - 24)/4} \quad 4-1$$

Where,  $P_L$  is limit pressure, and  $b$  is a constant determined with the soil condition: 1.8 (dry condition), 3.5 (wet condition). In this study, the wet condition was applied because all layers under the groundwater level.

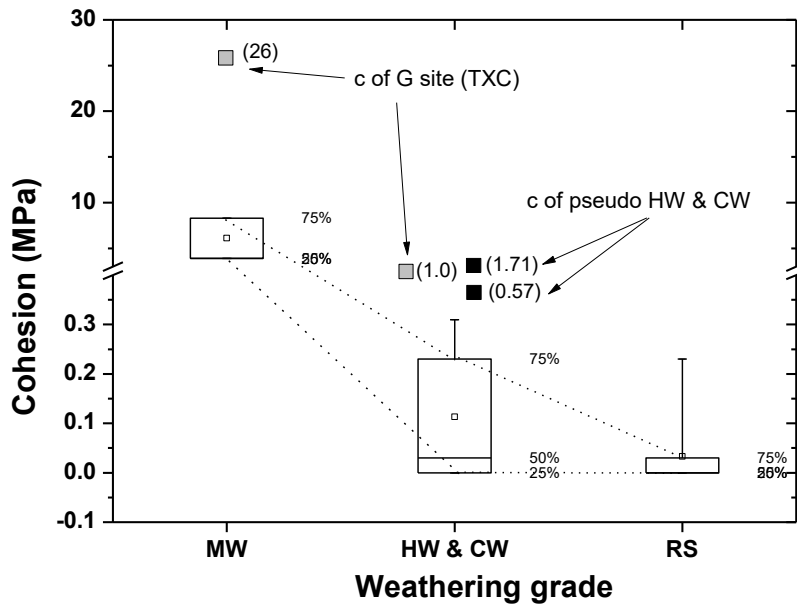
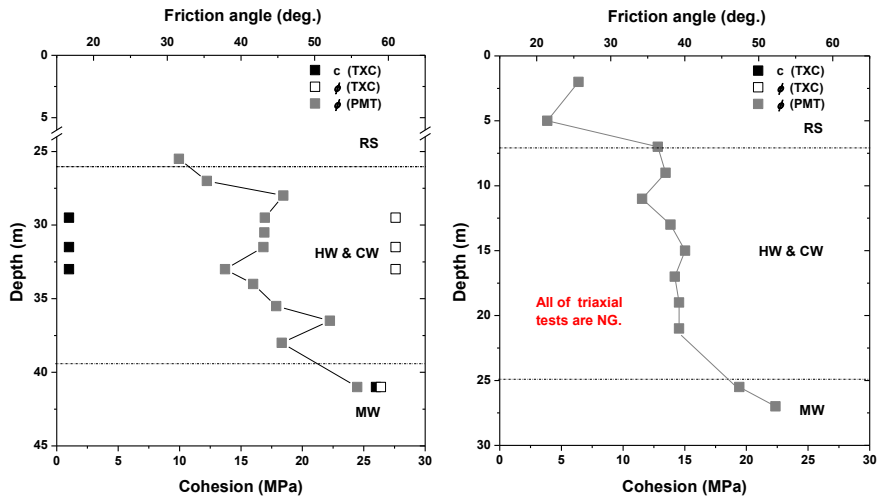
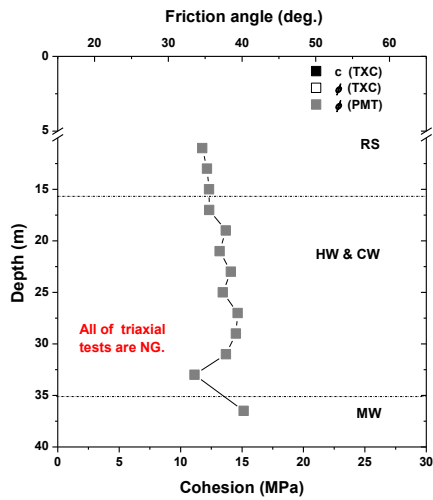


Figure 4-9 Distribution of cohesions suggested in the previous studies



(a) G site

(b) S site



(c) A site

Figure 4-10 Distribution of the equivalent friction angle at each site: (a) G site; (b) S site; (c) A site

Distribution of the equivalent friction angle evaluated using the limit pressure at each site was presented in Figure 4-10. The equivalent friction angles were generally increased at all of the test sites, as the layer changes from residual soil to moderately weathered granite. In G site, the equivalent friction angles were much lower than that of the triaxial compressive test (TXC) results, presumably, because of the size effect of the test material: intact rock cores were used for the triaxial compressive test, and the PMTs were conducted for in situ rock mass.

Comparing the mean value of the equivalent friction angles at each test site, G site had the highest values in the highly and completely weathered layer, and S site and A site had similar values (Table 4-9). On the other hand, the normalized mean value of the equivalent friction angle in highly and completely weathered granite layer was highest in A site and similar in G and S site (Table 4-10). The equivalent friction angles from the first quartile ( $Q_1$ ) to the third quartile ( $Q_3$ ) laid in the range from first quartile ( $Q_1$ ) to the third quartile ( $Q_3$ ) of the friction angles suggested in the previous studies, so the equivalent friction angles seem to be appropriately evaluated.

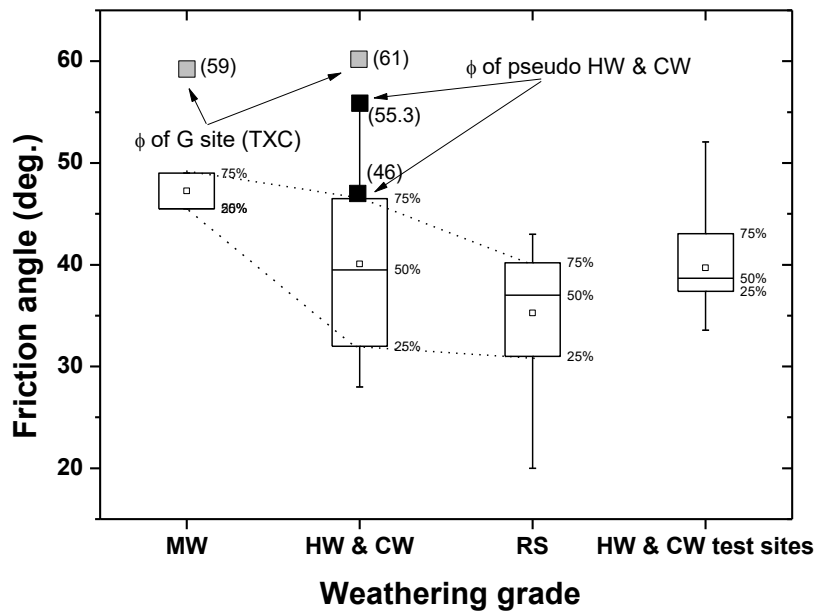


Figure 4-11 Comparison of the equivalent friction angles with the friction angles in previous studies

Table 4-9 Equivalent friction angle evaluated using limit pressure

Property	Layer	G site			S site			A site		
		Min.	Mean	Max.	Min.	Mean	Max.	Min.	Mean	Max.
$\phi$ (deg.)	RS	- *	31.6	-	21.4	23.5	25.7	34.6	35.1	35.5
	HW & CW	35.4	43.3	52.1	34.3	37.9	40.1	33.6	37.4	39.4
	MW	-	55.8	-	47.4	49.8	52.3	-	40.2	-

\* Not measured or invalid

Table 4-10 Normalized mean value of average unconfined compressive strength

Property	Layer	Normalized mean value		
		G site	S site	A site
$\phi$ (deg.)	RS	0.57	0.47	0.87
	HW & CW	0.78	0.76	0.93
	MW	1.00	1.00	1.00

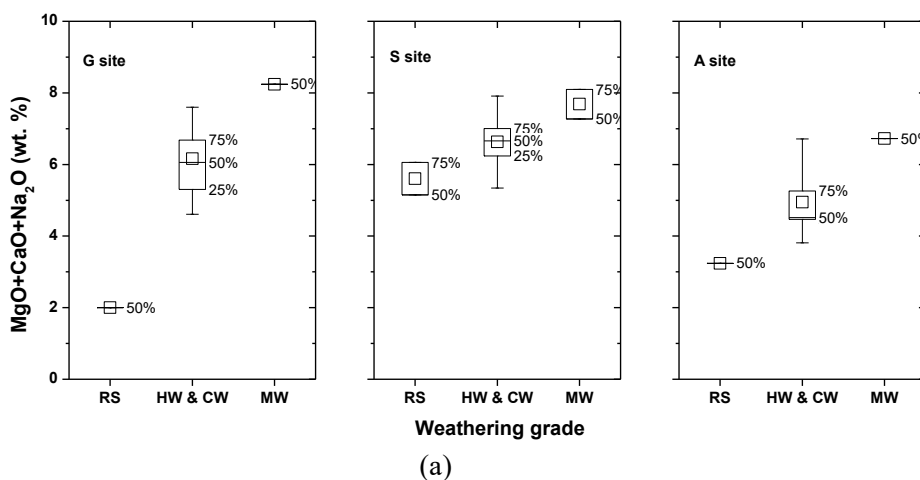


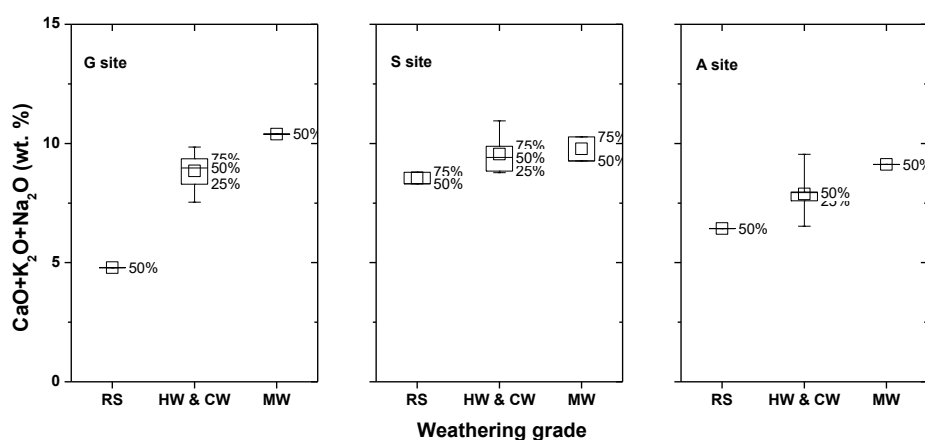
## 4.4 Geochemical Analysis Results

### 4.4.1 Major Oxide Composition

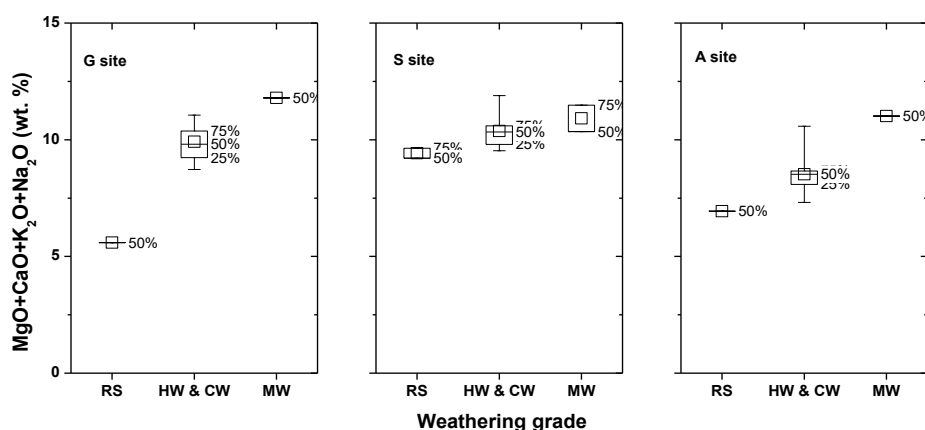
Major oxide composition from residual soil to moderately weathered granite layer at each test site was measured by XRF analysis (Table 4-11, Table 4-12, and Table 4-13). The weight percentages of the major oxide are directly related to a particular chemical weathering index, so it is very important to analyze the major oxide composition for selecting the suitable chemical weathering index representing the degree of weathering.

The composition of alkali and alkaline oxides used in the chemical weathering index equation (see Table 2-3) was analyzed to determine which chemical weathering indices are suitable for representing the degree of weathering (Figure 4-12).





(b)



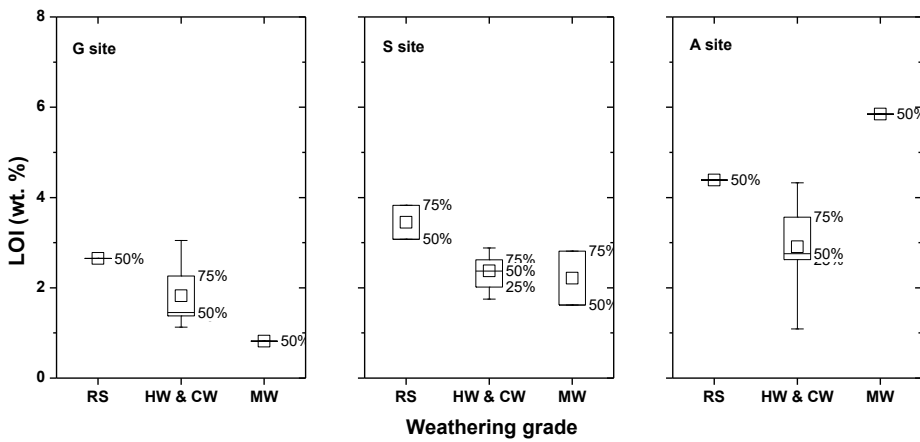
(c)

Figure 4-12 Distribution of the weight percentage of the alkalis and alkaline oxides with weathering grade: (a) used in VR, (b) used in CIA and  $I_{\text{mob}}$ , (c) used in MWPI

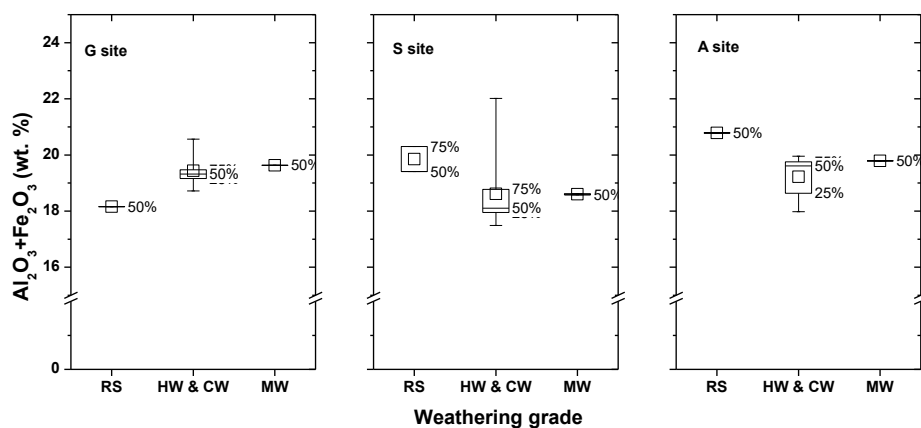
The weight percentage of the alkali and alkaline oxides laid from the first quartile ( $Q_1$ ) to the third quartile ( $Q_3$ ) at each site, which are used for calculating VR, CIA,  $I_{\text{mob}}$ , and MWPI, decreased as layers change from moderately

weathered granite to residual soil (i.e. the composition decreases as weathering intensity increases). This tendency is a general, and VR, CIA,  $I_{mob}$ , and MWPI were developed based on the decrease of the alkalis and alkaline oxide composition, as described in section 2.2.2.

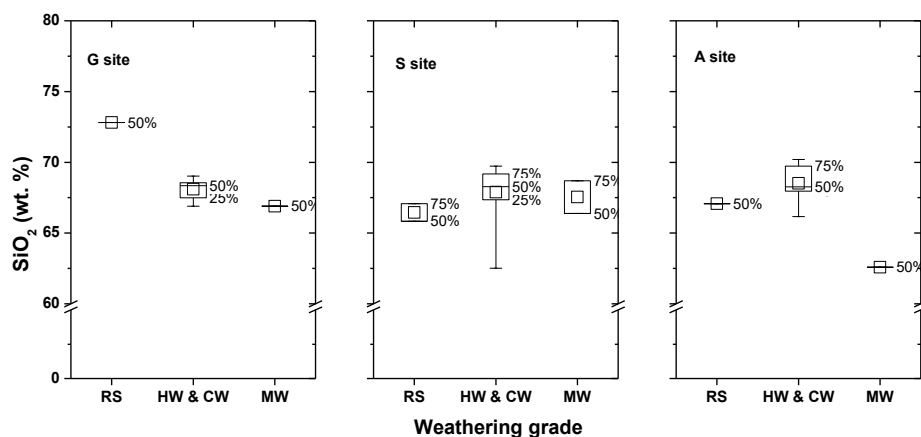
On the other hand, loss on ignition (LOI), sesquioxide containing three atoms of oxygen with two atoms of another element (e.g.,  $Al_2O_3$  and  $Fe_2O_3$ ), and  $SiO_2$  did not show a typical tendency as weathering intensity increases (Figure 4-13); In general, LOI and sesquioxide increase and  $SiO_2$  decreases with weathering intensity, as described in section 2.2.2. So, CWI, PI and RR, which was respectively developed based on the increasing tendency of sesquioxide and the decreasing tendency of  $SiO_2$ , are presumably unsuitable for representing the degree of weathering at all test sites.



(a)



(b)



(c)

Figure 4-13 Distribution of the weight percentage of LOI, sesquioxides, and SiO<sub>2</sub> with weathering grade: (a) used in LOI, (b) used in CWI, (c) used in PI and RR

Table 4-11 Weight percentage of major oxide measured by XRF (G site)

Layer	Depth (m)	Weight percentage of major oxide											
		SiO <sub>2</sub>	Al <sub>2</sub> O <sub>3</sub>	TiO <sub>2</sub>	Fe <sub>2</sub> O <sub>3</sub>	MgO	CaO	Na <sub>2</sub> O	K <sub>2</sub> O	MnO	P <sub>2</sub> O <sub>5</sub>	LOI	Total
RS	25.5	72.82	11.58	0.33	6.58	0.80	0.46	0.74	3.59	0.36	0.08	2.65	99.99
	27.0	69.02	15.90	0.40	3.41	0.89	0.66	3.67	3.96	0.06	0.17	1.82	99.97
	28.0	68.56	15.69	0.42	3.56	0.91	2.03	3.53	3.55	0.06	0.19	1.45	99.95
	29.5	68.39	15.58	0.43	3.59	1.02	2.21	3.46	3.69	0.06	0.18	1.35	99.95
	30.5	68.34	15.31	0.40	3.41	0.84	1.65	3.56	3.75	0.06	0.17	2.45	99.95
	31.5	67.49	15.52	0.47	3.82	1.21	3.00	3.39	3.46	0.06	0.19	1.38	99.98
	33.0	67.76	15.73	0.44	3.75	1.13	2.80	3.36	3.59	0.06	0.18	1.13	99.93
	34.0	67.33	15.45	0.42	4.70	1.19	0.73	2.69	4.12	0.10	0.18	3.05	99.95
	35.5	68.62	15.46	0.45	3.89	1.11	1.02	3.18	3.93	0.06	0.19	1.96	99.86
	36.5	66.90	16.25	0.43	4.31	1.28	0.83	3.69	3.79	0.04	0.18	2.26	99.96
MW	38.0	68.51	15.75	0.42	3.33	1.06	2.05	3.50	3.68	0.04	0.17	1.40	99.90
	41.0	66.89	15.94	0.45	3.69	1.40	3.32	3.52	3.55	0.06	0.17	0.82	99.82

Table 4-12 Weight percentage of major oxide measured by XRF (S site)

Layer	Depth (m)	Weight percentage of major oxide											
		SiO <sub>2</sub>	Al <sub>2</sub> O <sub>3</sub>	TiO <sub>2</sub>	Fe <sub>2</sub> O <sub>3</sub>	MgO	CaO	Na <sub>2</sub> O	K <sub>2</sub> O	MnO	P <sub>2</sub> O <sub>5</sub>	LOI	Total
RS	2.0	65.83	16.44	0.61	3.86	0.90	1.57	2.68	4.06	0.044	0.164	3.83	99.98
	5.0	67.07	15.89	0.50	3.51	0.85	1.58	3.64	3.58	0.073	0.206	3.08	99.98
HW & CW	7.0	67.35	15.23	0.48	3.65	0.78	2.18	3.70	3.76	0.049	0.200	2.59	99.97
	9.0	68.05	15.31	0.47	3.41	0.77	1.67	3.84	3.34	0.044	0.182	2.88	99.97
	11.0	69.73	14.56	0.46	2.93	0.76	1.30	3.36	4.11	0.034	0.174	2.56	99.98
	13.0	68.76	14.82	0.44	3.13	0.71	1.64	4.65	3.59	0.043	0.163	2.02	99.98
	15.0	67.13	15.37	0.52	3.40	0.77	2.03	3.44	4.84	0.042	0.186	2.25	99.98
	17.0	62.52	18.48	0.58	3.54	0.94	1.02	5.95	3.98	0.048	0.192	2.73	99.97
	19.0	68.71	15.16	0.51	2.95	0.72	0.89	3.73	5.12	0.042	0.157	1.99	99.97
	21.0	69.17	14.84	0.48	3.13	0.96	2.12	3.92	2.80	0.037	0.149	2.37	99.98
	23.0	68.28	15.00	0.51	3.33	0.87	2.53	4.16	2.46	0.041	0.158	2.62	99.96
	24.5	69.22	15.18	0.59	2.73	0.92	2.00	4.02	3.39	0.037	0.133	1.75	99.98
	25.5	68.69	14.74	0.51	3.88	1.08	2.67	3.53	3.07	0.050	0.146	1.62	99.99
MW	27.0	66.39	15.45	0.52	3.13	1.21	3.00	3.90	3.39	0.046	0.151	2.81	99.98

Table 4-13 Weight percentage of major oxide measured by XRF (A site)

Layer	Depth (m)	Weight percentage of major oxide											
		SiO <sub>2</sub>	Al <sub>2</sub> O <sub>3</sub>	TiO <sub>2</sub>	Fe <sub>2</sub> O <sub>3</sub>	MgO	CaO	Na <sub>2</sub> O	K <sub>2</sub> O	MnO	P <sub>2</sub> O <sub>5</sub>	LOI	Total
RS	11.0	66.93	16.83	0.68	3.80	0.51	0.64	2.06	3.71	0.053	0.245	4.47	99.92
	13.0	67.71	16.80	0.62	3.73	0.52	0.67	2.10	3.73	0.055	0.242	3.80	99.98
	15.0	67.07	16.81	0.56	3.98	0.51	0.65	2.08	3.70	0.05	0.22	4.39	100.01
HW & CW	17.0	67.96	16.34	0.65	3.32	0.51	0.69	2.99	3.68	0.05	0.22	3.58	99.99
	19.0	69.74	15.03	0.44	2.95	0.61	0.62	3.28	4.32	0.07	0.16	2.76	99.98
	21.0	69.31	15.50	0.56	3.13	0.76	0.48	3.46	3.85	0.04	0.19	2.70	99.99
	23.0	70.20	15.26	0.53	3.11	0.31	0.63	3.75	3.58	0.09	0.19	2.32	99.98
	25.0	66.17	15.78	0.59	3.97	1.03	2.13	3.55	3.87	0.06	0.20	2.63	99.98
	27.0	68.27	16.10	0.54	3.52	0.49	0.76	3.26	3.57	0.04	0.19	3.22	99.97
	29.0	68.22	15.52	0.59	3.78	0.79	0.63	2.39	3.51	0.06	0.20	4.33	100.02
	31.0	69.76	15.90	0.61	3.85	0.57	0.77	3.13	4.05	0.05	0.21	1.09	99.99
	33.0	66.99	16.30	0.59	3.66	0.72	0.80	3.74	3.40	0.02	0.21	3.56	99.99
MW	36.5	62.58	15.81	0.54	3.98	1.89	2.63	2.20	4.29	0.05	0.16	5.85	99.98

#### 4.4.2 Chemical Weathering Indices

The 8 types of chemical weathering indices described in section 2.2.2 were evaluated from residual soil to moderately weathered granite layer at each test site based on the results of the XRF analysis (Table 4-14, Table 4-15, and Table 4-16). Since the chemical weathering indices are affected by the complicated factors such as the types of rock, mineralogical characteristics, and *in situ* conditions, it is very important to analyze the various chemical weathering indices and determine the suitable one representing the degree of weathering in the study area.

The distribution of the chemical weathering indices at each site are presented in Figure 4-16, Figure 4-17, and Figure 4-18 with depth. As described in section 2.2.2, each chemical weathering index has a typical tendency as the weathering intensity increases: VR, CIA,  $I_{mob}$ , LOI, and CWI increase; PI, RR, and MWPI decrease. Comparing the tendency presented at each test site with the ideal tendency, the suitable chemical weathering indices well representing the degree of weathering at each site could be presumably identified.

In G site, VR, CIA,  $I_{mob}$ , LOI, and CWI showed a generally decreasing tendency as the layers change from residual soil to moderately weathered granite, and these indices, also, locally increased at a depth of 34 m. The distribution of MWPI well represented the weathering profile described above, but PI and RR rarely changed below a depth of 27 m, especially RR showed the highest value in the residual soil layer in spite of the decreasing ideal tendency as weathering intensity increased. In S site, VR, CIA,  $I_{mob}$ , and MWPI presented



a similar weathering profile, but LOI and CWI, whose ideal tendency is the same with VR, CIA, and  $I_{mob}$ , showed the weathering profile in reverse below a depth of 17 m. Also, the PI was nearly constant in all the layers, and RR showed the opposite tendency with MWPI in spite of the same ideal tendency with respect to weathering. In A site, the distributions of each chemical weathering indices were very similar those of the G site and S site: VR, CIA,  $I_{mob}$ , and MWPI reasonably represented the weathering profile, because these indices assessed the layer was less weathered as it changes from residual soil to moderately weathered granite; PI was nearly constant in all the layers; RR showed the opposite tendency with MWPI. Therefore, it seems that VR, CIA,  $I_{mob}$ , and MWPI rationally evaluated the degree of weathering of the weathered granite in the all the test sites, and the suitable chemical weathering indices, also, can be confirmed by examining whether the tendency of the weathering index according to the weathering grade is the same at all the test sites (Figure 4-17, Figure 4-18).

The reason why VR, CIA,  $I_{mob}$ , and MWPI represent the degree of weathering better than PI and RR can be found out from the results of the major oxide analysis described in section 4.4.1. As presented in Figure 4-12, the composition of alkalis and alkaline oxide used to calculate VR, CIA,  $I_{mob}$ , and MWPI continuously decreased as the layers changed from moderately weathered granite to residual soil, which corresponds to the basic assumption used for developing VR, CIA,  $I_{mob}$ , and MWPI. On the other hand, the compositions of  $SiO_2$ , sesquioxides, and LOI did not always correspond to the basic assumption used for developing PI, RR, LOI, and CWI. The assumptions

applied to each chemical weathering index were described in section 2.2.2.

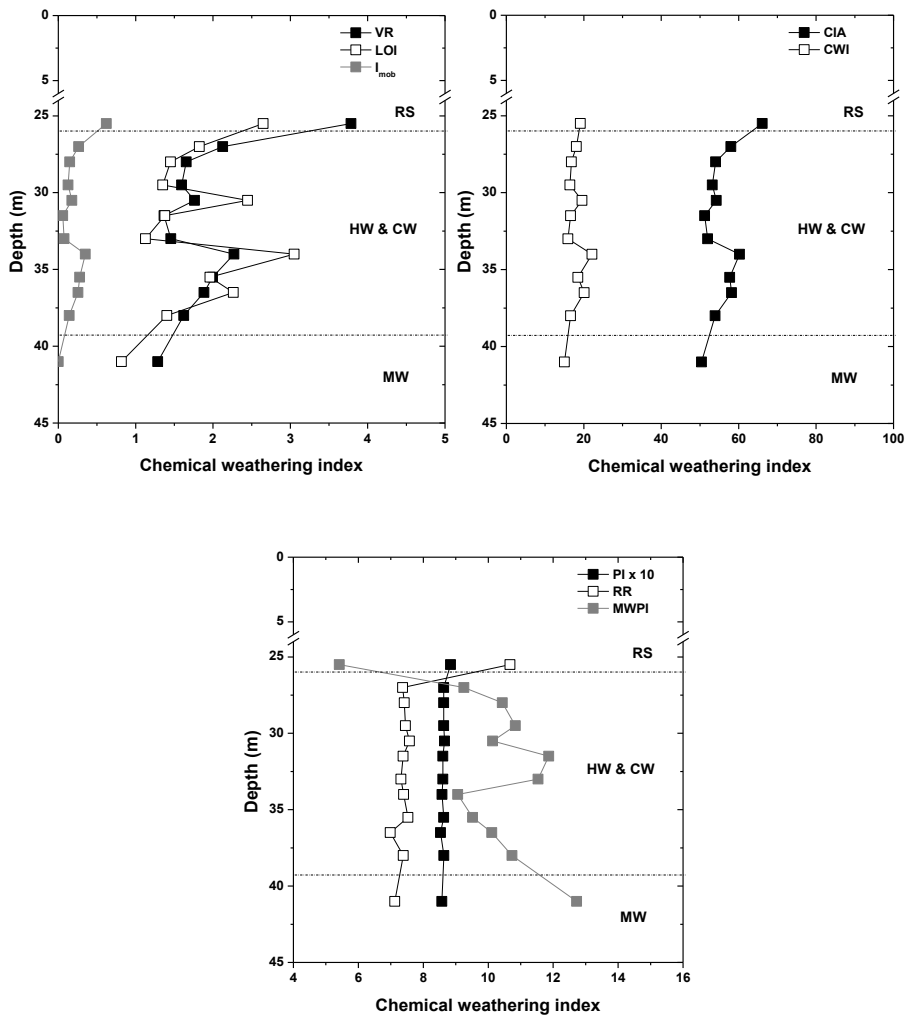


Figure 4-14 Distribution of the chemical weathering indices evaluated at G site

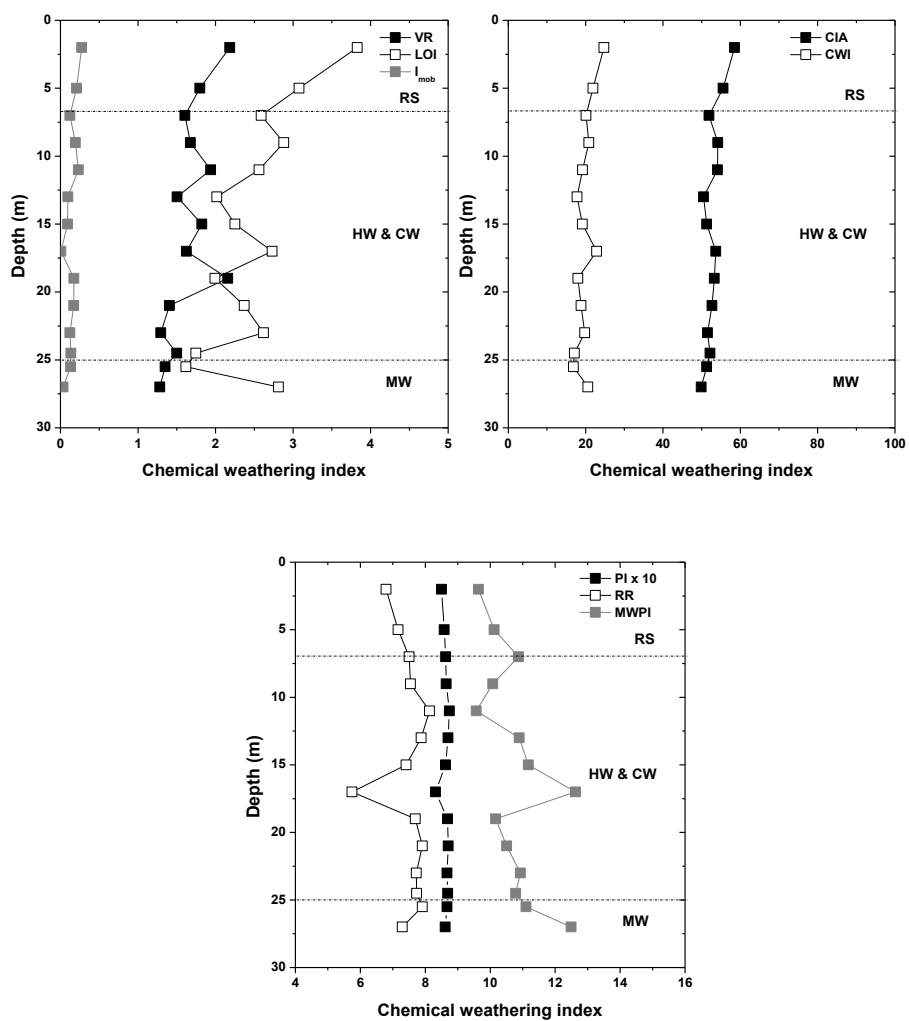


Figure 4-15 Distribution of the chemical weathering indices evaluated at S site

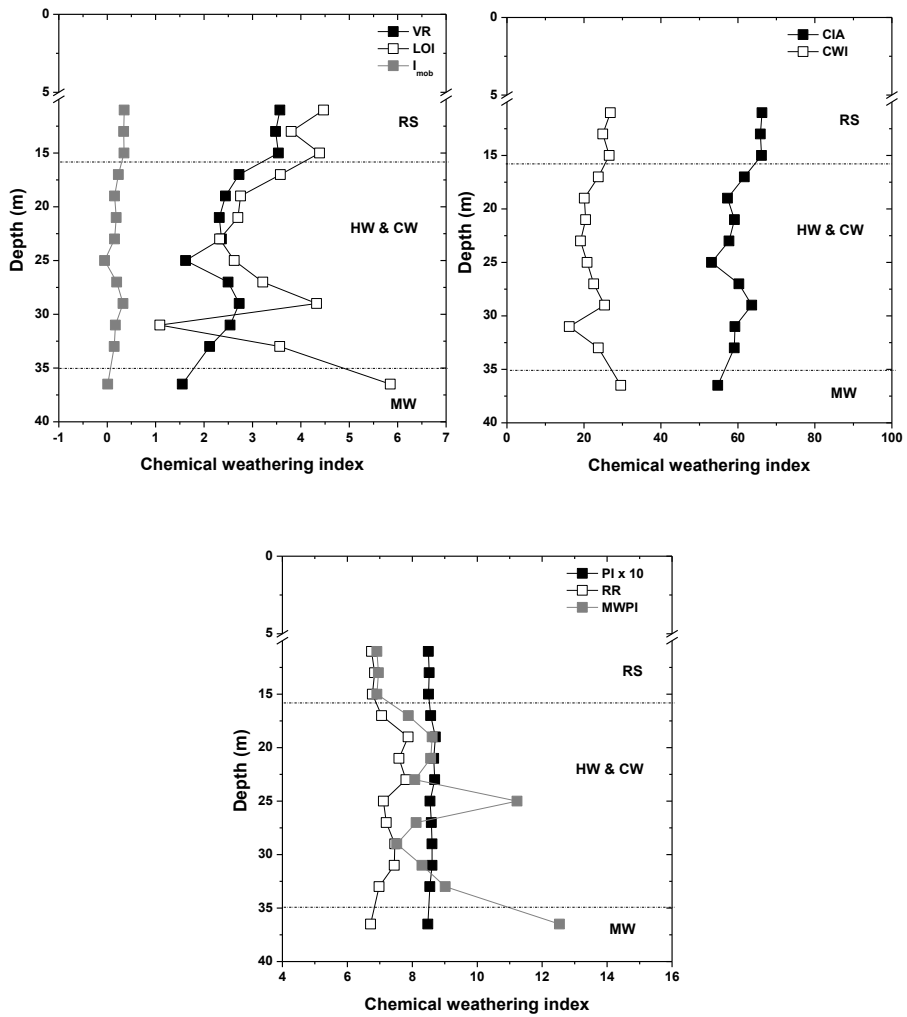
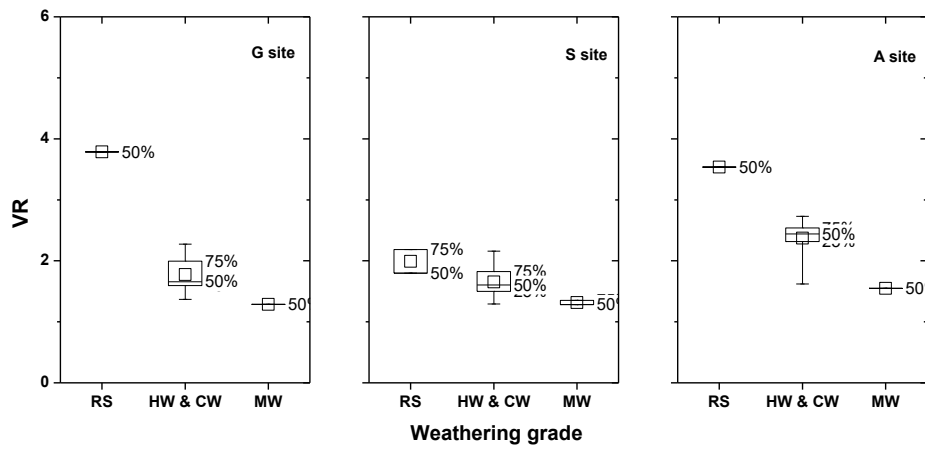
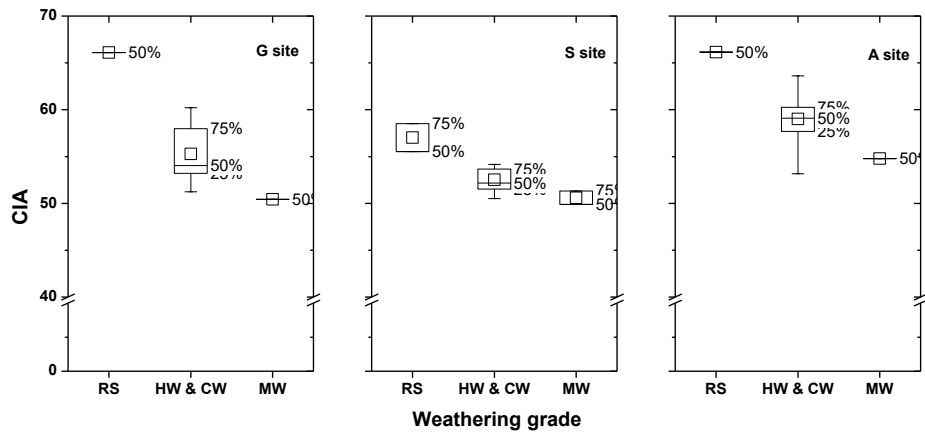


Figure 4-16 Distribution of the chemical weathering indices evaluated at A site

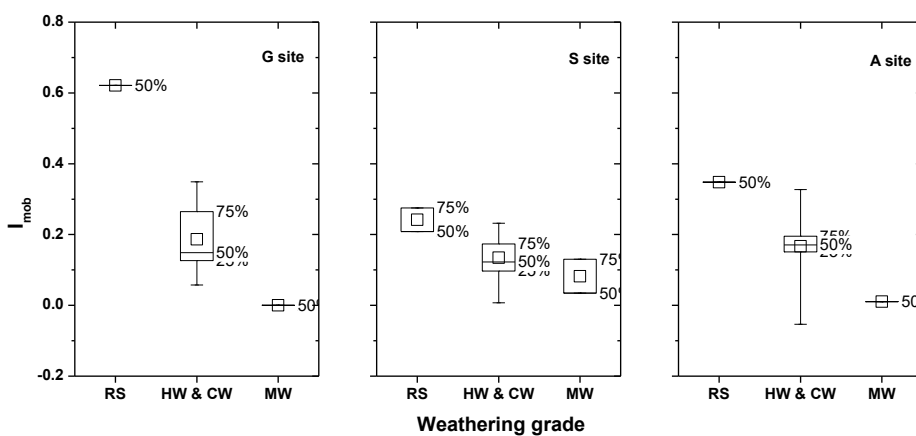


(a)

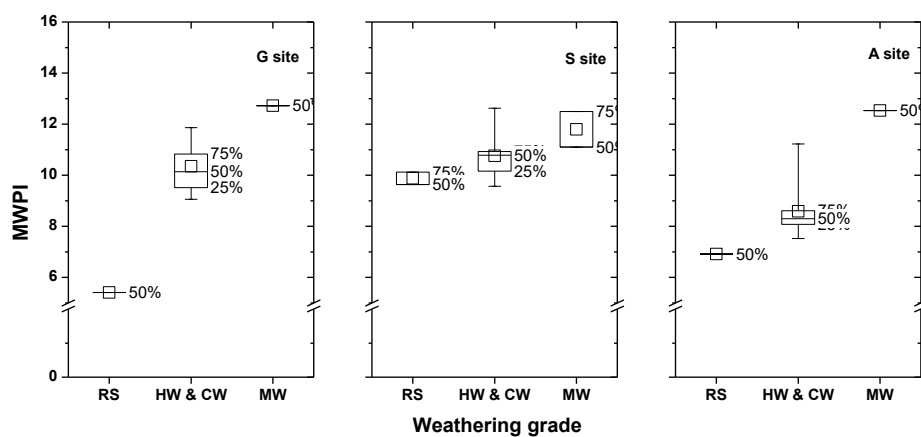


(b)

Figure 4-17 Distribution of the chemical weathering indices with weathering grade : (a) VR, (b) CIA, (c)  $I_{mob}$ , (d) MWPI (continue on next page)

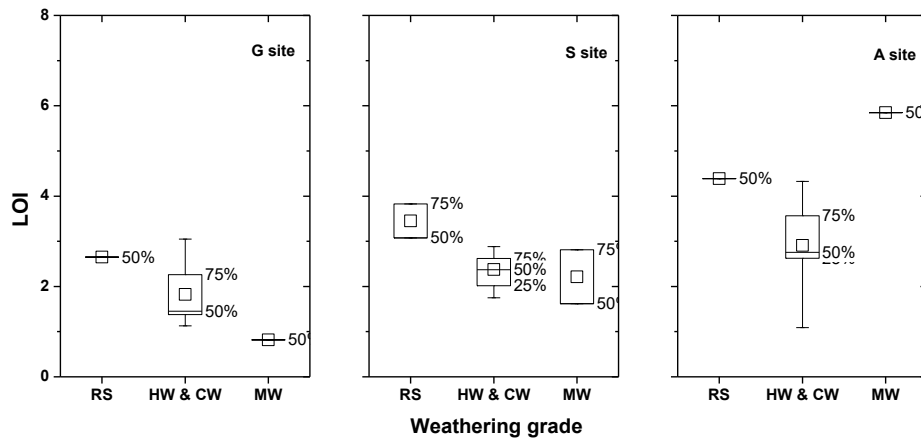


(c)

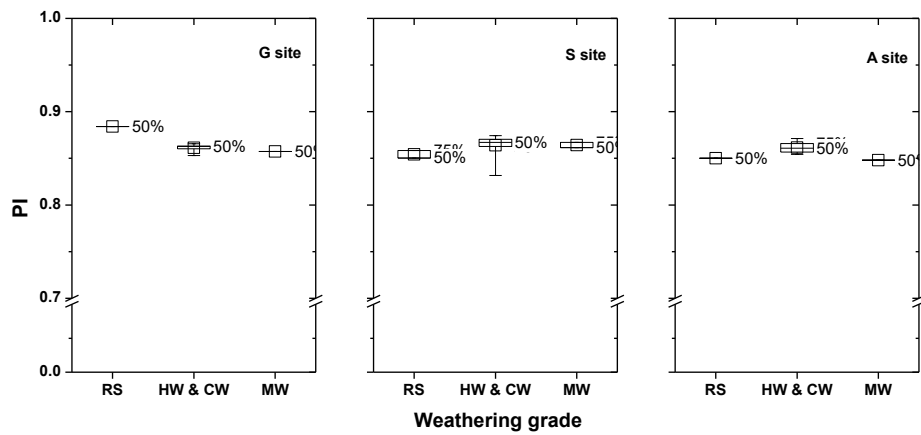


(d)

Figure 4-17 Distribution of the chemical weathering indices with weathering grade : (a) VR, (b) CIA, (c)  $I_{mob}$ , (d) MWPI

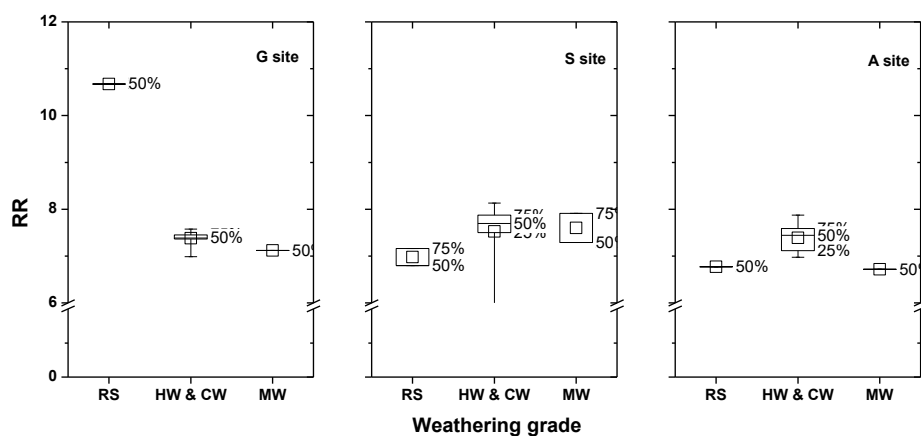


(a)

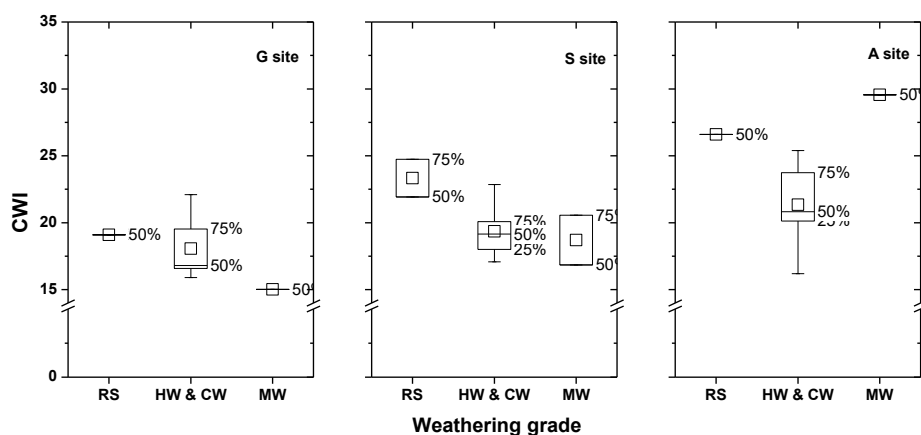


(b)

Figure 4-18 Distribution of the chemical weathering indices with weathering grade : (a) LOI, (b) PI, (c) RR, (d) CWI (*continue on next page*)



(c)



(d)

Figure 4-18 Distribution of the chemical weathering indices with weathering grade : (a) LOI, (b) PI, (c) RR, (d) CWI



Table 4-14 Chemical weathering indices (G site)

Layer	Depth (m)	Chemical weathering indices							
		VR	CIA	LOI	I <sub>mob</sub>	PI	RR	MWPI	CWI
RS	25.5	3.785	66.094	2.649	0.621	0.884	10.672	5.413	19.100
HW & CW	27.0	2.127	57.980	1.824	0.265	0.863	7.364	9.253	18.071
	28.0	1.655	54.037	1.452	0.149	0.863	7.417	10.436	16.806
	29.5	1.594	53.214	1.351	0.126	0.863	7.452	10.834	16.429
	30.5	1.762	54.215	2.447	0.175	0.866	7.576	10.137	19.529
	31.5	1.368	51.236	1.377	0.057	0.861	7.377	11.864	16.584
	33.0	1.456	52.013	1.128	0.074	0.860	7.312	11.538	15.903
	34.0	2.273	60.216	3.050	0.349	0.858	7.397	9.060	22.102
	35.5	1.995	57.705	1.960	0.277	0.863	7.531	9.518	18.460
	36.5	1.883	58.178	2.262	0.254	0.853	6.985	10.113	20.101
	38.0	1.623	53.912	1.403	0.141	0.863	7.383	10.735	16.580
MW	41.0	1.287	50.428	0.816	0.000	0.857	7.120	12.725	15.017

Table 4-15 Chemical weathering indices (S site)

Layer	Depth (m)	Weight percentage of major oxide							
		VR	CIA	LOI	I <sub>mob</sub>	PI	RR	MWPI	CWI
RS	2.0	2.185	58.516	3.828	0.275	0.850	6.795	9.637	24.733
	5.0	1.799	55.538	3.077	0.209	0.858	7.162	10.122	21.919
HW & CW	7.0	1.605	51.905	2.588	0.122	0.863	7.503	10.874	20.086
	9.0	1.676	54.158	2.881	0.194	0.865	7.543	10.080	20.850
	11.0	1.937	54.109	2.561	0.232	0.874	8.130	9.569	19.183
	13.0	1.505	50.511	2.017	0.097	0.870	7.872	10.892	17.780
	15.0	1.824	51.301	2.251	0.093	0.862	7.413	11.176	19.149
	17.0	1.625	53.661	2.730	0.007	0.832	5.741	12.624	22.856
	19.0	2.159	53.274	1.994	0.173	0.868	7.694	10.165	18.007
	21.0	1.405	52.673	2.370	0.171	0.871	7.910	10.507	18.803
	23.0	1.294	51.532	2.619	0.123	0.867	7.725	10.930	19.761
	24.5	1.500	52.167	1.748	0.134	0.869	7.736	10.782	17.082
MW	25.5	1.350	51.312	1.618	0.130	0.867	7.910	11.102	16.843
	27.0	1.282	49.886	2.811	0.034	0.862	7.290	12.493	20.564

Table 4-16 Chemical weathering indices (A site)

Layer	Depth (m)	Weight percentage of major oxide							
		VR	CIA	LOI	I <sub>mob</sub>	PI	RR	MWPI	CWI
RS	11.0	3.568	66.264	4.470	0.350	0.849	6.748	6.909	26.861
	13.0	3.480	65.855	3.800	0.340	0.852	6.839	6.957	24.889
	15.0	3.536	66.139	4.388	0.348	0.850	6.773	6.912	26.590
HW & CW	17.0	2.725	61.675	3.579	0.230	0.857	7.058	7.880	23.745
	19.0	2.441	57.302	2.755	0.151	0.871	7.874	8.612	20.117
	21.0	2.316	59.088	2.701	0.186	0.866	7.588	8.568	20.431
	23.0	2.362	57.681	2.322	0.151	0.869	7.804	8.077	19.128
	25.0	1.620	53.172	2.626	-0.054	0.855	7.114	11.225	20.828
	27.0	2.497	60.259	3.215	0.195	0.859	7.198	8.122	22.541
	29.0	2.729	63.610	4.327	0.327	0.861	7.460	7.522	25.393
	31.0	2.539	59.246	1.089	0.171	0.861	7.445	8.301	16.189
	33.0	2.118	59.078	3.564	0.144	0.854	6.976	9.018	23.751
	36.5	1.550	54.782	5.849	0.011	0.848	6.717	12.531	29.563

## 4.5 Discussion of Geotechnical Properties

### 4.5.1 Comparative study

In this section, the geotechnical properties of the highly and completely weathered granite measured at each test site were compared with the values suggested in the various classification criteria that were presented in chapter 2 and previous researches.

The pressuremeter modulus measured at all test sites were compared with the classification criterion suggested in site investigation manual (Seoul, 2006), and the previous researches for weathered granite in South Korea (Seo et al., 2016; Lee et al., 2001). As shown in Figure 4-19, the  $E_m$  measured at S site and A site showed a similar range with that of the previous study performed by Lee et al (2001). On the other hand, the  $E_m$  measured at G site were much higher than the range of the  $E_m$  suggested in the previous researches, it was presumably due to the higher overburden pressure. However, the effect of the overburden pressure on the  $E_m$  of the highly and completely weathered granite is likely to be still vague, because the range of the  $E_m$  measured at A was a little lower than that of the S site which has a higher overburden pressure.

As presented in Figure 4-19, also, the range of the  $E_m$  suggested by Seoul (2006) is narrow (100 MPa - 200 MPa) comparing to the measured  $E_m$ . Since many engineers still apply the  $E_m$  suggested in the criterion as an input parameter of numerical analysis, it would be advisable to be modified with considering the measured  $E_m$  in further.

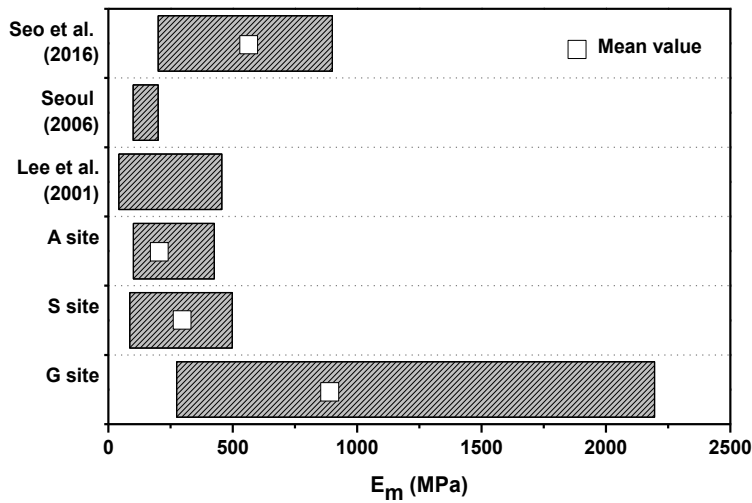


Figure 4-19 Comparison of pressuremeter modulus ( $E_m$ )

Also, the unit weight ( $\gamma_t$ ), P-wave velocity ( $V_p$ ), and S-wave velocity ( $V_s$ ) measured at all test sites using geophysical tests were compared with those suggested in classification criteria and previous researches (Figure 4-20 to Figure 4-22). The measured  $\gamma_t$  showed a little different with test sites but the range of the measured  $\gamma_t$  was from 20 kN/m<sup>3</sup> to 25 kN/m<sup>3</sup>. The measured  $V_p$  at all test sites were within the classification criteria except for the criterion suggested by KRANA (2011) in which the range of  $V_p$  is relatively low compared to the other criteria. Since any criteria did not include  $V_s$  as a classification property, the measured  $V_s$  were compared with the previous research about the representative  $V_s$  for the subsurface layer in South Korea (Sun et al., 2012). As presented in Figure 4-22, the range of the  $V_s$  measured at S site and A site was similar to the previous research, but that of the G site was relatively higher. The higher  $V_p$  and  $V_s$  of the G site is presumably due to the higher overburden pressure but it is still vague as described in the discussion of

the  $E_m$ :  $V_p$  and  $V_s$  of the S site was higher than that of the A site.

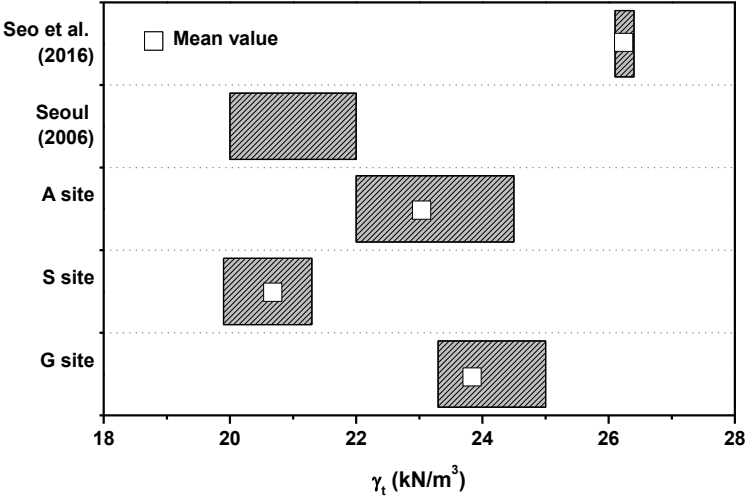


Figure 4-20 Comparison of unit weight ( $\gamma_t$ )

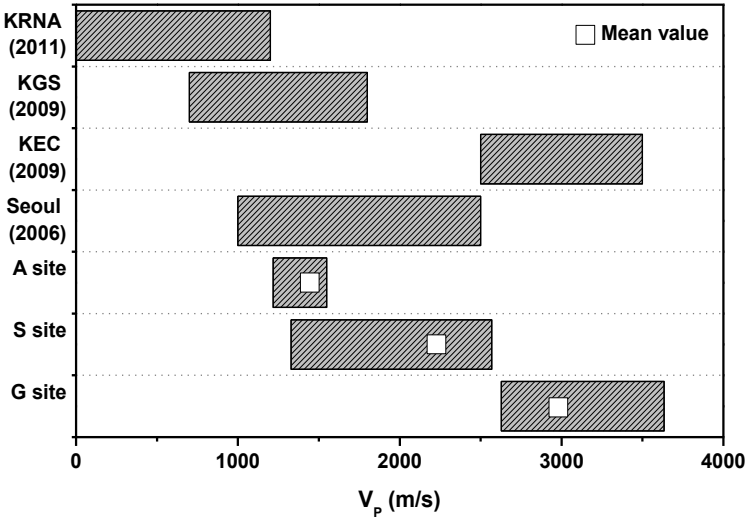


Figure 4-21 Comparison of P-wave velocity ( $V_p$ )

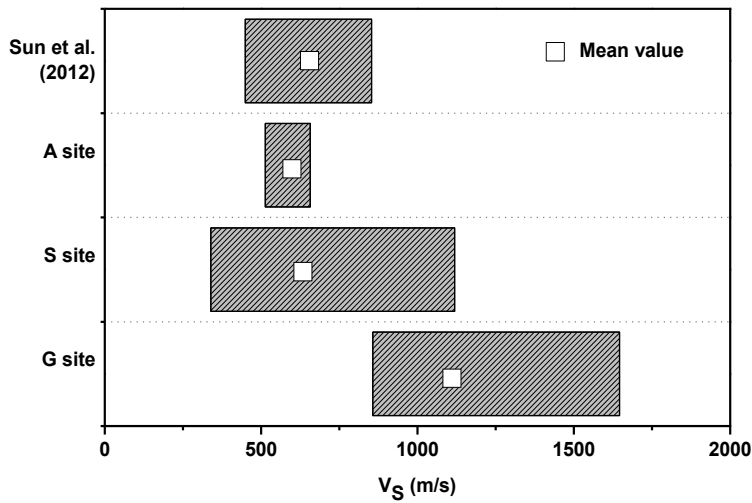


Figure 4-22 Comparison of S-wave velocity ( $V_s$ )

The most of the unconfined compressive strengths ( $q_u$ ) measured at all test sites were below 10 MPa, which are similar to the previous classification criteria and researches. However, the criteria suggested by KGS (2009) and KEC (2009) are much higher than the measured  $q_u$ . It is not appropriate for applying the highly and completely weathered granite, considering the suitable specimens for the uniaxial test are rarely retrieved. So, it would be advisable to be modified with considering the measured  $q_u$  in further (Figure 4-23).

The equivalent friction angles ( $\phi_{\text{equi.}}$ ) interpreted using the limit pressure ( $P_L$ ) were included in the range of friction angles suggested by the previous researches but were little higher than those suggested by Seoul (2006). Considering the SPT-N value of the highly and completely weathered rock, which is higher than 50, the criterion suggested by Seoul (2006) seems to be conservative (Figure 4-24 and Table 4-17).

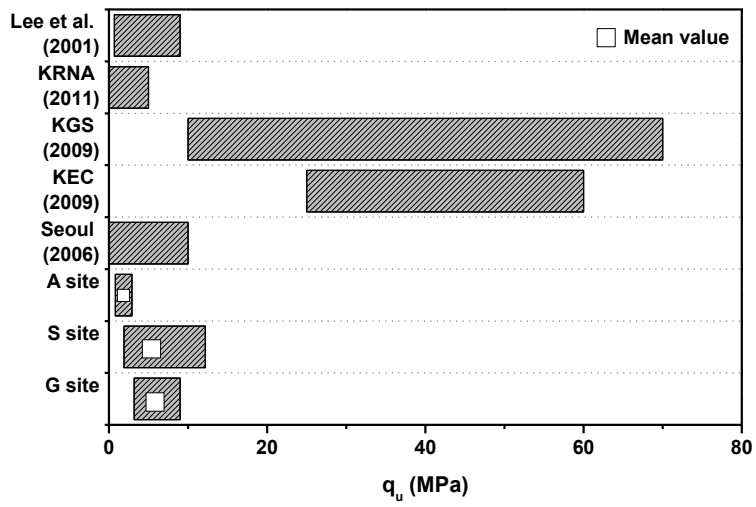


Figure 4-23 Comparison of unconfined compressive strength ( $q_u$ )

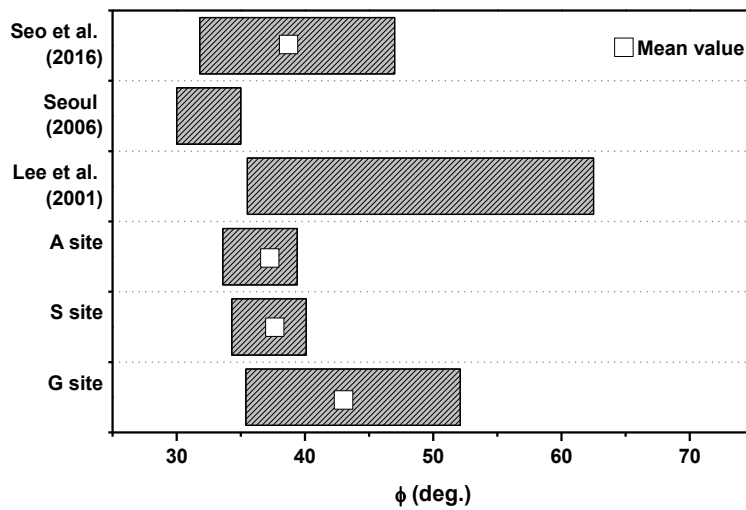


Figure 4-24 Comparison of equivalent friction angle ( $\phi_{\text{equi.}}$ )



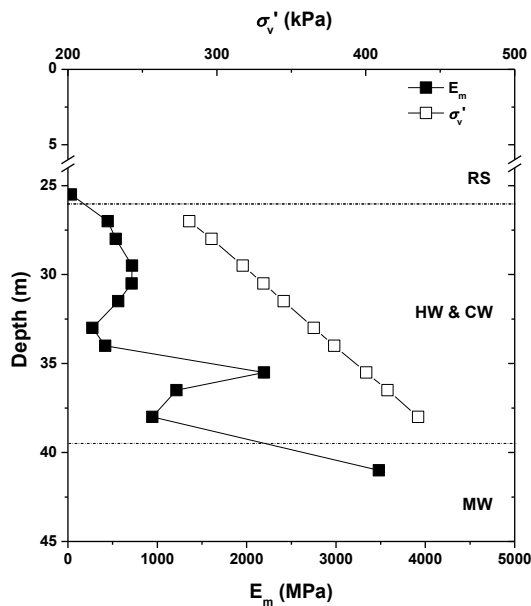
Table 4-17 Relationship between SPT-N and friction angle of sand (Terzaghi and Peck, 1948)

SPT-N <sub>60</sub>	Friction angle (deg.)	
	Peck	Meyerhof
0 ~ 4	< 28.5	< 30
4 ~ 10	28.5 ~ 30.0	30 ~ 35
10 ~ 30	30.0 ~ 36.0	35 ~ 40
30 ~ 50	36.0 ~ 41.0	40 ~ 45
> 50	> 41.0	> 45

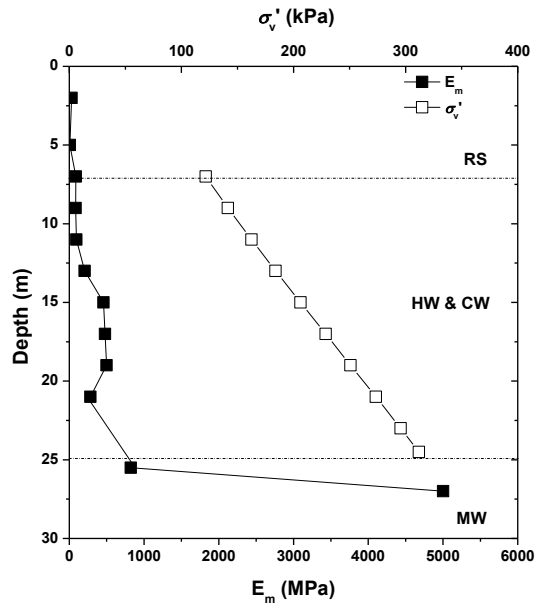
In summary, the quantitative classification criteria are very different with the institutions, so many engineers are likely to be confused in determining the subsurface layer or geotechnical properties as input parameters for numerical analysis or design. The geotechnical properties of the highly and completely weathered rock. Also, the highly and completely weathered granite has a wide range of geotechnical properties values resulted from its location, the characteristics of its parent rock, and surrounding conditions, so it is necessary that the degree of weathering and site-specific characteristics should be considered.

#### 4.5.2 Soil – Rock Transition State

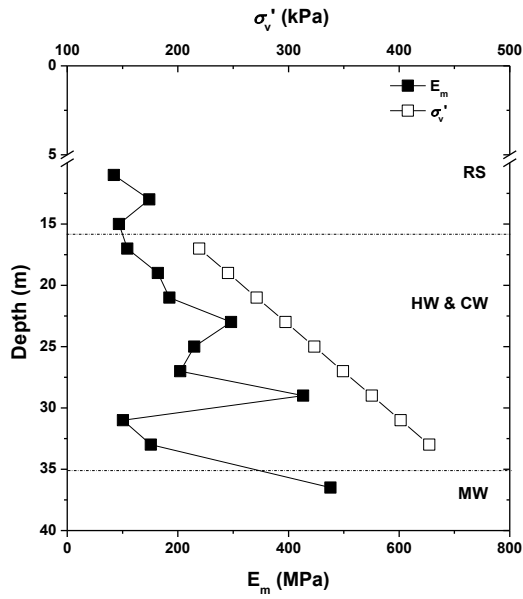
As described in chapter 1, the highly and completely weathered rock is an intermediate geo-material that shows the soil-rock transitional characteristics. It is known that the geotechnical properties of soil are affected by the vertical effective stress ( $\sigma_v'$ ): the properties usually increased with the vertical effective stress. However, the properties of the highly and completely weathered granite measured at each test site were not showed a typical distribution with vertical effective stress. It is showed that the properties were decreased or dramatically increased in spite of the linear increase of vertical effective stress. This irregular tendency, especially, was observed in the distribution of the pressuremeter modulus (Figure 4-25), it is presumably due to the effect of the weathering.



(a)



(b)



(c)

Figure 4-25 Distribution both  $E_m$  and  $\sigma_v'$ : (a) G site; (b) S site; (c) A site

The SPT-N measured by standard penetration test has been generally applied to estimate the geotechnical properties of soil material. SPT (Standard penetration test) has been usually applied in site investigation of the highly and completely weathered rock layer, so many engineers have been using the relationship between SPT-N and geotechnical properties of the weathered rock. To examine the applicability of the relationship, several empirical equations of geotechnical properties derived using SPT-N were compared with the measured properties at all test sites. The applied empirical equations are presented from Table 4-18 to Table 4-20.

Most of the measured pressuremeter modulus were lower than that calculated using the equations suggested by Schmertmann (1978), and the estimated pressuremeter modulus using the equation suggested by Yoshinaka (1968) were similar to those of median in the same SPT-N level (Figure 4-26 (a)). However, the variation of measured pressuremeter modulus was increased in which the SPT-N was larger than 300 blows. In addition, several measured pressuremeter modulus at G site were not included (the number of data: 6) because SPT could not penetrate below the depth of 31 m, so the variation maybe increases, if the missed data would be included.

All empirical equations for friction angle overestimated the friction angle of the highly and completely weathered granite (Figure 4-26 (b)). It is because that the equations were derived using the test results of sand, so very high or unreasonable friction angles will be calculated when SPT-N of the highly and completely weathered rock is just applied to the equations. So, it would be advisable to be modified with considering the measured friction angles in

further.

The estimated S-wave velocities using the equations suggested by Imai (1977) and Sun et al. (2008) were similar to the measured S-wave velocities because these equations were derived using the test results conducted in all soil including the highly and completely weathered rock. However, the other equations derived using the test results of silty sand soils overestimated the S-wave velocities of the highly and completely weathered granite with the same reason described in the discussion of the friction angle.

Table 4-18 Empirical equations of  $E_m$ .

Researcher	$E_m$ (MPa)
Yoshinaka (1968)	$7N$
Schmertmann (1978)	$\alpha N$

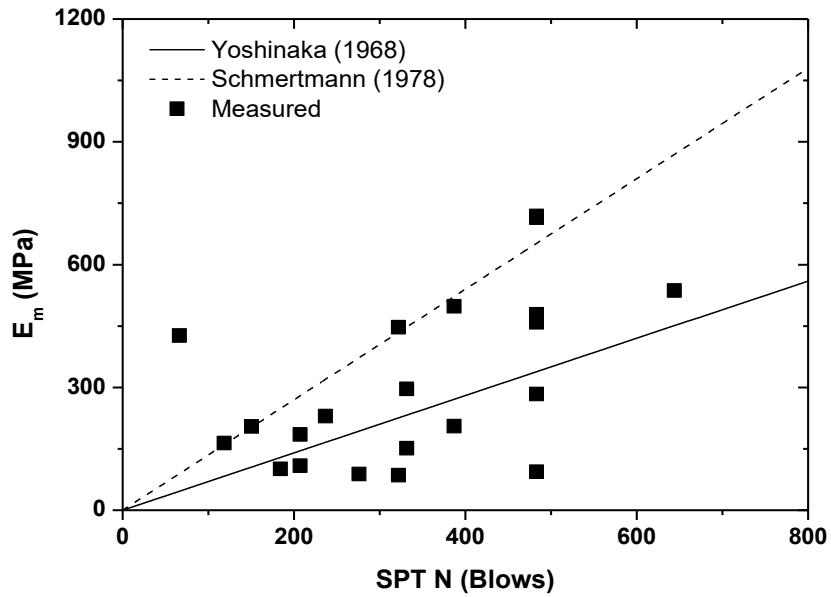
\*  $\alpha = 4$  (silt or sandy silt), 7 (medium sand), 10 (coarse sand), and 12 ~ 15 (sandy gravel, gravel). In this study,  $\alpha = 13.5$  was applied.

Table 4-19 Empirical equations of  $\phi$ .

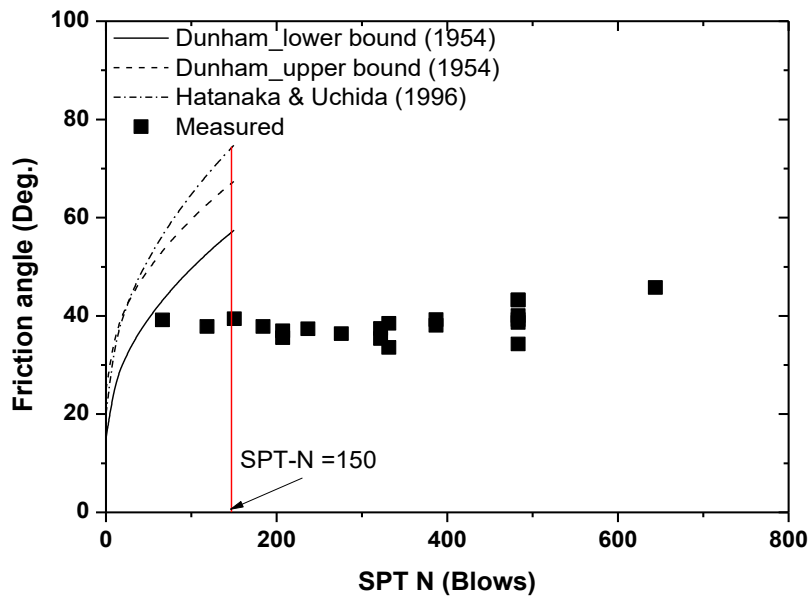
Researcher	$\phi$ (deg.)
Duham (1954)	$\sqrt{12N} + 15$ (lower bound)
	$\sqrt{12N} + 25$ (upper bound)
Hatanaka & Uchida (1996)	$\sqrt{20N} + 25$

Table 4-20 Empirical equations of  $V_s$ .

Researcher	$V_s$ (m/s)
Imai (1977)	$91N^{0.337}$
Chein et al. (2000)	$22N^{0.76}$
Jafari et al. (2002)	$19N^{0.85}$
Sun et al. (2008)	$65.64N^{0.457}$



(a)



(b)

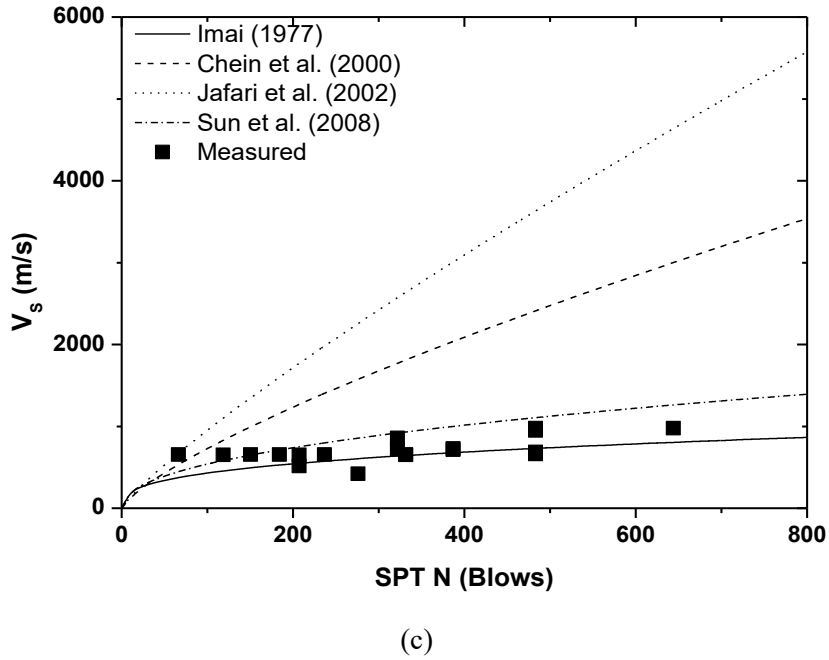


Figure 4-26 Relationship between geotechnical properties and SPT  $N$ : (a)  $E_m$ ; (b)  $\phi$ ; (c)  $V_s$

Many rock mechanical engineers have been developed the empirical equations for evaluating the rock mass mechanical properties. As presented in Table 4-21 and

Table 4-22, the equations used unconfined compressive strength of intact rock, rock mass rating (RMR), and rock quality designation (RQD) as parameters. Using the measured parameters in this study such as unconfined compressive strength and RQD, the RMR of the highly and completely weathered granite was 12, and the geological strength index (GSI) was 10 based on Figure 4-27. The  $E_m$  and  $\phi$  estimated using the previously suggested empirical equations, and the results were presented in Table 4-23 and Table 4-24. The estimated  $E_m$  using



the equations except for that suggested by Aydan (1997) were included in the range of the  $E_m$  measured at all test sites. However, the friction angles estimated using the previously suggested equation were very low, which was not reasonable for the highly and completely weathered granite. Also, the RMR and GSI was a rough method to evaluate the characteristics of highly and completely weathered rock because its many parameters used in RMR and GSI are rarely obtained; the suitable specimens for uniaxial compressive strength tests are rarely retrieved, and the RQD of highly and completely weathered rock is considered as zero as described in ASTM D6032. Therefore, it is not appropriate to apply the equations presented in Table 4-21 and Table 4-22 to the highly and completely weathered rock.

In summary, it is vague that the empirical equations derived for soil or rock are applied to the highly and completely weathered rock, which is the soil-rock transition state, for evaluating its geotechnical properties. So, in this study, the estimation method of the highly and completely weathered rock was newly proposed and applied to the geotechnical properties measured at all the test sites. The details about the estimation method were specifically described in chapter 5.

Table 4-21 Empirical equations of  $E_m$ 

Researcher	$E_m$ (GPa)
Bieniawski (1978)	$10^{(RMR-10)/40}$ (RMR < 50)
Kim (1993)	$0.3e^{0.07 RMR}$
Aydan (1997)	$0.0097 RMR^{3.54} \times 10^{-3}$
Hoek & Brown (1998)	$\sqrt{\frac{\sigma_c}{100}} \times 10^{\left(\frac{GSI-10}{40}\right)}$

\*  $\sigma_c$  is an unconfined compressive strength of intact rock (in MPa),  $\sigma_c < 100$  MPa.

Table 4-22 Empirical equations of  $\phi$ 

Researcher	$\phi$ (Deg.)
Trueman (1986)	$0.5RMR + 5$
Bieniawski (1989)	$-0.086 + 0.7891RMR - 0.0031RMR^2$
Kim (1993)	$0.25RMR + 27.5$
Honisch (1994)	$17 + 0.25RQD$


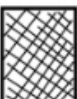




GEOLOGICAL STRENGTH INDEX FOR JOINTED ROCKS		SURFACE CONDITIONS				
		VERY GOOD	GOOD	FAIR	POOR	VERY POOR
STRUCTURE		DECREASING SURFACE QUALITY →				
	INTACT OR MASSIVE—intact rock specimens or massive in situ rock with few widely spaced discontinuities	90	80	70	60	50
	BLOCKY—well interlocked undisturbed rock mass consisting of cubical blocks formed by three intersecting discontinuity sets					
	VERY BLOCKY—interlocked, partially disturbed mass with multi-faceted angular blocks formed by 4 or more joint sets	40	30	20	10	0
	BLOCKY/DISTURBED/SEAMY—folded with angular blocks formed by many intersecting discontinuity sets. Persistence of bedding planes or schistosity					
	DISINTEGRATED—poorly interlocked, heavily broken rock mass with mixture of angular and rounded rock pieces	0	0	0	0	0
	LAMINATED/SHEARED—Lack of blockiness due to close spacing of weak schistosity or shear planes					

Figure 4-27 Chart for determining GSI (Hoek and Brown, 1997)

Table 4-23 Estimated  $E_m$ 

Researcher	$E_m$ (MPa)
Bieniawski (1978)	1122
Kim (1993)	695
Aydan (1997)	64
Hoek & Brown (1998)	298

\*  $\sigma_c$  is an unconfined compressive strength of intact rock (in MPa),  $\sigma_c < 100$  MPa.

Table 4-24 Estimated  $\phi$ 

Researcher	$\phi$ (Deg.)
Trueman (1986)	11
Bieniawski (1989)	9
Kim (1993)	30
Honisch (1994)	17

## **Chapter 5. Proposed Method for Estimating Geotechnical Properties**

### **5.1 Correlation Analysis**

To evaluate the relationship between the geotechnical properties of highly and completely weathered granite, the correlation analysis between the property ratio ( $R_p$ ) and the weathering index ratio ( $R_w$ ) was conducted. The  $R_p$  and  $R_w$  are defined in section 3.5.

$R_p$  values for each geotechnical property were calculated using the in situ test results and  $R_w$  values for the VR, CIA,  $I_{mob}$ , and MWPI, which well represented the degree of weathering at all the test sites, were determined by the chemical weathering indices results of the retrieved sample. Then, the curve fitting parameter  $k$  values defining the relationship between  $R_p$  and  $R_w$  for given sets of calculated data ( $R_p$  and  $R_w$ ) were obtained by choosing the best fit curve (i.e., minimizing the root mean square error, RMSE). From Figure 5-1 to Figure 5-4 shows the correlation between  $R_p$  and  $R_w$ , and Table 5-1 lists the  $k$  value and coefficient of determination ( $R^2$ ) calculated using each chemical weathering index. For the sake of simplicity, each geotechnical property and chemical weathering index used to calculate  $R_p$  and  $R_w$  is shown in brackets (e.g.  $R_p (E_m)$ , and  $R_w (VR)$  mean the property ratio of  $E_m$  and the weathering index ratio of VR, respectively).

The correlations between  $R_p$  and  $R_w$  were analyzed in four categories as

suggested by Rigopoulos et al. (2015): weak ( $R^2 < 0.5$ ), moderate ( $0.5 \leq R^2 < 0.7$ ), strong ( $0.7 \leq R^2 < 0.9$ ), and very strong ( $0.9 \leq R^2$ ). The  $R_P(E_m)$ , and  $R_P(G_{max})$  showed almost very strong correlations with  $(R_W)^k$  calculated through the VR, CIA,  $I_{mob}$ , and MWPI ( $0.88 \leq R^2 \leq 0.93$ ), and the  $R_P(E_{ur})$ ,  $R_P(P_L)$ ,  $R_P(V_s)$ , and  $R_P(q_u)$  showed strong correlations ( $0.70 \leq R^2 \leq 0.87$ ) with  $(R_W)^k$  resulted from all the analyzed chemical weathering indices. On the other hand,  $R_P(\gamma_t)$  and  $R_P(\phi_{equi})$  generally showed moderate correlation, and  $R_P(V_P)$  showed weak correlations were presented. Thus, the  $V_P$  evaluated with the proposed method in this study should only be used as a rough reference.

To evaluate the proposed method's applicability, the correlation of  $R_P$  that represents the geotechnical properties with  $R_W$  that represents the degree of weathering was examined; they mostly showed a strong correlation. Therefore, the proposed method estimated the geotechnical properties relatively well. However, applying the proposed method crucially requires determining the chemical weathering indices that can represent the degree of weathering at the target sites. Thus, as described in section 4.4, various chemical weathering indices must be selected and analyzed closely based on the XRF analysis results before evaluating the geotechnical properties through the proposed method.

The proposed method can simply predict the geotechnical properties of highly weathered granite based on the measured chemical weathering indices from residual soil to moderately weathered granite, and the geotechnical properties of residual soil and moderately weathered granite. The geotechnical properties of residual soil and moderately weathered granite can be determined relatively easily and the chemical weathering indices can be evaluated using a

small number of samples retrieved from the SPT.

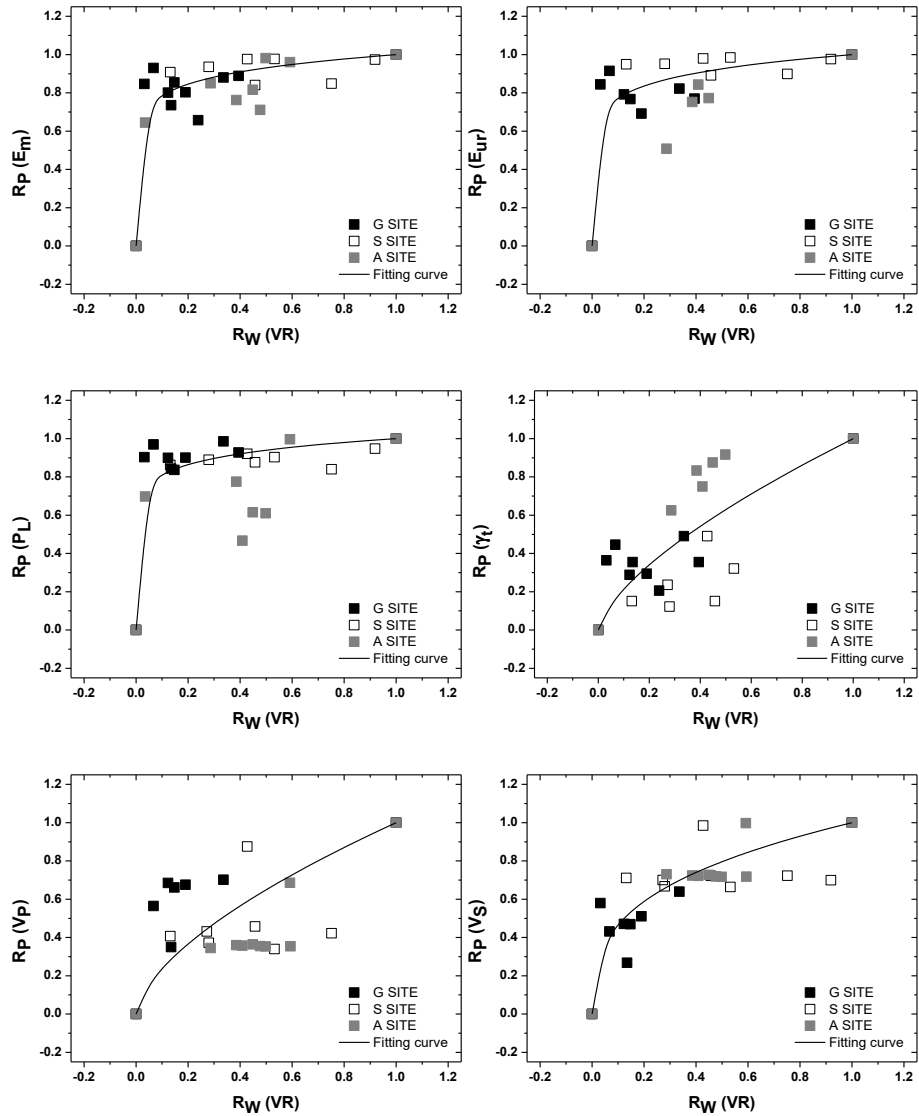


Figure 5-1 The relationship between the property ratio ( $R_p$ ) and the weathering index ratio ( $R_w$ ) based on VR (continue on next page)

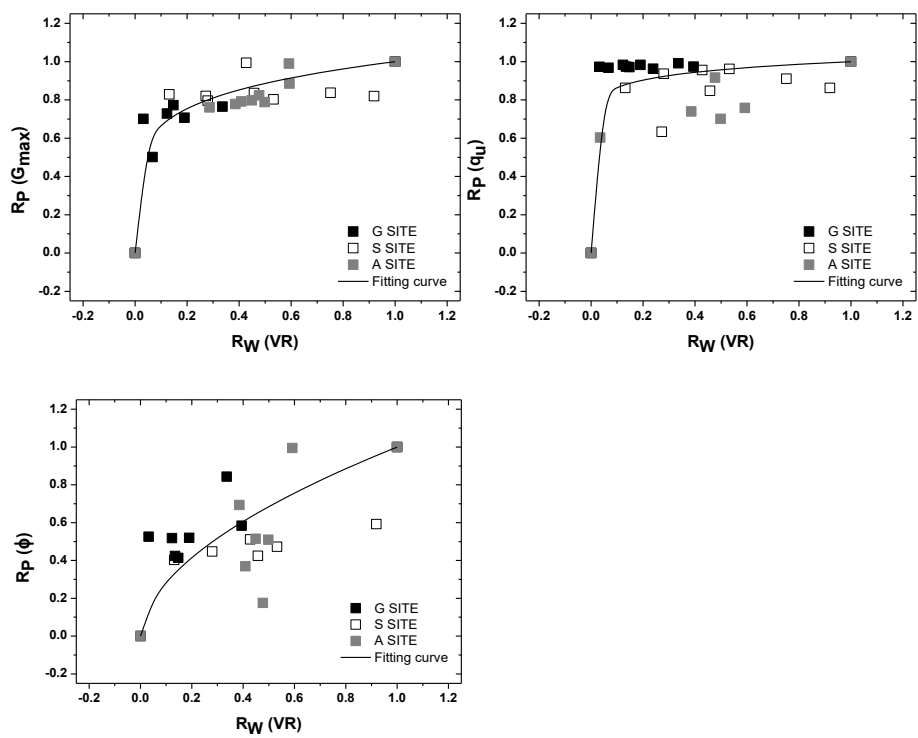


Figure 5-1 The relationship between the property ratio ( $R_p$ ) and the weathering index ratio ( $R_w$ ) based on VR



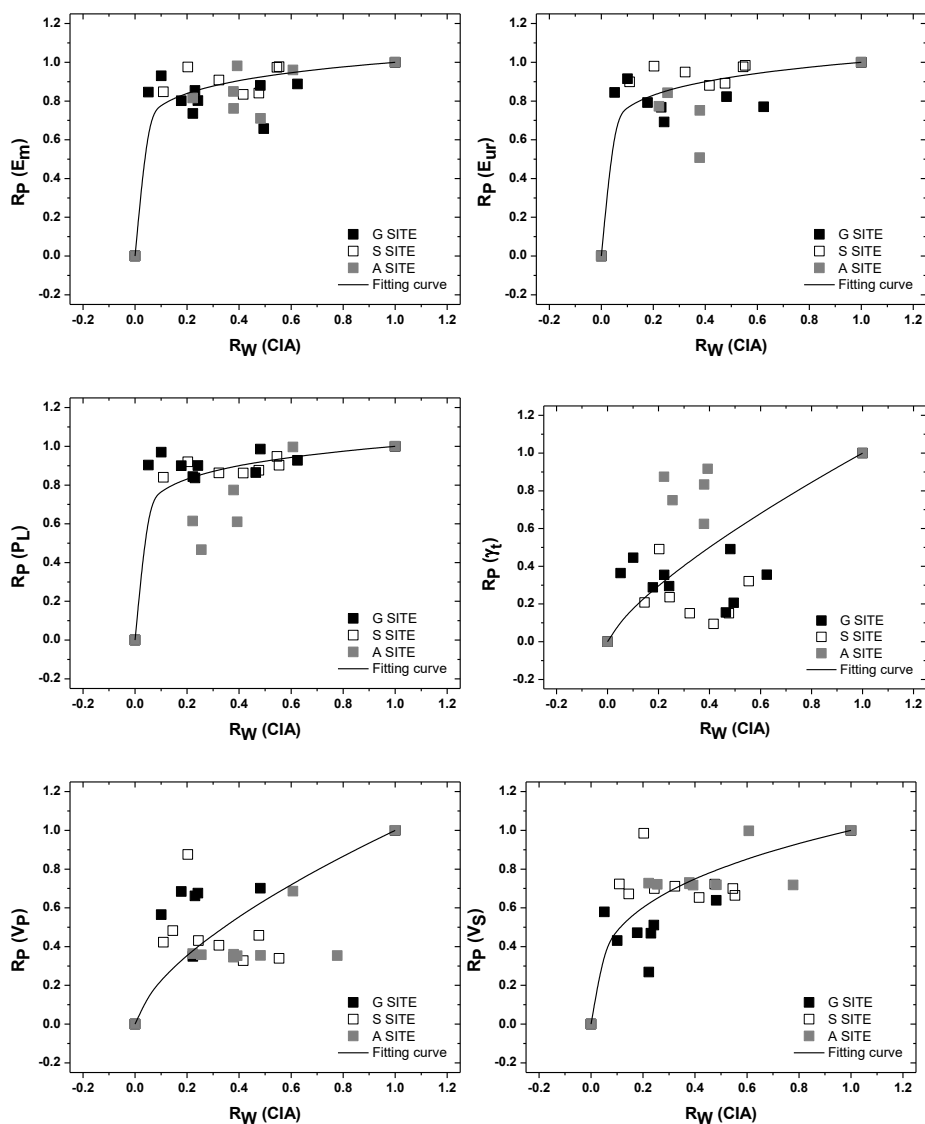


Figure 5-2 The relationship between the property ratio ( $R_p$ ) and the weathering index ratio ( $R_w$ ) based on CIA (continue on next page)

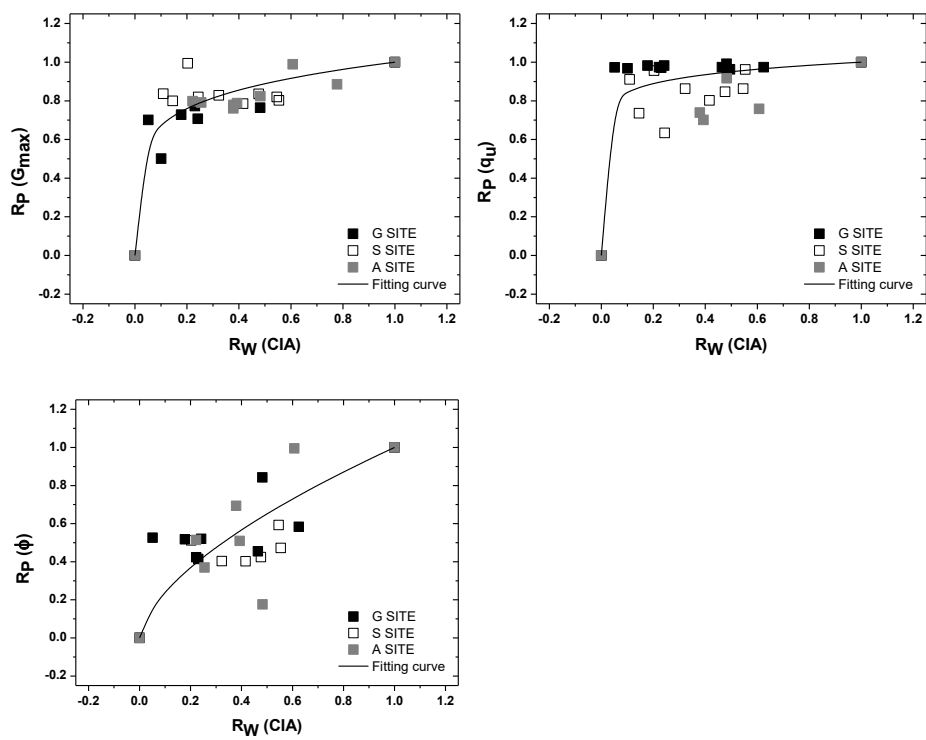


Figure 5-2 The relationship between the property ratio ( $R_p$ ) and the weathering index ratio ( $R_w$ ) based on CIA

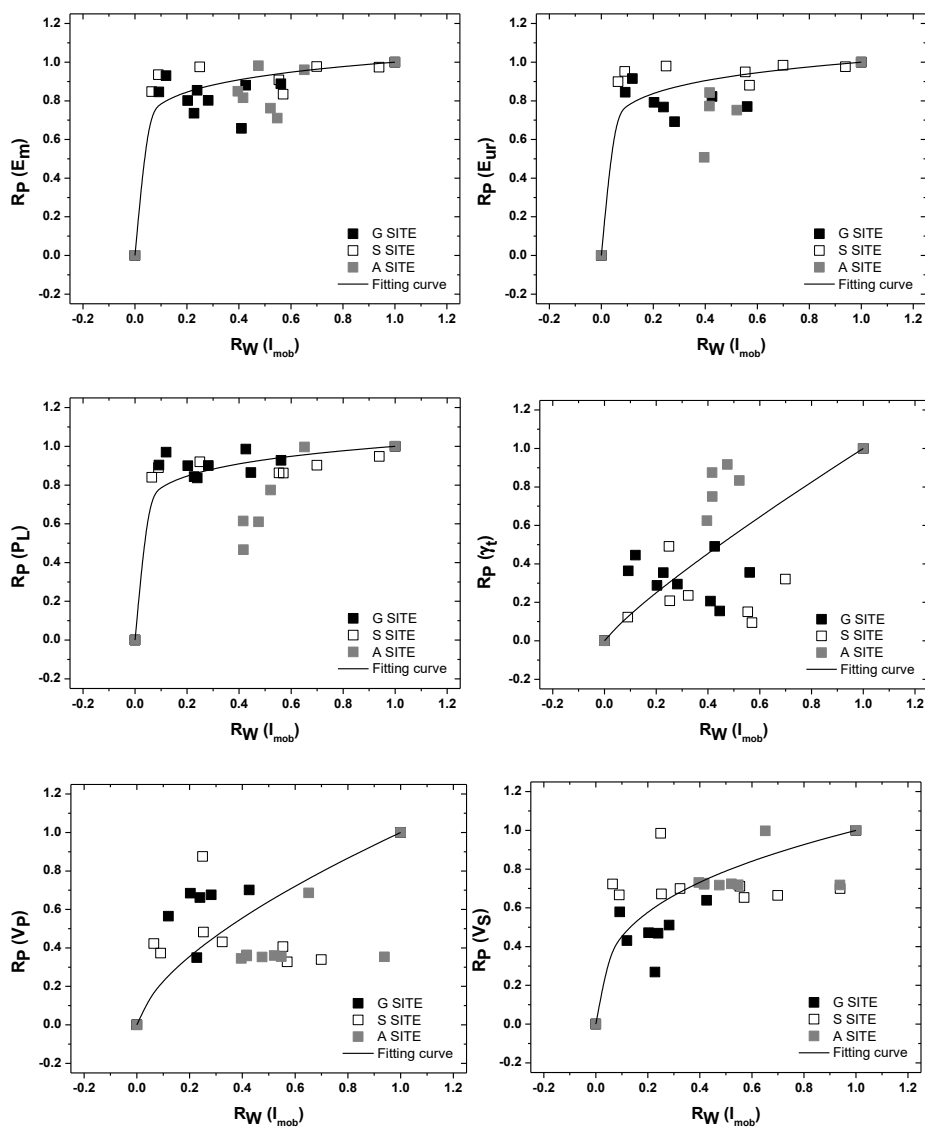


Figure 5-3 The relationship between the property ratio ( $R_p$ ) and the weathering index ratio ( $R_w$ ) based on  $I_{mob}$  (continue on next page)

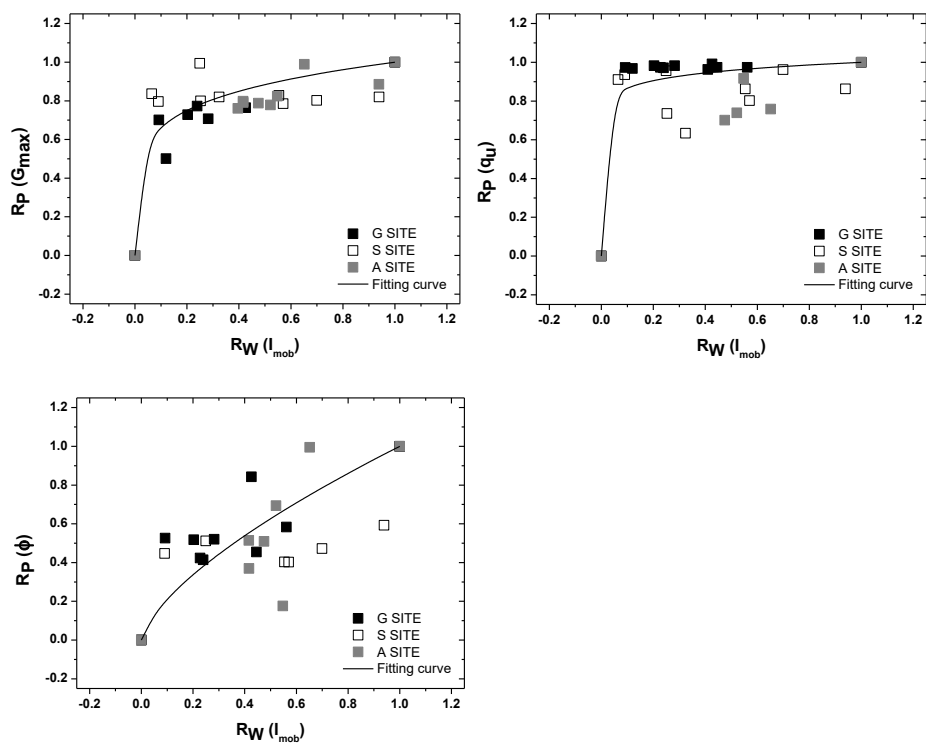


Figure 5-3 The relationship between the property ratio ( $R_p$ ) and the weathering index ratio ( $R_w$ ) based on  $I_{mob}$

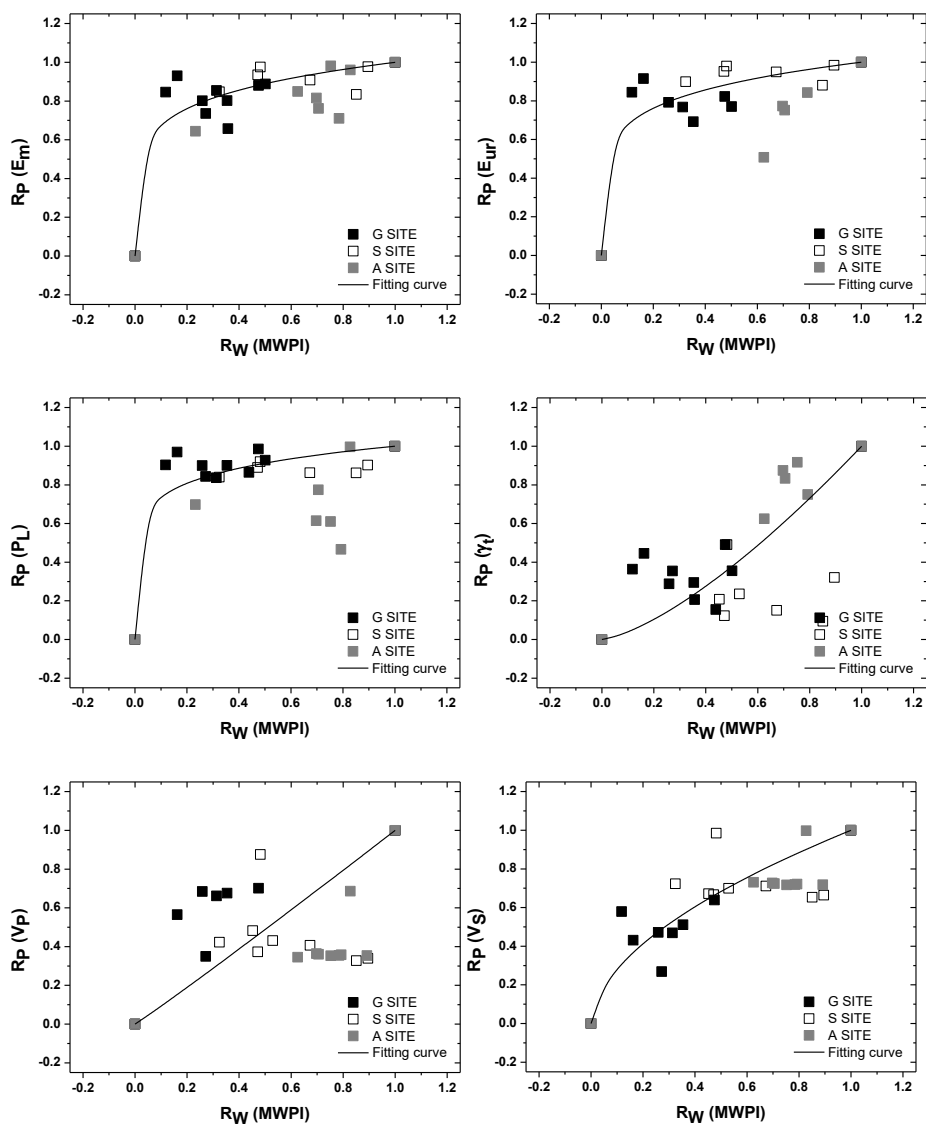


Figure 5-4 The relationship between the property ratio ( $R_p$ ) and the weathering index ratio ( $R_w$ ) based on MWPI (continue on next page)

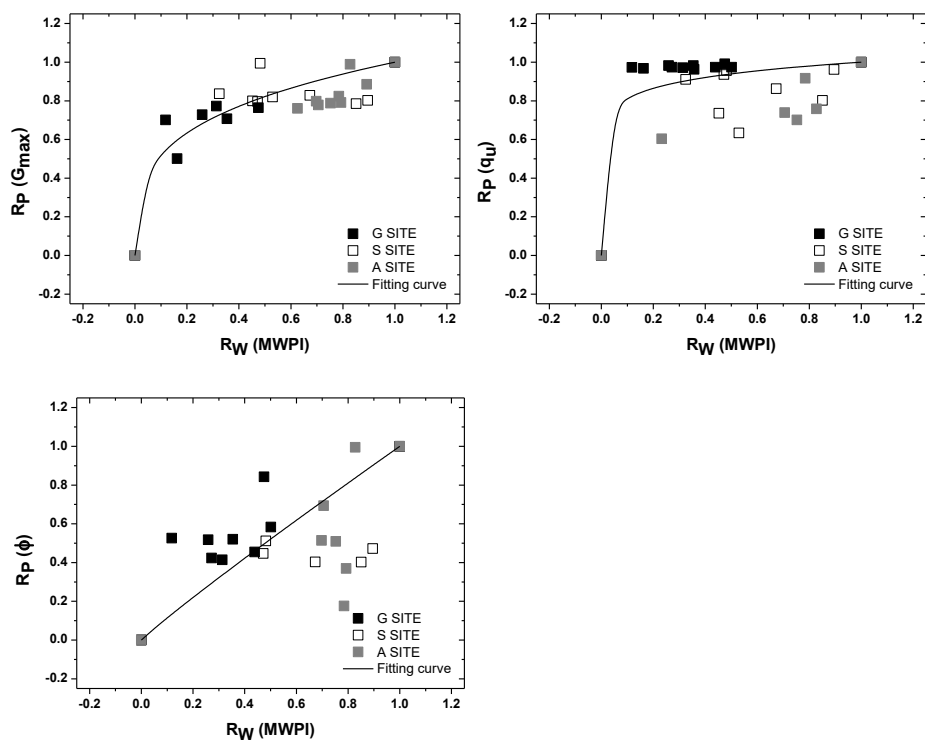


Figure 5-4 The relationship between the property ratio ( $R_p$ ) and the weathering index ratio ( $R_w$ ) based on MWPI

Table 5-1 Relationship between the property ratio and the weathering index ratio ( $R_P = (R_W)^k$ )

Weathering index ratio ( $R_W$ )		Property ratio ( $R_P$ )								
		$E_m$	$E_{ur}$	$P_L$	$\gamma_t$	$V_P$	$V_S$	$G_{max}$	$q_u$	$\phi_{eq.}^*$
VR	$k$	0.104	0.111	0.090	0.669	0.623	0.329	0.174	0.063	0.722
	$R^2$	0.91	0.87	0.80	0.63	0.43	0.82	0.93	0.85	0.58
CIA	$k$	0.108	0.115	0.115	0.755	0.645	0.314	0.170	0.073	0.619
	$R^2$	0.90	0.86	0.83	0.37	0.44	0.74	0.91	0.87	0.66
$I_{mob}$	$k$	0.104	0.110	0.103	0.862	0.641	0.340	0.178	0.061	0.675
	$R^2$	0.89	0.84	0.81	0.47	0.35	0.70	0.88	0.86	0.57
MWPI	$k$	0.169	0.169	0.132	1.409	1.034	0.500	0.282	0.090	0.941
	$R^2$	0.89	0.85	0.77	0.50	0.23	0.79	0.90	0.82	0.45

\* Equivalent friction angle

## 5.2 Prediction of Geotechnical Property

To validate the proposed estimation method, the predicted geotechnical properties using the developed relationship between the property ratio ( $R_p$ ) and the weathering index ratio ( $R_w$ ) were compared with the measured geotechnical properties. The geotechnical properties of highly and completely weathered granite can be easily calculated converting the developed  $R_p$  -  $R_w$  relationship, as shown in equation 5-1.

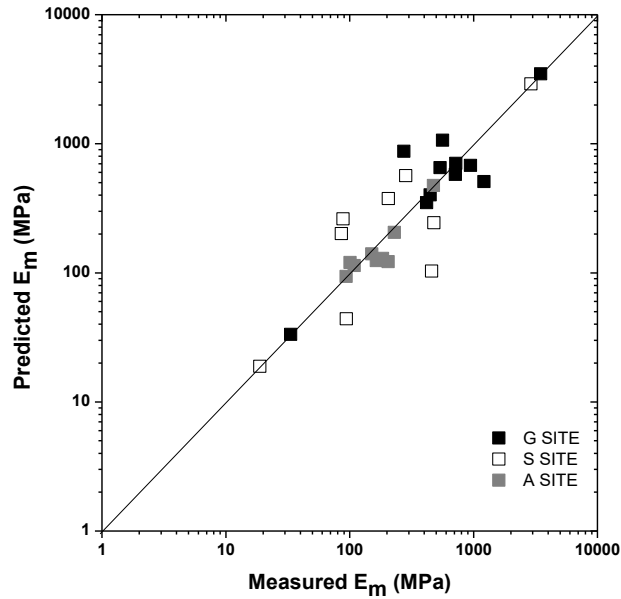
$$\zeta_{HW\&CW} = \zeta_{MW} - (\zeta_{MW} - \zeta_{RS})(R_w)^k \quad 5-1$$

The fitting constant,  $k$ , is determined using Table 5-1, according to the geotechnical property to be predicted. In this section, the geotechnical properties predicted using VR compared the measured properties, and the ratio of the predicted properties to the measured properties were analyzed.

$E_m$  and  $G_{max}$  whose property ratio showed a very strong correlation ( $0.9 \leq R^2$ ) with the chemical weathering index ratio of VR were analyzed. As shown in Figure 5-5-(a) and Figure 5-6-(a), most of the predicted values of  $E_m$  and  $G_{max}$  were close to the 1:1-line. Also, ratio of the predicted  $E_m$  and  $G_{max}$  to measured one were analyzed for quantitative evaluating how exact the proposed model predicts the measured  $E_m$  and  $G_{max}$ . Most of the ratio of the predicted  $E_m$  and the measured  $E_m$  were distributed near the 1.0, and the mean value of the ratio was 1.14 (Figure 5-5-b), which means 14 % overestimation as average.

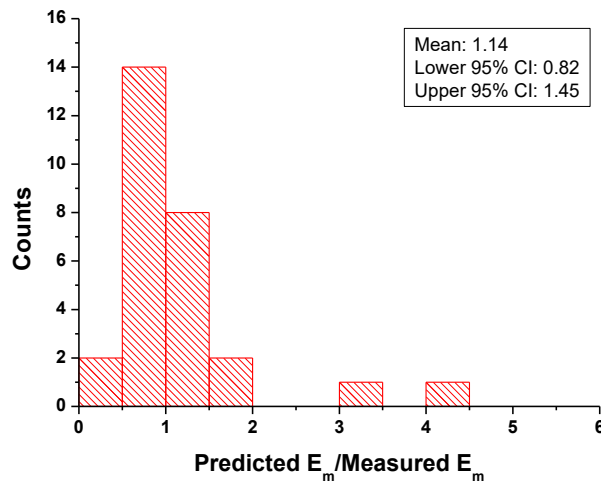


On the other hand, the mean value of the ratio to the  $G_{\max}$  was 1.00 and most ratios were concentrated from 0.8 to 1.2 (Figure 5-6-b).



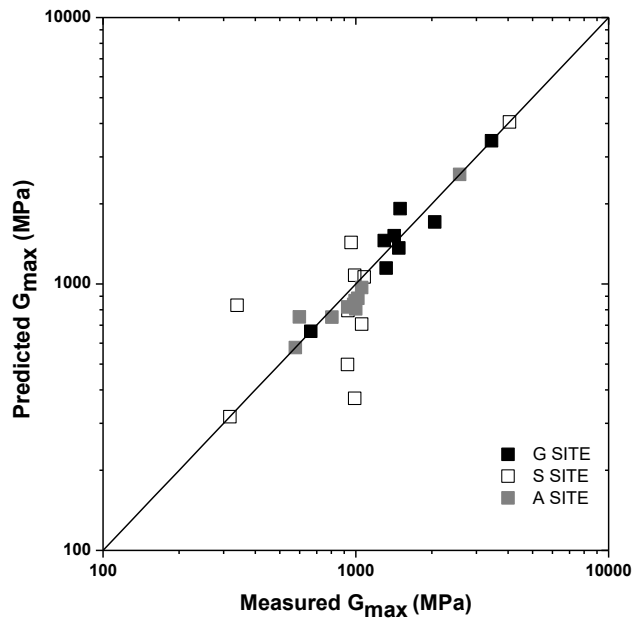
(a)

Figure 5-5 Comparison the predicted and measured  $E_m$ : (a) Plot of predicted  $E_m$  – measured  $E_m$ ; (b) Histogram of predicted  $E_m$  / measured  $E_m$   
(continue on next page)

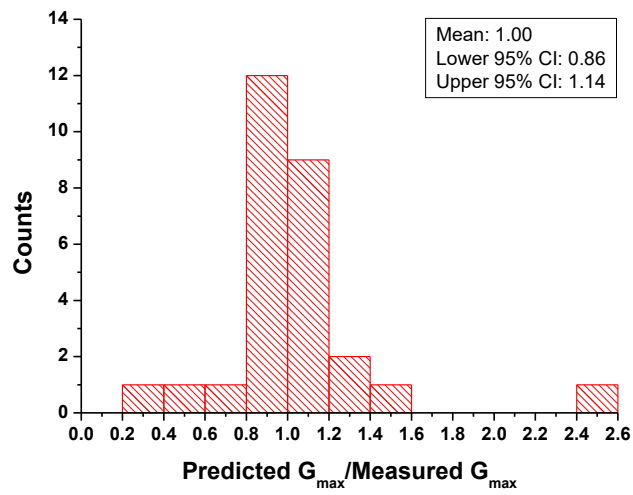


(b)

Figure 5-5 Comparison the predicted and measured  $E_m$ : (a) Plot of predicted  $E_m$  – measured  $E_m$ ; (b) Histogram of predicted  $E_m$  / measured  $E_m$



(a)



(b)

Figure 5-6 Comparison the predicted and measured  $G_{\max}$ : (a) Plot of predicted  $G_{\max}$  – measured  $G_{\max}$ ; (b) Histogram of predicted  $G_{\max}$  / measured  $G_{\max}$

Also,  $E_{ur}$ ,  $P_L$ ,  $V_s$ , and  $q_u$  whose property ratio showed a strong correlations ( $0.80 \leq R^2 \leq 0.87$ ) with the chemical weathering index ratio of VR were predicted using the proposed method and compared with the measured properties. As shown in Figure 5-7, most of the predicted geotechnical properties ( $E_{ur}$ ,  $P_L$ ,  $V_s$ , and  $q_u$ ) were close to the 1:1-line. However, the predicted  $q_u$  of G site was generally overestimated comparing to the measured  $q_u$ , so it is recommended to use the predicted  $q_u$  as a rough reference value. Also, ratio of the predicted geotechnical properties ( $E_{ur}$ ,  $P_L$ ,  $V_s$ , and  $q_u$ ) to measured one were analyzed for quantitative evaluating how exact the proposed model predicts the measured properties. Most of the ratio of the predicted geotechnical properties ( $E_{ur}$ ,  $P_L$ ,  $V_s$ , and  $q_u$ ) and the measured properties were distributed near 1.0, and the mean values of the ratio were range from 0.96 to 1.74, which represents that the proposed method generally well predict the geotechnical properties (Figure 5-8).

$\gamma_t$ ,  $\phi$ , and  $V_p$  whose property ratio showed a moderate and weak correlations ( $0.43 \leq R^2 \leq 0.63$ ) with the chemical weathering index ratio of VR were also analyzed. Although these geotechnical properties showed a relatively low coefficient of determination comparing to the other properties, most of the predicted properties were close to 1:1 line, and the ratio of the predicted properties to the measured one was distributed near 1.0 (Figure 5-9, Figure 5-10). Based on these results, it can be concluded that the proposed prediction model provides a reliable estimation of the geotechnical properties of highly and completely weathered granite. Using the relationship derived in section 5.1, the geotechnical properties of highly and completely weathered granite can be

easily and reliably predicted, however, for the more accuracy, additional data acquisition and analysis are needed.

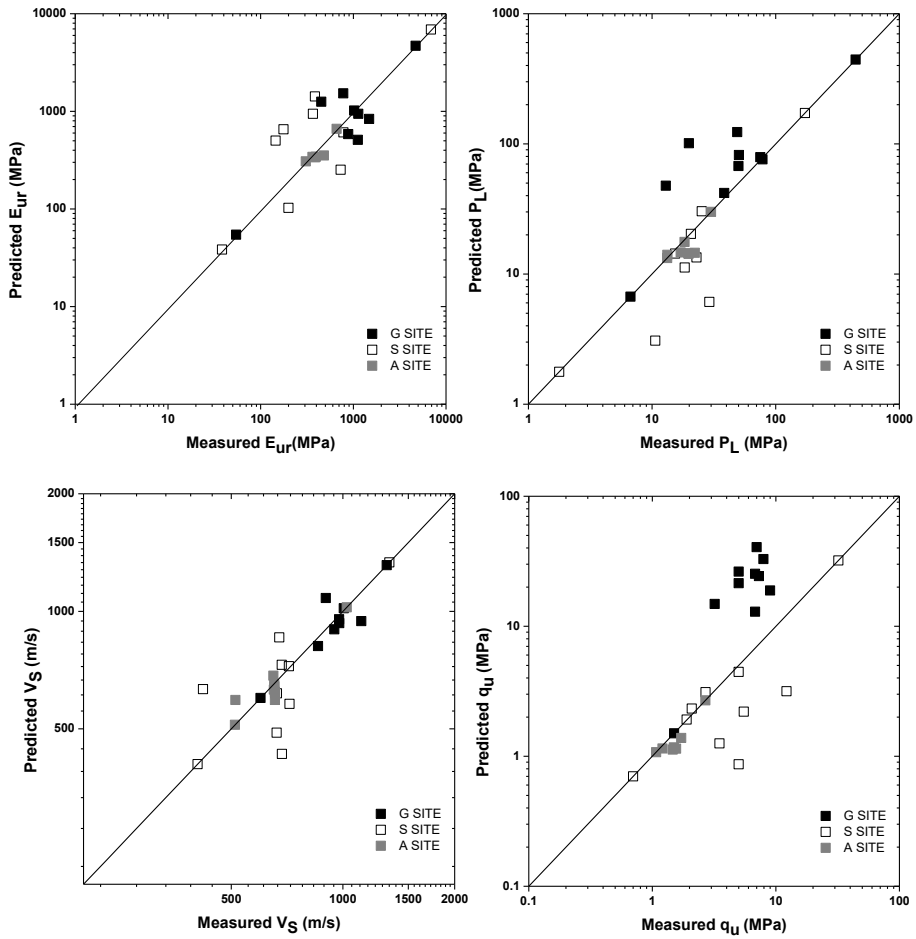


Figure 5-7 Comparison the predicted and measured geotechnical properties:  $E_{ur}$ ,  $P_L$ ,  $V_S$ , and  $q_u$

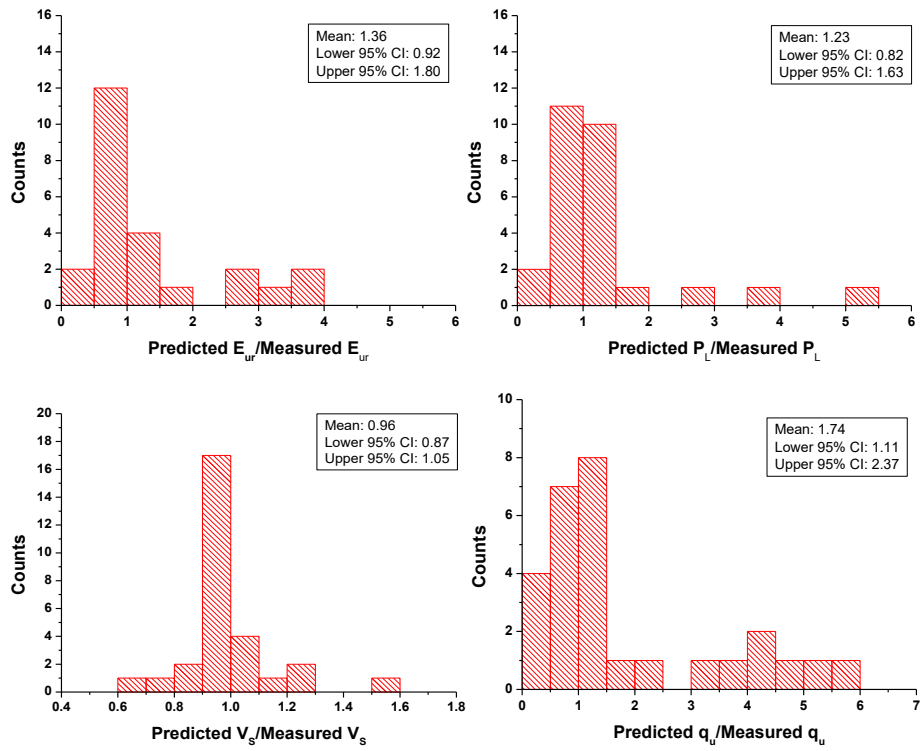


Figure 5-8 Histogram of predicted properties / measured properties:  $E_{ur}$ ,  $P_L$ ,  $V_s$ , and  $q_u$

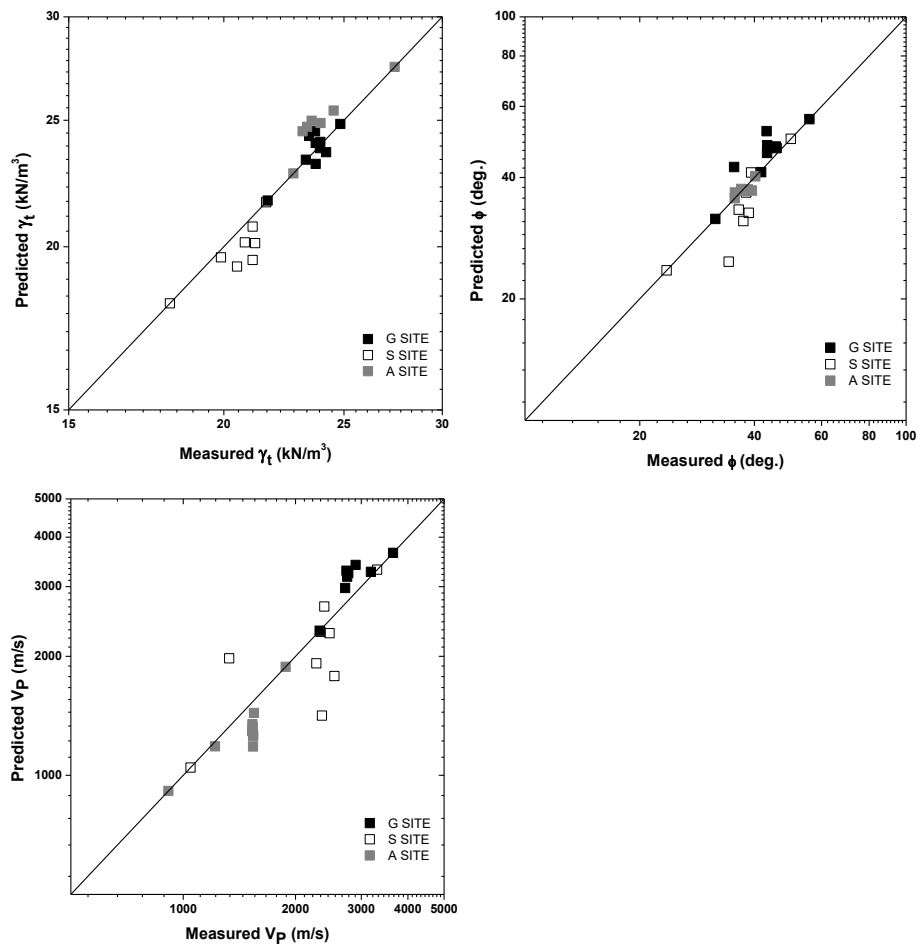


Figure 5-9 Comparison the predicted and measured geotechnical properties:  $\gamma_t$ ,  $\phi$ , and  $V_p$

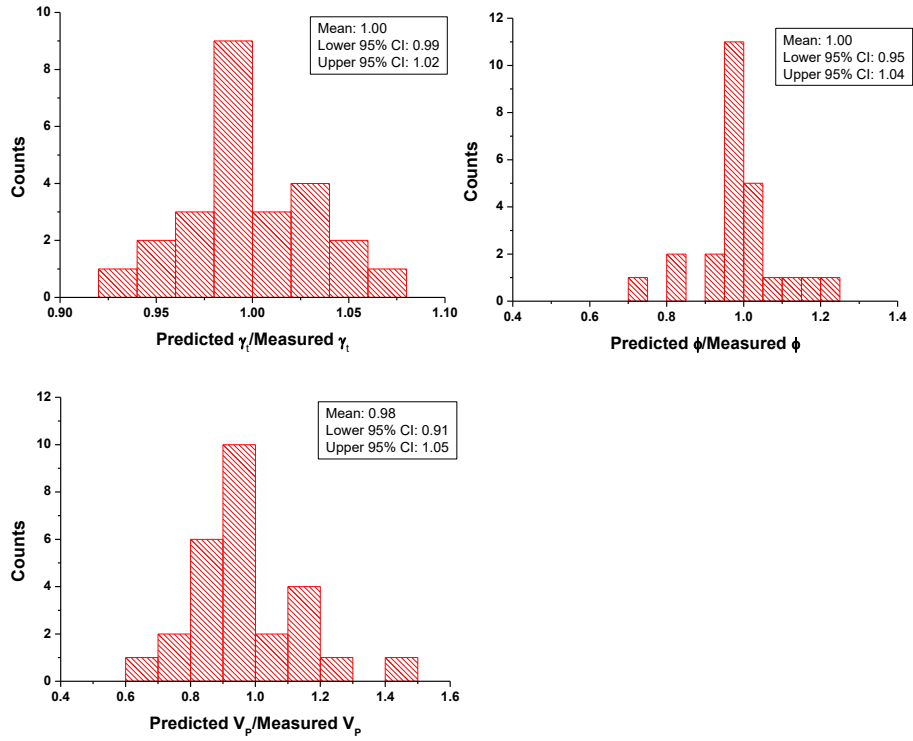


Figure 5-10 Histogram of predicted properties / measured properties:  $\gamma_t$ ,  $\phi$ , and  $V_p$



### 5.3 Application of the Proposed method

The estimation equations of the geotechnical properties of highly and completely weathered granite can be directly applied to the granite. However, appropriate relationships between the geotechnical properties and the chemical weathering indices should be determined to apply the proposed method to other types of rock.

Figure 5-11 shows the procedure for determining the fitting constant  $k$  of the other types of rock. Firstly, the geotechnical properties should be measured using *in situ* and laboratory tests from residual soil to moderately weathered rock layer, and then chemical weathering indices of the samples retrieved at each test depth should be calculated and analyzed as described in section 4.4. Finally, using correlation analysis between  $R_p$  and  $R_w$ , the fitting constant  $k$  that represents each geotechnical property and the suitable chemical weathering indices can be determined.

Once the fitting constant was determined, the properties of highly and completely weathered rock can be predicted following the procedure as shown in Figure 5-12. Firstly, the geotechnical properties of residual soil and moderately weathered rock should be measured, and then chemical weathering indices from residual soil to moderately weathered rock should be calculated. Finally, the geotechnical properties of the highly and completely weathered rock can be determined by applying the known values to the relationship between  $R_p$  and  $R_w$ .

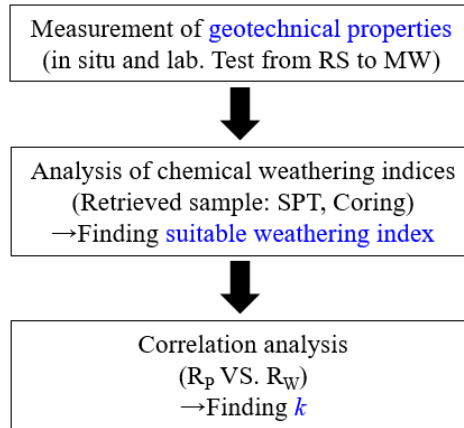


Figure 5-11 Procedure for determining fitting constant k (other types of rock)

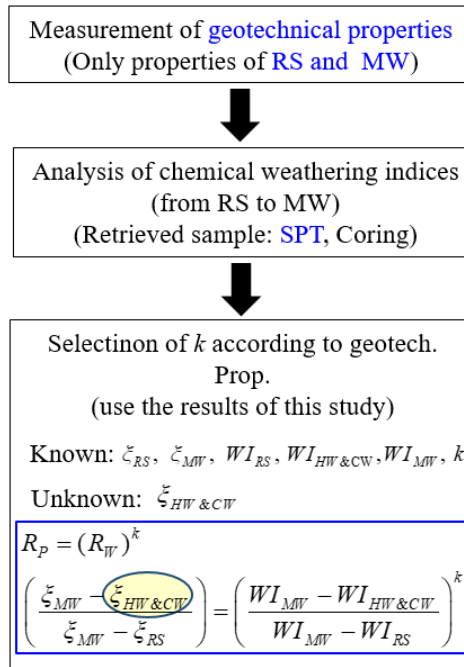


Figure 5-12 Application of k for HW and CW granite

## Chapter 6. Conclusions and Recommendations

This dissertation experimentally investigated the geotechnical properties and the chemical weathering indices of highly and completely weathered granite and evaluated their relationship. Several *in situ* tests were performed to estimate the geotechnical properties and obtain the basic data for deriving the relationship. Also, all samples from residual soil to moderately weathered granite layer were retrieved for laboratory tests and XRF analysis. Various chemical weathering indices were calculated using the percentage of the major oxide element resulted from XRF analysis. Particular attention was given to the development of the highly and completely weathered granite geotechnical property estimation model that could consider the site-specific characteristics. The main conclusions and recommendations draw from the experiment and analysis research in this dissertation are summarized as follows.

### *Geotechnical properties from residual soil to moderately weathering granite*

Several *in situ* tests and laboratory tests were conducted to evaluate geotechnical properties, and the result of each property showed a general increasing tendency with depth, but in a particular range of the highly and completely weathered granite layer, the properties were locally decreased. It indicated that the degree of weathering is always not to be continuously decreased. So, it is more reasonable to use the chemical weathering indices that show the degree of the weathering at each test depth for estimating the

geotechnical properties of the highly and completely weathered granite.

Also, the magnitude of geotechnical properties measured at each test site was widely distributed and differ from each other, in spite of the layers that were classified the same weathering condition (e.g. residual soil, highly and completely weathered granite, and moderately weathered granite). It indicated that the geotechnical properties are dependent on site-specific characteristics. therefore, considering the site-specific characteristics is important in order to reliably evaluate the geotechnical properties using not a local empirical relationship but a general empirical relationship.

#### *Chemical weathering indices from residual soil to moderately weathering granite*

Several chemical weathering indices were evaluated based on the percentage of major oxide elements analyzed by the XRF, and the appropriate chemical weathering indices for the weathered granite were determined based on the distribution of the major oxide element and the chemical weathering indices. VR, CIA,  $I_{mob}$ , and MWPI which were developed based on the decreasing tendency of alkalis and alkaline oxide represent the degree of weathering at all the test sites, and showed similar tendency with the geotechnical properties evaluated at each test site (i.e., the general decreasing weathering intensity with depth including the locally less weathered area).

Since the determination of the suitable chemical weathering indices representing the *in situ* degree of weathering is very important to derive reliable

relationships between the geotechnical properties and the chemical weathering indices, the sufficient analysis for the major oxide and the chemical weathering indices have to be conducted.

*Relationship between geotechnical properties and chemical weathering indices*

A new estimation method of the geotechnical properties of highly and completely weathered granite was proposed, and the acquired test data including the geotechnical properties and the chemical weathering indices were applied for determining the fitting constant indicating the relationships between the geotechnical properties and the chemical weathering indices. As a result, the suggested method generally showed a strong correlation, and especially very strong correlations were identified when the suggested method was applied to the pressuremeter modulus and maximum shear modulus. So, the results of this thesis can be utilized for the simple and reliable estimation of the geotechnical properties of highly weathered granite based on the measured chemical weathering indices from residual soil to moderately weathered granite, and the geotechnical properties of residual soil and moderately weathered granite. With additional researches using more data, it is expected that the more reliable estimation model can be acquired and utilized for economical evaluation of the geotechnical properties of highly and completely weathered granite.

### *Limitations and recommendations*

The result of this paper showed a basic concept and procedure for estimating the geotechnical properties of highly and completely weathered granite using the chemical weathering indices and the properties of residual soil and moderately weathered granite.

Some cautions should be exercised, however, when predicting the geotechnical properties. A sufficient analysis of chemical weathering indices which one well represents the *in situ* degree of weathering have to be conducted before applying the suggested estimation method. A simple application of the fitting constants suggested in this paper without considering the suitable chemical weathering indices may lead the totally different geotechnical properties comparing the real value. So, it is recommended to apply the fitting constant suggested in this paper when the chemical weathering indices (i.e., VR, CIA,  $I_{mob}$ , and MWPI) of the target site well represent the general degree of weathering, which can be identified by the distribution of the chemical weathering indices in each weathered layer (i.e., residual soil, highly and completely weathered granite, and moderately weathered granite layer).

Also, since the results presented in this paper were derived based on limited data of the three test sites, additional researches using more data have to be conducted to advance the reliability of the proposed method.

## List of References

- Arel, E., Tugrul, A., 2001. Weathering and its relation to geomechanical properties of Cavusbasi granitic rocks in Northwestern Turkey. *Bulletin of Engineering Geology and the Environment* 60, 123–133.  
doi:10.1007/s100640000091
- Baynes, F.J., Dearman, W.R., 1978. The relationship between the microfabric and the engineering properties of weathered granite. *Bulletin of the International Association of Engineering Geology* 18, 191–197.  
doi:10.1007/BF02635370
- Blyth, F., Freitas, M. De, 2017. A geology for engineers.
- Chiu, C.F., Ng, C.W.W., 2014. Relationships between chemical weathering indices and physical and mechanical properties of decomposed granite. *Engineering Geology* 179, 76–89. doi:10.1016/J.ENGGEOL.2014.06.021
- Dearman, W.R., Baynes, F.J., Irfan, T.Y., 1978. Engineering grading of weathered granite. *Engineering Geology* 12, 345–374.  
doi:10.1016/0013-7952(78)90018-2
- Duzgoren-Aydin, N., Aydin, A., Malpas, J., 2002. Re-assessment of chemical weathering indices: case study on pyroclastic rocks of Hong Kong. *Engineering Geology* 63, 99–119. doi:10.1016/S0013-7952(01)00073-4
- Franklin, J.A., Chandra, R., 1972. The slake-durability test. *International Journal of Rock Mechanics and Mining Sciences & Geomechanics Abstracts* 9, 325–328. doi:10.1016/0148-9062(72)90001-0
- Gannon, J., Masterton, G., Wallace, W., 1999. *Piled foundations in weak rock*. London.
- Gardner, L.R., Kkeoruenromne, I., Chen, H.S., 1978. *Isovolumetric geochemical investigation of a buried granite saprolite near Columbia, SC, U.S.A.* Pergamon Press.
- Hamrol, A., 1961. A quantitative classification of the weathering and

- weatherability of rocks, in: International Conference of Soil and Mechanical Engineers, Vol. 2. pp. 771–774.
- Iliev, I.G., 1966. AN ATTEMPT TO ESTIMATE THE DEGREE OF WEATHERING OF INTRUSIVE ROCKS FROM THEIR PHYSICO-MECHANICAL PROPERTIES, in: International Society of Rock Mechanics. pp. 109–114.
- Irfan, T.Y., 1996. Mineralogy, fabric properties and classification of weathered granites in Hong Kong. *Quarterly Journal of Engineering Geology and Hydrogeology* 29, 5–35.  
doi:10.1144/GSL.QJEGH.1996.029.P1.02
- Irfan, T.Y., Dearman, W.R., 1978. The engineering petrography of a weathered granite in Cornwall, England. *Quarterly Journal of Engineering Geology and Hydrogeology* 11, 233–244.  
doi:10.1144/GSL.QJEG.1978.011.03.03
- Kanji, M.A., 2014. Critical issues in soft rocks. *Journal of Rock Mechanics and Geotechnical Engineering* 6, 186–195.  
doi:10.1016/J.JRMGE.2014.04.002
- Kim, S., Park, H.-D., 2003. The relationship between physical and chemical weathering indices of granites around Seoul, Korea. *Bulletin of Engineering Geology and the Environment* 62, 207–212.  
doi:10.1007/s10064-003-0192-7
- Kwon, O.S., 1998. Experimental study on the shear strength and deformation characteristics of weathered soil.
- Lacerda, W.A., 2010. Shear strength of soils derived from the weathering of granite and gneiss in Brazil. *Geological Society, London, Engineering Geology Special Publications* 23, 167–182. doi:10.1144/EGSP23.10
- Lech, M.E., Trewin, C.L., 2013. Weathering, erosion, landforms and regolith Teacher notes and student activities.
- Lee, S.G., 1993. Weathering of granite. *Journal of the geological society of Korea* 29, 396–413.



- Menard, L., 1975. The Menard Pressuremeter: Interpretation and Application of Pressuremeter Test Results to Foundation Design.
- Nesbitt, H.W., 1979. Mobility and fractionation of rare earth elements during weathering of a granodiorite. *Nature* 279, 206–210.  
doi:10.1038/279206a0
- Nesbitt, H.W., Young, G.M., 1982. Early Proterozoic climates and plate motions inferred from major element chemistry of lutites. *Nature* 299, 715–717. doi:10.1038/299715a0
- Ollier, C., 1984. Weathering. Weathering.
- Onodera, T., Yoshinaka, R., Oda, M., 1974. Weathering and its relation to mechanical properties of granite., in: 3rd Congr of ISRM Advances in Rock Mechanics. Denver, pp. 71–78.
- Peltier, L.C., 1950. The Geographic Cycle in Periglacial Regions as it is Related to Climatic Geomorphology. *Annals of the Association of American Geographers* 40, 214–236. doi:10.1080/00045605009352070
- Price, D., 1995. Weathering and weathering processes. *Quarterly Journal of Engineering Geology and Hydrogeology* 28, 243–252.
- Reiche, P., 1943. Graphic Representation of Chemical Weathering. *SEPM Journal of Sedimentary Research* Vol. 13, 58–68.  
doi:10.1306/D4269198-2B26-11D7-8648000102C1865D
- Rigopoulos, I., Tsikouras, B., Pomonis, P., Hatzipanagiotou, K., 2015. Assessment of the engineering behavior of ultramafic and mafic rocks using chemical indices. doi:10.1016/j.enggeo.2015.07.019
- Ruxton, B.P., 1968. Measures of the Degree of Chemical Weathering of Rocks. *The Journal of Geology* 76, 518–527. doi:10.1086/627357
- Seo, Y.-S., Yun, H.-S., Kim, D.-G., Kwon, O.-I., 2016. Analysis on Physical and Mechanical Properties of Rock Mass in Korea. *The Journal of Engineering Geology* 26, 593–600. doi:10.9720/kseg.2016.4.593
- Seoul, 2006. Site investigation manual. Seoul, Korea.
- Shirlaw, J.N., Hencher, S.R., Zhao, J., 2000. Design and construction issues

- for excavation and tunnelling in some tropically weathered rocks and soils, in: ISRM International Symposium. International Society of Rock Mechanics and Rock Engineering.
- Sueoka, T., 1988. Identification and Classification of Granite residual Soils Using Chemical Weathering Index, in: Symposium on The Weathering Residual Soil. pp. 89–94.
- Sueoka, T., I. K., L., Muramatu, M., Imamura, S., 1985. Geomechanical properties and engineering classification for decomposed granite soils in Kaduna district, Nigeria, in: First International Conference on Geomechanics in Tropical Lateritic and Saprolitic Soils. Brasilia, pp. 175–186.
- Udagedara, D.T., Oguchi, C.T., Gunatilake, A.A.J.K., 2017. Combination of chemical indices and physical properties in the assessment of weathering grades of sillimanite-garnet gneiss in tropical environment. *Bulletin of Engineering Geology and the Environment* 76, 145–157.  
doi:10.1007/s10064-016-0878-2
- Ulsay, R., Hudson, J.A., 2007. The complete ISRM suggested methods for rock characterization, testing and monitoring; 1974–2006. *International Society on Rock Mechanics* 628.
- Vogel, D.E., 1975. Precambrian Weathering in Acid Metavolcanic Rocks from the Superior Province, Villebon Township, South-Central Québec. *Canadian Journal of Earth Sciences* 12, 2080–2085. doi:10.1139/e75-183
- Vogt, T., 1927. Sulitjelmafeltets geologi og petrografi. *Norges Geologiske Undersøkelse* 121, 1–560.

## 초 록

화강암은 국내 지질의 약 35 % 이상을 구성하고 있는 주요 암종이며 풍화대가 두껍게 발달되어 있다. 화강 풍화암은 도로, 교량, 터널 등 대부분의 주요 건설사업에서 지반구조물의 지지층으로 활용되고 있으므로 화강 풍화암의 지반특성 및 지반정수를 평가하는 것은 구조물의 성능과 안전성 확보를 위해서 중요하다. 그러나 실내 역학시험에 적합한 상태의 시료를 채취하기 어렵고 지반조사 시 광범위하게 사용되는 표준관입시험(SPT: Standard penetration test) 수행 시 관입량이 매우 작기 때문에 신뢰도 있는 지반정수를 평가하기 어렵다. 또한, 프레스미터시험(PMT: Pressuremeter test)과 같이 시추공 내에서 지반특성을 평가하는 현장시험의 경우 신뢰도 있는 지반정수 평가가 가능하지만 시험 소요 시간 및 비용의 제약으로 매우 제한적으로 수행되고 있다.

기존 연구자들은 풍화암의 지반정수 평가를 위해 풍화 현상에 따른 암의 특성 변화에 대한 연구를 수행하였다. 풍화 현상을 정량적으로 평가하기 위해 풍화지수의 대한 연구가 활발히 수행되었으며, 풍화지수와 암의 공학적 특성 사이의 관계를 평가하는 연구가 다수 수행되었다. 그러나, 기존 연구는 대부분 실내 시험이 가능한 신선암 ~ 연암을 대상으로 수행되었으며 단순히 풍화지수와 암의 공학적 특성을 1:1로 비교하여 현장 조건을 반영하지 못한 한계가

있다. 이에 본 연구에서는 화강 풍화암을 대상으로 현장시험을 주로 적용하여 지반정수를 평가하였으며, 시료의 교란과 무관하게 풍화를 정량적으로 평가할 수 있는 화학적 풍화지수를 이용하여 현장 조건을 반영한 지반정수 평가 방법을 새로이 제안하였다. 국내 3개 현장에서 화강 풍화암을 대상으로 PMT, 밀도검층, 다운홀테스트를 수행하였으며, 풍화대(풍화토와 풍화암)와 연암 전구간의 시료를 채취하여 실내시험 및 X선 형광분석을 수행하였다.

현장시험 통해 화강 풍화암의 변형계수, 제하-재제하 탄성계수, 극한압력, 현장 전단위중량, 압축과 및 전단파 속도, 동적 전단탄성계수를 평가하였고, 실내시험을 통해 일축압축강도와 전단강도 정수를 평가하였다. 풍화암의 지반정수는 풍화토와 연암의 지반정수 사이 값을 갖는 것으로 확인되었으며, 심도에 따라 전반적으로 증가하는 경향을 보였으나 풍화정도에 따라 국부적인 감소 현상을 확인할 수 있었다. 3 개 현장의 측정된 지반정수는 현장의 특성에 따라 그 크기가 달랐으며, 본 연구에서는 이러한 현장 특성을 반영하여 화학적 풍화지수와 지반정수 사이의 일반적인 관계를 평가하고자 하였다.

화학적 풍화지수를 이용하여 풍화암의 지반정수를 평가하기 위해 풍화에 따른 암의 지반정수 모델을 제안하였다. 제안한 지반 정수 모델은 대상 현장의 특성을 반영하기 위해 해당 현장 풍화암 상부에 존재하는 풍화토와 하부에 존재하는 연암의 지반정수를 경계값으로 적용하였고, 동일한 방법으로 해당현장의 화학적 풍화지수를 사용하여 풍화도를 평가할 수 있도록 구성하였다. 3개 현장에서 측정된 지반정수 및 화학적 풍화지수를 이용하여 제안한 평가모델에 적

용하여 각각의 지반정수 평가를 위한 추정식을 제안하였다.

본 연구는 풍화에 따른 화강암의 지반정수 변화 경향을 바탕으로 국내 화강 풍화암의 지반정수를 평가하기 위해 수행되었으며, 3개 현장의 실측한 지반정수와 화학적 풍화지수를 제안한 지반정수 평가 모델에 적용하여 지반정수 추정식을 제안하였다. 본 연구결과를 바탕으로 본 연구결과를 바탕으로 지반구조물의 설계 및 시공 시 화강 풍화암의 지반정수를 보다 경제적이고 정확하게 평가할 수 있을 것이라 기대된다.

**주요어:** 지반조사, 지반정수, 풍화, 화학적 풍화지수, 화강 풍화암  
**학 번:** 2015-30281